CalVal Jason-2

Jason-2 validation and cross calibration activities (Annual report 2013)

Contract No 104685/00 - lot 1.2A

Reference : CLS.DOS/NT/13-227

Nomenclature : SALP-RP-MA-EA-22270-CLS

Issue : 1rev 0

Date : January 30, 2014

CLS - 8-10 Rue Hermès - Parc Technologique du Canal - 31520 Ramonville St-Agne - FRANCE
Telephone 33 5 61 39 47 00 / Fax 33 5 61 75 10 14

Chronology Issues:		
Issue:	Date:	Reason for change:
1rev0	December 10, 2013	Creation

People involved in this issue :				
	AUTHORS	**COMPANY**	**DATE**	**INITIALS**
Written by:	S. Philipps H. Roinard	CLS CLS		
Checked by:		CLS		
Approved by:		CLS CLS		
Application authorised by:				

Index Sheet :	
Context:	
Keywords:	
Hyperlink:	

Distribution:		
Company	Means of distribution	Names
CLS/DOS	electronic copy	G.DIBARBOURE V.ROSMORDUC
CNES	electronic copy	thierry.guinle@cnes.fr emilie.bronner@cnes.fr nicolas.picot@cnes.fr aqgp_rs@cnes.fr dominique.chermain@cnes.fr delphine.vergnoux@cnes.fr

List of tables and figures

List of Tables

List of Figures

List of items to be defined or to be confirmed

Applicable documents / reference documents

Contents

1. Introduction

This document presents the synthesis report concerning validation activities of Jason-2 GDRs under SALP contract (N° 104685/00 Lot 1.2A) supported by CNES at the CLS Space Oceanography Division. It covers several points: CAL/VAL Jason-2 activities, Jason-2 / Jason-1 cross-calibration, particular studies and investigations.
The OSTM/Jason-2 satellite was successfully launched on June, 20th 2008. Since July, 4th, Jason-2 is on its operational orbit. Until January 2009, it was flying in tandem with Jason-1, only 55s apart. Note that from May 2012 onwards, Jason-1 is on a geodetic orbit (see note on Jason-1 geodetic mision [7]). Jason-1 sent its last measurement on 21st June 2013, after about 11.5 years in orbit. Since the beginning of the mission, Jason-2 data have been analyzed and monitored in order to assess the quality of Jason-2 products. Cycle per cycle reports are available on AVISO webpage (http://www.aviso.oceanobs.com/en/calval/systematic-calval/validation-reports.html).
This present report assesses the Jason-2 data quality. Missing and edited measurements are monitored. Furthermore relevant parameters derived from instrumental measurements and geophysical corrections are analyzed.
During 2012, the whole Jason-2 mission was reprocessed in GDR-D standard. For more details, please refer to the reprocessing report ([11]), spanning the reprocessing period (cycles 001 to 145), which contains comparisons between previous GDR-T and current GDR-D standard, as well as comparison between Jason-2 GDR-D and Jason-1 and Envisat data. Another report ([12]) focuses on the comparison of Jason-2 GDR-T and GDR-D with Jason-1 data during the first 20 Jason-2 cycles (the formation flight phase, when both satellites were on the same ground-track only 55s apart).

Hereafter, analyzes focus on Jason-1/Jason-2 cross-calibration. During the formation flight configuration (4th July 2008 to 26th January 2009) both satellites were on the same ground track. This allowed to precisely assess parameter discrepancies between both missions in order to detect geographically correlated biases, jumps or drifts. The SLA performances and consistency with Jason-1 are also described. But even after the end of the flight formation phase, and after Jason-1 moved to its geodetic orbit, comparison were still possible until the end of the Jason-1 mission in June 2013. Even if only low order statistics are mainly presented here, other analyzes including histograms, plots and maps are continuously produced and used in the quality assessment process. Indeed, it is now well recognized that the usefulness of any altimeter data only makes sense in a multi-mission context, given the growing importance of scientific needs and applications, in particular for operational oceanography. One major objective of the Jason-2 mission is to continue the Jason-1 and T/P high precision altimetry and to allow combination with other missions (ENVISAT, Jason-1, Saral-AltiKa). This kind of comparisons between different altimeter missions flying together provides a large number of estimations and consequently efficient long term monitoring of instrument measurements.
An Isro (Indian Space Research Organization) satellite, Saral (Satellite with ARgos and ALtika), embarks the AltiKa altimeter (working in Ka-band, 35 GHz), built by Cnes, as well as a Doris instrument. The launch of this mission on 25th of February 2013 allows to complete the altimetry constellation from 2013 onwards, re-occupying the long-term ERS and Envisat ground track. Comparisons between AltiKa and Jason-2 data are available in [18].

2. Processing status

2.1. Processing

End of 2008 Jason-2 data were already available to end users in OGDR (3h data latency) and IGDR (1-2 days data latency). They were first released in version T and switched at cycle 015 to version C. They stayed in this version till cycle 149 (till 2012/07/31 12:01:59 for OGDR), this is the same version (concerning the geophysical standards) as Jason-1 data (for better compatibility). GDR data were released in version T during August 2009. During 2012 the whole GDR dataset was reprocessed in GDR-D version. **In this report, GDR-D from cycle 1 to 195 are used (until 27/10/2013)**. A description of the different Jason-2 products is available in the OSTM/Jason-2 Products handbook ([42]).
The purpose of this document is to report the major features of the data quality from the Jason-2 mission. As Jason-2 was in formation flight with Jason-1 (only 55 s apart) until January 2009, this report also uses results from intercalibration with Jason-1.

2.2. CAL/VAL status

2.2.1. List of events

The following table shows the major plannified events during the Jason-2 mission.

Dates	Events	Impacts
4 July 2008 5h57	Start of Jason-2 Cycle 0	
4 July 2008 12h15	Start of Poseidon3 altimeter. Tracking mode : autonomous acquisition, median	Start of level2 product generation.
04 July 2008 13:47:52 to 04 July 2008 14:13:36	Poseidon3 altimeter. Tracking mode : Diode acquisition, median	
04 July 2008 14:14:39 to 17 July 2008 15:30:22	Poseidon3 altimeter. Tracking mode : Diode acquisition, SGT	
8 July 2008 4h45 - 5h25	Poseidon3 altimeter. Dedicated period for validation of tracking mode performances	small data gaps on corresponding passes [Cycle 0]
		.../...

Dates	Events	Impacts
11 July 2008 13h00-13h01 and 13h04-13h12	Poseidon3 altimeter. Tracking mode : Diode-DEM (functional)	Functional test of DIODE-DEM tracking mode while onboard DEM was not correct, leading to wrong waveforms and so impacts on altimeter retracking outputs.
12 July 2008 1h20	Start of Jason-2 Cycle 1	
16 July 2008 7h10-17h08	upload POS3 - DEM	Data gap on corresponding passes [Cycle 1, Pass 108-144]
17 July 2008 7h29-11h30	upload POS3 - DEM	Data gap on corresponding passes [Cycle 1, Pass 108-144]
17 July 2008 15:30:22 to 31 July 2008 21:17:08 UTC	Poseidon3 altimeter. Tracking mode : Diode acquisition, median	
21 July 2008 23h18	Start of Jason-2 Cycle 2	
31 July 2008 21:17:09 to 10 August 2008 19:15:39	Jason-2 Cycle 3: Poseidon3 altimeter. Tracking mode : Diode-DEM	
10 August 2008 19:15:40 to 20 August 2008 17:14:10	Jason-2 Cycle 4: Poseidon3 altimeter. Tracking mode : Diode acquisition, median	
20 August 2008 17:14:11 to 30 August 2008 15:12:43	Jason-2 Cycle 5: Poseidon3 altimeter. Tracking mode : Diode-DEM	
30 August 2008 15:12:43 to 9 September 2008 13:11:15	Jason-2 Cycle 6: Poseidon3 altimeter. Tracking mode : Diode acquisition, median	
9 September 2008 13:11:15 to 19 September 2008 11:09:47	Jason-2 Cycle 7: Poseidon3 altimeter. Tracking mode : Diode-DEM	
19 September 2008 11:09:47 to 29 September 2008 09:08:19	Jason-2 Cycle 8: Poseidon3 altimeter. Tracking mode : Diode acquisition, median	
11 Mai 2009 12:09 to 14 Mai 2009 13:09	Upload POS3 (new DEM)	data gaps (northern hemisphere) for passes 154 to 231
		.../...

Dates	Events	Impacts
2 February 2009 06:55:11 to 15:58:05	software upload to Poseidon-3	data gap between passes 204 and 213
4 June 2009 06:31:27 to 14 June 2008 04:29:59	Jason-2 Cycle 34: Poseidon3 altimeter. Tracking mode : Diode-DEM	
12 February 2010	Upload of Doris V8.0 flight software	improved OGDR orbit accuracy
16 September 2010	Jason-2 Cycle 81: Upload of DEM patch for Gavdos transponder calibration	data gap for passes 087 and 237
17 February 2011	GPSP OBS revert upload	
12-14 September 2012	DORIS OBS upload (DORIS restart on 19th September)	OGDR data gap (during the DORIS restart)
15 May 2013	update on Usingen receiver was done on 15-May-2013 at 11:05Z in order to solve a problem with the TM receiver	

Table 1: *P*lannified events

2.2.2. Missing measurements

This section presents a summary of major satellite or ground segment events that occurred from cycle 0 to 195. Table 2 gives a status about the number of missing passes (or partly missing) for GDRs, as well as the associated events for each cycle.
Up to beginning of 2013, Jason-2 had little missing measurements. In the beginning, they were mainly caused by station acquisition problems. During 2013, three safe hold modes occured. During 2011, there was a telemetry outage at Usingen station leading to approximatly 2h of missing data on 04/04/2011. During 2012, less than 2h of altimetry data were missing due to technical or operator problems. Except these cases, missing measurements are mostly due to scheduled events (like altimeter expert calibrations performed every 6 month or software upload).

During 2013, cycles 165 to 195 were analysed. Jason-2 turned into a first safe hold mode between 2013-03-25 and 2013-03-29 - so that no Jason-2 measurement is available from 2013-03-25 02:42 to 2013-03-29 17:53 (cycle 174) - and into a second safe hold mode between 2013-03-30 and 2013-04-05 so that no Jason-2 measurement was available from 2013-03-30 21:57 to 2013-04-05 14:19 (cycles 174 and 175). After the second SHM, Jason-2 was switched from payload module A to payload module B. Finally Jason-2 entered a third safe hold mode this year, so that there is no measurements between 2013-09-05 at 7:44:17 and 2013-09-12 at 12:25:52.
A problem on Usingen receiver (incomplete TM dumps over Usingen leading to missing data) has also been solved thanks to an update on 15-May-2013 at 11:05, during cycle 179.

The following table gives an overview over missing data and why it is missing.

Jason-2 Cycles/Pass	Dates	Events
000/222-224	10/07/2008 - 18:28:02 to 20:25:04	Missing telemetry (Usingen station pb)
000/232	11/07/2008 - 03:57:08 to 04:30:30	Partly missing due to altimeter calibration (long LPF)
000/235	11/07/2008 - 07:01:28 to 07:27:41	Partly missing due to altimeter calibration (CNG step)
001/44-46	13/07/2008 - 17:40:00 to 19:37:30	Missing telemetry (Usingen station pb)
001/48-50	13/07/2008 - 21:37:02 to 23:30:00	Missing telemetry (NOAA station pb)
001/108-144		several passes partly missing due to upload of new DEM (plannified unavailability)
003/032-035	02/08/2008 - 02:23:45 to 05:46:30	Passes 32 and 35 are partly missing, passes 33 and 34 are completely missing due to missing telemetry (Usingen)
005/236-241	29/08/2008 - 21:44:56 to 30/08/2008 02:52:07	Missing telemetry (Usingen station pb): passes 237 to 240 completely missing, passes 236 and 241 partly missing
006/232	08/09/2008 - 15:48:00 to 16:21:22	pass 232 partially missing due to altimeter calibration (long LPF)
006/235	08/09/2008 - 18:53:00 to 19:19:10	pass 235 partially missing due to altimeter calibration (CNG step)
016/73	10/12/2008 - 15:11:19 to 15:13:27	pass 73 partially missing due to 1) upload of correction for low signal tracking anomaly and 2) memory dumps (planned unavailability)
026/33	18/03/2009 - 05:09:15 to 05:10:44	pass 33 has approximatly 90 seconds of missing ocean measurements in gulf of guinea (probably due to missing telemetry)
029/209-210	23/04/2009 - 20:18:36 to 20:35:11	data gap over land (on transition between passes 209 and 210) due to missing telemetry
031/154-231	11/05/2009 12:09 to 14/05/2009 13:09	Upload of new DEM leading to missing portions (northern hemisphere) for passes 154 to 231
		.../...

Jason-2 Cycles/Pass	Dates	Events
033/204-213	02/06/2009 - 06:55:11 to 15:58:05	Passes 205 to 212 are completely missing. Passes 204 and 213 are partly missing with respectively 100% and 96% of missing measurements over ocean. This is due to software upload to Poseidon-3.
034/232	13/06/2009 - 07:07:03 to 07:40:23	Due to long calibration, pass 232 is partly missing with 65% of missing measurements over ocean.
034/235	13/06/2009 - 10:11:41 to 10:37:50	Due to calibration CNG step, pass 235 is partly missing with 8% of missing measurements over ocean.
037/54	06/07/2009 - 02:33:12 to 02:34:33	pass 054 has a small data gap due to missing PLTM
053/57	11/12/2009 - 20:38:19 to 21:29:43	passes 57 and 58 have a data gap due to Gyro calibration
053/232	18/12/2009 - 16:39 to 17:12	pass 232 has a data gap due to CAL2 calibration
053/235	18/12/2009 - 19:43	pass 235 has a 26 minutes data gap due to CNG calibration (mostly over land)
072/199	23/06/2010 - 19:15:37 to 19:16:59	pass 199 has small data gap due to missing telemetry
073/232	05/07/2010 - 00:09:33 to 00:42:54	pass 232 has a data gap due to CAL2 calibration
073/235	05/07/2010 - 03:14:11 to 03:40:20	pass 235 has a data gap due to CNG calibration (mostly over land)
081/087	16/09/2010 - 16:40:22 to 16:52:48	pass 087 has a data gap due to upload of DEM update (for GAVDOS transponder calibration)
081/237	22/09/2010 - 13:07:27 to 13:18:12	pass 237 has a data gap due to upload of DEM update (for GAVDOS transponder calibration)
084/031	14/10/2010 - 06:02 to 06:11:15	Calibration (I2 and Q2)
084/031-032	14/10/2010 - 06:12 to 06:21:15	Calibration (I and Q)
084/043	14/10/2010 - 17:00:57 to 17:02:39	pass 043 has a small data gap due to missing PLTM
094/231	29/01/2011 - 04:50 to 04:55	Calibration CAL1 (14% of missing ocean data)
094/232	29/01/2011 - 05:38 to 06:11	Calibration CAL2 (65% of missing ocean data)

.../...

Jason-2 Cycles/Pass	Dates	Events
094/235	29/01/2011 - 08:37 to 09:03	Calibration CNG (mostly over land, 9% of missing ocean data)
101/133-135	04/04/2011 - 18:49:08 to 21:03:48	Telemery outage at Usingen, passes 133 to 135 have respectively 23%, 100%, and 91% of missing ocean data
110/158-159	04/07/2011 - 00:27:29 to 01:27:29	Gyro calibration. Passes 158 and 159 have respectively 18% and 88% of missing ocean data
115/232	25/08/2011 - 11:07:35 to 11:40:56	Calibration CAL2: 65% of missing ocean data
115/235	25/08/2011 - 14:12 to 14:38	Calibration CNG: mostly over land, 8% of missing ocean data
132/232	10/02/2012 - 00:42:26 to 01:14:03	Calibration CAL2: 65% of missing ocean data
132/235	10/02/2012 - 03:47:11 to 04:13:20	Calibration CNG: mostly over land, 8% of missing ocean data
135/105	05/03/2012 - 19:54:49 to 20:26:14	technical problem and operator error: 25% of missing ocean data
136/191	19/03/2012 - 02:15:18 to 02:50:11	problem of ACK: 56% of missing ocean data
145/143	14/06/2012 - 11:41:15 to 11:42:58	pass 143 has a small data gap due to missing telemetry
145/248	18/06/2012 - 13:20:10 to 13:21:29	pass 248 has a small data gap
147/022	29/06/2012 - 13:45:30 to 13:49:46	pass 022 has a small data gap due to missing telemetry (8% of missing ocean data)
147/134	03/07/2012 - 22:41:25 to 22:43:58	pass 134 has a small data gap due to operator error (5% of missing ocean data)
154/210	14/09/2012 - 07:45:08 to 07:46:07	pass 210 has a small portion of missing data in central Pacific
156/232	05/10/2012 - 00:07:08 to 00:40:30	Calibration CAL2: 66% of missing ocean data
156/235	05/10/2012 - 03:11:47 to 03:37:57	Calibration CNG: mostly over land, 9% of missing ocean data

.../...

Jason-2 Cycles/Pass	Dates	Events
168/158-159	29/01/2013 - 03:08:20 to 04:02:37	Gyro calibration. Passes 158 and 159 have respectively 14% and 100% of missing ocean data
172/96-97	07/03/2013 - 08:18:37 to 09:30:49	Operator error. Passes 96 and 97 have respectively 72% and 52% of missing ocean data
174/43-161	25/03/2013 - 02:42 to 29/03/2013 17:53	First Safe Hold Mode. Pass 43 has 63% of missing ocean data and passes 44 to 161 are entirely missing
174-191/175-83	30/03/2013 - 21:57 to 05/04/2013 14:49	Second Safe Hold Mode. About cycle 174, pass 191 has 9% of missing ocean data and passes 192 to 254 are entirely missing. About cycle 175, passes 1 to 82 are entirely missing and pass 83 has 90% of missing measurements over ocean.
178/234		Due to a problem with TM receiver, pass 234 is partly missing (north of pacific) and has 10% of missing measurements over ocean
179/ 38		Due to a problem with TM receiver, pass 38 has 6.8% of missing measurements over ocean
182/235	2013-06-19 from 22 :33 :29 to 22 :59 :37	pass 235 has a data gap due to CNG calibration (mostly over land)
190/185 - 191/116	2013-09-05 at 7 :44 :17 to 2013-09-12 at 12 :25 :52	Third Safe Hold Mode. About cycle 190, pass 185 has 10.2% of missing measurements over sea and passes 186 to 254 are entirely missing. About cycle 191, passes 1 to 115 are missing.

Table 2: *M*issing pass status

2.2.3. Edited measurements

Table 3 indicates particular high editing periods (see section 3.2.1.). Most of the occurrences correspond to radiometer wet troposphere correction at default value (due to AMR unavailability) or altimeter low signal tracking anomaly (AGC anomaly), though the latter concerns only few measurements and was corrected during cycle 16 (see section **??**).

Jason-2 Cycles/Passes	Date	Comments
000/89	05/07/08 - 14:22:07 to 14:23:38	Partly edited by several parameters out of threshold (AGC anomaly)
		.../...

Jason-2 Cycles/Passes	Date	Comments
000/134	07/07/08 - 08:06:37 to 08:28:57	Partly edited by several parameters out of threshold (AGC anomaly)
000/156	08/07/08 - 04:35:12 to 05:31:01	rain flag is set (dotted), probably related to start/stop sequence (from 04:45 to 05:24)
000/234	11/07/08 - 05:45:12 to 05:49:03	Partly edited by several parameters out of threshold (AGC anomaly)
000/241	11/07/08 - 13:04:27 to 13:09:11	Partly edited by ice flag (number of elementary Ku-band measurements at 0, AGC=16.88) due to test of altimeter DEM mode
001/		several passes partly edited by several parameters out of threshold (AGC anomaly)
002/		several passes partly edited by several parameters out of threshold (AGC anomaly)
004/		several passes partly edited by several parameters out of threshold (AGC anomaly)
006/		several passes partly edited by several parameters out of threshold (AGC anomaly)
008/		several passes partly edited by several parameters out of threshold (AGC anomaly)
009/		several passes partly edited by several parameters out of threshold (AGC anomaly)
010/		several passes partly edited by several parameters out of threshold (AGC anomaly)
011/		several passes partly edited by several parameters out of threshold (AGC anomaly)
012/		several passes partly edited by several parameters out of threshold (AGC anomaly)
013/		several passes partly edited by several parameters out of threshold (AGC anomaly)
014/		several passes partly edited by several parameters out of threshold (AGC anomaly)
015/		several passes partly edited by several parameters out of threshold (AGC anomaly)
.../...		

Jason-2 Cycles/Passes	Date	Comments
019/024-042	07/01/ 11:00:35 to 08/01/2009 03:23:34	radiometer wet troposphere correction at default value due to AMR unavailability
019/119-161	11/01/ 03:56:38 to 12/01/2009 19:26:14	radiometer wet troposphere correction at default value due to AMR unavailability
110/047	29/09/2011 16:14 to 16:20	a portion of pass 47 is edited by radiometer wet troposphere correction out of threshold or at default values (radio-frequency interference from a ground based source)
168/141-144	28/01/2013 10:50 to 13:22	radiometer wet troposphere correction at default value due to AMR unavailability
169/176-181	08/02/2013 17:37 to 22:44	radiometer wet troposphere correction at default value due to AMR unavailability
174/162-163	29/03/2013 17:53 to 29/03/2013 19:36	radiometer wet troposphere correction at default value after first Safe Hold Mode
175/83-85	05/04/2013 14:18 to 16:27	radiometer wet troposphere correction at default value after second Safe Hold Mode
191/116-125	12/09/2013 12:25:52 to 21:56:39	radiometer wet troposphere correction at default value after third Safe Hold Mode
194/227	16/10/2013 15:02:08 to 15:04:17	a part of pass 227 is rejected near Kamchatka Peninsula because of ice flag (linked to high radiometer minus model wet tropophere difference, and probably related to typhon WIPHA that happened in the region between the 15th and 17th October 2013)

Table 3: *E*dited measurement status

2.3. Models and Standards History

Three versions of the Jason-2 Operational Geophysical Data Records (OGDRs) and Interim Geophysical Data Records (IGDRs) have been generated up to now. These three versions are identified by the version numbers "T" (for test), "c" and "d" in the product filename. For example, version "T" IGDRs are named "JA2_IPN_2PT", version "c" IGDRs are named "JA2_IPN_2Pc", and version "d" IGDRs are named "JA2_IPN_2Pd". All three versions adopt an identical data record format as described in Jason-2 User Handbook ([42]). Versions "T" and "c" differ only sligthly (names of variables are corrected and 3 variables added). Version "T" O/IGDRs were the first version released soon after launch and was disseminated only to OSTST community. Version "c" O/IGDRs were first implemented operationally from data segment 141 of cycle 15 for the OGDRs (3rd December 2008) and cycle 15 for the IGDRs. Version "c" of Jason-2 data is consistent with version "c" of Jason-1 data. Version "d" O/IGDRs were first implemented operationally from data segment 78 of cycle 150 for the OGDRs (31st July 2012) and cycle 150 for the IGDRs. GDR data switched to version "d" from cycle 146 onwards, but previous cycles 1 to 145 were reprocessed in version "d" during 2012. Therefore the whole Jason-2 mission is available in GDR version "d". The tables 4 and 5 below summarize the models and standards that are adopted for versions "T" / "c" and "d" of Jason-2 data. More details on some of these models are provided in Jason-2 User Handbook document ([42]).
Impact of GDR reprocessing can be found in the reprocessing reports [11] and [12].

From cycle 170 to 178, the flag "qual_inst_corr_1hz_sig0_ku" was set to one because of an out of thresholds criterion. From cycle 179 onwards, the flag "qual_inst_corr_1hz_sig0_ku" won't constantly be set as the threshold used to set this flag has been adjusted in the processing chain, in order to take into account the natural instrumental drift.

Model	Product version "T" and "c"
Orbit	Based on Doris onboard navigator solution for OGDRS. DORIS tracking data for IGDRs (DORIS + SLR tracking for cycles 20 to 78) DORIS+SLR+GPS tracking data for GDRs. Using POE-C
Altimeter Retracking	"Ocean" retracking: MLE4 fit from 2nd order Brown model: MLE4 simultaneously retrieves the following 4 parameters from the altimeter waveforms: • Epoch (tracker range offset) → altimeter range • Composite Sigma → SWH • Amplitude → Sigma0 • Trailing Edge slope → Square of mispointing angle

.../...

Model	Product version "T" and "c"
	"Ice" retracking: Geometrical analysis of the altimeter waveforms, which retrieves the following parameters: • Epoch (tracker range offset) → altimeter range • Amplitude → Sigma0
Altimeter Instrument Corrections	Consistent with MLE4 retracking algorithm.
Jason-2 Advanced Microwave Radiometer (AMR) Parameters	Using calibration parameters derived from long term calibration tool developed and operated by NASA/JPL.
Dry Troposphere Range Correction	From ECMWF atmospheric pressures and model for S1 and S2 atmospheric tides
Wet Troposphere Range Correction from Model	From ECMWF model
Ionosphere correction from model	Based on Global Ionosphere TEC Maps from JPL
Sea State Bias Model	Empirical model derived from 3 years of MLE4 Jason-1 altimeter data with version "b" geophysical models.
Mean Sea Surface Model	CLS01
Mean Dynamic Topography Model	MDT_RIO_2005
Geoid	EGM96
Bathymetry Model	DTM2000.1
Inverse Barometer Correction	Computed from ECMWF atmospheric pressures after removing S1 and S2 atmospheric tides
Non-tidal High-frequency De-aliasing Correction	Mog2D high resolution ocean model on I/GDRs. None on OGDRs. Ocean model forced by ECMWF atmospheric pressures after removing S1 and S2 atmospheric tides.
Tide Solution 1	GOT00.2 + S1 ocean tide . S1 load tide ignored
Tide Solution 2	FES2004 + S1 and M4 ocean tides. S1 and M4 load tides ignored
Equilibrium long-period ocean tide model.	From Cartwright and Taylor tidal potential.

.../...

Model	Product version "T" and "c"
Non-equilibrium long-period ocean tide model.	Mm, Mf, Mtm, and Msqm from FES2004
Solid Earth Tide Model	From Cartwright and Taylor tidal potential.
Pole Tide Model	Equilibrium model
Wind Speed from Model	ECMWF model
Altimeter Wind Speed	Wind speed table derived from Jason-1 data (Collard, [30]).

Table 4: *M*odels and standards adopted for the Jason-2 version "T" and "c" products. Adapted from [42]

Model	Product version "d"
Orbit	Based on Doris onboard navigator solution for OGDRS. DORIS tracking data for IGDRs (DORIS + SLR tracking for cycles 20 to 78) DORIS+SLR+GPS tracking data for GDRs. Using POE-D
Altimeter Retracking	"Ocean MLE4" retracking: MLE4 fit from 2nd order Brown analytical model: MLE4 simultaneously retrieves the 4 parameters that can be inverted from the altimeter waveforms: • Epoch (tracker range offset) → altimeter range • Composite Sigma → SWH • Amplitude → Sigma0 • Square of mispointing angle (Ku band only, a null value is used in input of the C band retracking algorithm) "Ocean MLE3" retracking: MLE3 fit from 1st order Brown analytical model: MLE3 simultaneously retrieves the 3 parameters that can be inverted from the altimeter waveforms: • Epoch (tracker range offset) → altimeter range • Composite Sigma → SWH • Amplitude → Sigma0

.../...

Model	Product version "d"
	"Ice" retracking: Geometrical analysis of the altimeter waveforms, which retrieves the following parameters: • Epoch (tracker range offset) → altimeter range • Amplitude → Sigma0
Altimeter Instrument Corrections	Two sets: • on set consistent with MLE4 retracking • on set consistent with MLE3 retracking
Jason-2 Advanced Microwave Radiometer (AMR) Parameters	Using calibration parameters derived from long term calibration tool developed and operated by NASA/JPL.
Dry Troposphere Range Correction	From ECMWF atmospheric pressures and model for S1 and S2 atmospheric tides
Wet Troposphere Range Correction from Model	From ECMWF model
Ionosphere correction from model	Based on Global Ionosphere TEC Maps from JPL
Sea State Bias Model	Two empirical models: • MLE4 version derived from 1 year of MLE4 Jason-2 altimeter data with version "d" geophysical models • MLE3 version derived from 1 year of MLE3 Jason-2 altimeter data with version "d" geophysical models
Mean Sea Surface Model	MSS_CNES_CLS11
Mean Dynamic Topography Model	MDT_CNES-CLS09
Geoid	EGM96
Bathymetry Model	DTM2000.1
Inverse Barometer Correction	Computed from ECMWF atmospheric pressures after removing S1 and S2 atmospheric tides
	.../...

Model	Product version "d"
Non-tidal High-frequency De-aliasing Correction	Mog2D high resolution ocean model on I/GDRs. None on OGDRs. Ocean model forced by ECMWF atmospheric pressures after removing S1 and S2 atmospheric tides.
Tide Solution 1	GOT4.8 + S1 ocean tide. S1 and M4 load tide included.
Tide Solution 2	FES2004 + S1 and M4 ocean tides. S1 and M4 load tides ignored
Equilibrium long-period ocean tide model.	From Cartwright and Taylor tidal potential.
Non-equilibrium long-period ocean tide model.	Mm, Mf, Mtm, and Msqm from FES2004
Solid Earth Tide Model	From Cartwright and Taylor tidal potential.
Pole Tide Model	Equilibrium model
Wind Speed from Model	ECMWF model
Altimeter Wind Speed	Wind speed table derived from Jason-1 data (Collard, [30]). In addition, a calibration bias of 0.32 is applied to JA2 Ku-band sigma0 prior wind speed computation.
Rain flag	Derived from comparisons to thresholds of the radiometer-derived integrated liquid water content and of the difference between the measured and the expected Ku-band backscatter coefficient
Ice flag	Derived from comparison of the model wet tropospheric correction to a dual-frequency wet tropospheric correction retrieved from radiometer brightness temperatures, with a default value issued from a climatology table

Table 5: *M*odels and standards adopted for the Jason-2 version "d" products. Adapted from [42]

The differences between GDR-T and GDR-D products are listed in the table 6.

Model	Product Version "T"	Product Version "D"
Orbit	EIGEN-GL04S with time-varying gravity (annual and semi-annual terms up to deg/ord 50) + ITRF 2005	EIGEN-GRGS_RL02bis_MEAN_FIELD with time-varying gravity (annual, semi-annual, and drifts up to deg/ord 50) + ITRF 2008

.../...

Model	Product Version "T"	Product Version "D"
	DORIS+SLR+GPS	DORIS+SLR+GPS (increased weight for GPS)
Altimeter Retracking	MLE4 + 2nd order Brown model : MLE4 simultaneously retrieves the 4 parameters that can be inverted from the altimeter waveforms: epoch, SWH, Sigma0 and mispointing angle. This algorithm is more robust for large off-nadir angles (up to 0.8°).	Identical to version "T", in addition altimeter parameters are also available for MLE3 retracking
Altimeter Instrument Corrections	Consistent with MLE4 retracking algorithm.	One consistent with MLE4 retracking + One consistent with MLE3 retracking
Jason-2 Microwave Radiometer Parameters	Using calibration parameters derived from long term calibration tool developed and operated by NASA/JPL	Using calibration parameters derived from long term calibration tool developed and operated by NASA/JPL + enhancement in coastal regions + correction of anomaly in 34 GHz channel addition of radiometer rain and ice flag addition of radiometer 18.7 GHz/ 23.8 GHz/ 34 GHz antenna gain weighted land fraction in main beam
Dry Troposphere Range Correction	From ECMWF atmospheric pressures and model for S1 and S2 atmospheric tides.	Identical to version "T"
Wet Troposphere Range Correction from Model	From ECMWF model.	Identical to version "T"
Back up model for Ku-band ionospheric range correction.	Derived from JPL's Global Ionosphere Model (GIM) maps	Identical to version "T"
Sea State Bias Model	Empirical model derived from 3 years of Jason-1 MLE4 altimeter data with version "b" geophysical models	Empirical models derived from Jason-2 data (One consistent with MLE4 retracking + One consistent with MLE3 retracking)

.../...

Model	Product Version "T"	Product Version "D"
Mean Sea Surface Model	CLS01	CNES_CLS_2011
Geoid	EGM96	Identical to version "T"
Bathymetry Model	DTM2000.1	Identical to version "T"
Mean Dynamic Topography	Rio 2005 solution	CNES_CLS2009 solution
Inverse Barometer Correction	Computed from ECMWF atmospheric pressures after removing model for S1 and S2 atmospheric tides.	Identical to version "T"
Non-tidal High-frequency De-aliasing Correction	Mog2D high resolution ocean model. Ocean model forced by ECMWF atmospheric pressures after removing model for S1 and S2 atmospheric tides.	Identical to version "T"
Tide Solution 1	GOT00.2 + S1 ocean tide . S1 load tide ignored.	GOT4.8 (S1 ocean tide and S1 load tide are included).
Tide Solution 2	FES2004 + S1 and M4 ocean tides. S1 and M4 load tides ignored	Identical to version "T"
Equilibrium long-period ocean tide model.	From Cartwright and Taylor tidal potential.	Identical to version "T"
Non-equilibrium long-period ocean tide model.	Mm, Mf, Mtm, and Msqm from FES2004.	Mm, Mf, Mtm, and Msqm from FES2004 + correction for a bug
Solid Earth Tide Model	From Cartwright and Taylor tidal potential.	Identical to version "T"
Pole Tide Model	Equilibrium model.	Equilibrium model + correction of error which was present over lakes and enclosed seas.
Wind Speed from Model	ECMWF model	Identical to version "T"
Altimeter Wind Speed	Table derived from Jason-1 GDR data.	Table is identical to version "T", but the inputs differ.
		.../...

Model	Product Version "T"	Product Version "D"
Altimeter Rain Flag	Set to default values	Derived from Jason-2 sigma naught MLE3 values
Altimeter Ice Flag	Flag based on the comparison of the model wet tropospheric correction and of a radiometer bi frequency wet tropospheric correction (derived from 23.8 GHz and 34.0 GHz), accounting for a backup solution based on climatologic estimates of the latitudinal boundary of the ice shelf, and from altimeter wind speed.	Identical to version "T"
Update of the altimeter characterization file		PRF value is no longer truncated (2058.513239 Hz) Bias of 18.092 cm applied for Ku- and C-band range (corrects the value of the distance between center of gravity and the reference point of the altimeter antenna) Antenna aperture angle (at 3 dB) changed to 1.29 deg MQE setting is applied during 20 Hz to 1 Hz compression Tracker_range_res at a more precise value
other	LTM calculated over 1 day	LTM calculated over 7 days (sliding window) and applied for one day. the origin of the constant part of the time tag bias was found and is directly corrected in the Gdr-D datation.

Table 6: *M*odels and standards adopted for the Jason-2 product version "T", and "D"

3. Data coverage and edited measurements

3.1. Missing measurements

3.1.1. Over land and ocean

Determination of missing measurements relative to the theoretically expected orbit ground pattern is an essential tool to detect missing telemetry or satellite events for instance. Applying the same procedure for Jason-1 and Jason-2, the comparison of the percentage of missing measurements has been performed. Jason-2 can use several onboard tracking modes: Split Gate Tracker (ie the Jason-1 tracking mode, and used for cycle 0 and half of cycle 1), Diode/DEM (used for cycles 3, 5, 7, and 34) and median tracker (used for the other cycles). These different tracking modes are described by [35]. Thanks to the new modes of onboard tracking (median tracker and Diode/DEM), the data coverage over land surface was dramatically increased in comparison with Jason-1 depending on the tracker mode and the period. Figure 1 shows the percentage of missing measurements for Jason-2 and Jason-1 (all surfaces) computed with respect to a theoretical possible number of measurements. Due to differences between altimeter tracking algorithms, the number of available data is greater for Jason-2 than for Jason-1. Differences appear on land surfaces as shown in figure 2. The missing data are highly correlated with the mountains location. The monitoring shows a slight annual signal. The slight increase of Jason-2 missing measurements end of 2008 (during cycle 16) is related to the correction of the low signal tracking anomaly (see section **??**). During 2013, Jason-2 entered safe hold mode twice in March (from 25/03/2013 to 29/03/2013 and from 30/03/2013 until 05/04/2013, during cycles 174 and 175) and a third time in September (from 05/09/2013 to 12/09/2013, during cycles 190-191).

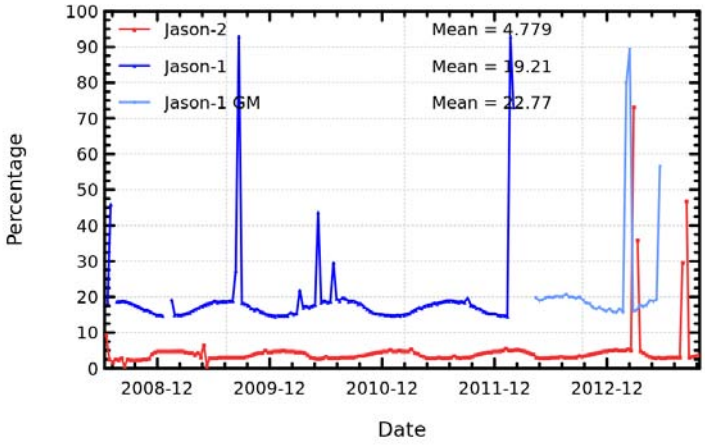

Figure 1: *Percentage of missing measurements over ocean and land for JA2 and JA1*

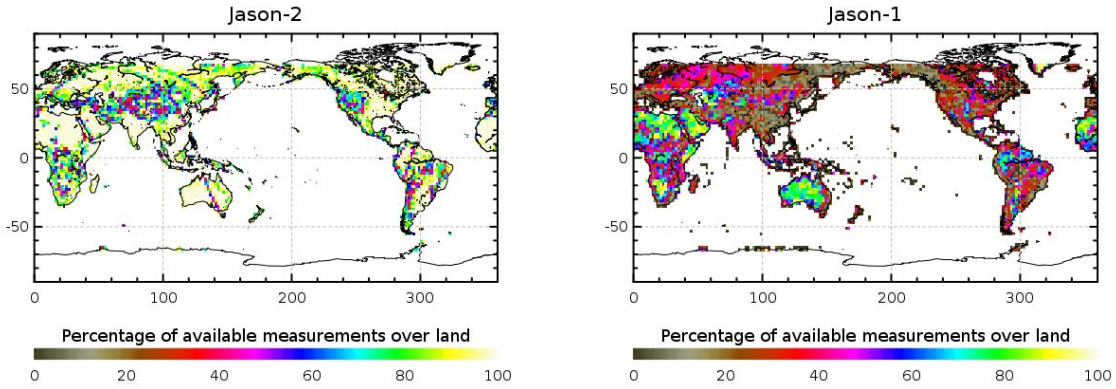

Figure 2: *Map of percentage of available measurements over land for Jason-2 on cycle 154 (left) and for Jason-1 on cycle 511 (right)*

3.1.2. Over ocean

When considering ocean surface, the same analysis method leads also to an improvement of Jason-2 data coverage, as plotted on the top left figure 3. It represents the percentage of missing measurements relative to the theory, when limited to ocean surfaces. The mean value is about 1.0% for Jason-2, 4.6% for Jason-1 on its repeat ground-track and 7.7% for Jason-1 on its geodetic ground-track. Note that since Jason-1 is on a geodetic ground-track, it is roughly once per month during about 2 h in INIT mode (no science data), due to Jason-2 overflight. Even if already very low, this figure of missing measurements is not significant due to several events where the measurements are missing. All these events are described on table 2.
On figure 3 on the top right, the percentage of missing measurements is plotted without taking into account the cycles where instrumental events or other big anomalies occurred. The mean value of missing measurements lowers down to 0.03% for Jason-2 and 1.9% (2.4%) for Jason-1 (Jason-1 geodetic). These additional Jason-1 missing measurements are mainly located over sea ice and near the coasts and are related to the altimeter tracking method. Indeed, selecting latitudes lower than 50° and bathymetry area lower than -1000m (see bottom of figure 3), the Jason-1 percentage becomes very weak (close to 0.02%) which represents less than 100 missing measurements per cycle over open ocean. For Jason-2, the same statistic is smaller with around 0.007% of missing measurements over open oean. This weak percentage of missing measurements is mainly explained by the rain cells and sigma0 blooms. These sea states can disturb significantly the Ku band waveform shape leading to an altimeter lost of tracking.

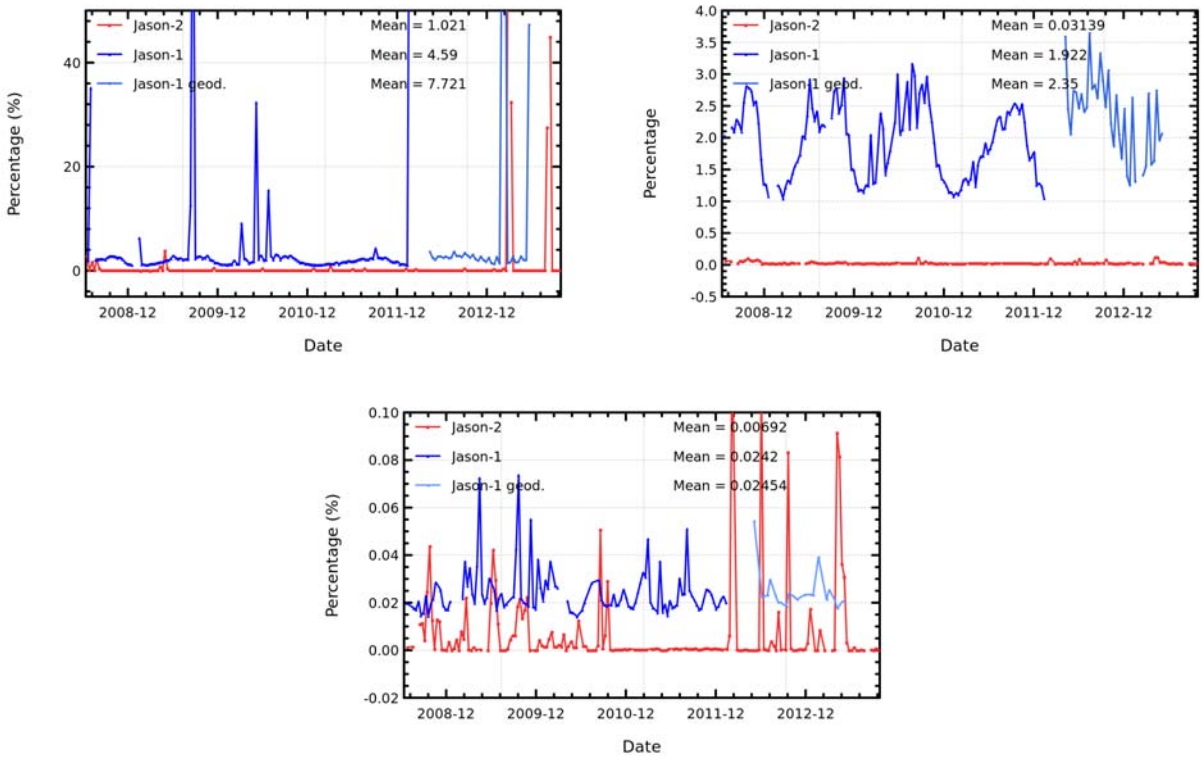

Figure 3: *Cycle per cycle percentage of missing measurements over ocean (top left), without anomalies (top right), without anomalies and with geographical selections (bottom).*

3.2. Edited measurements

3.2.1. Editing criteria definition

Editing criteria are used to select valid measurements over ocean. The editing process is divided into 4 parts. First, only measurements over ocean and lakes are kept (see section 3.2.2.). Second, some flags are used as described in section 3.2.3.. Note that though the altimeter rain flag is now available in the current release of GDR (D), it is not used hereafter in the editing procedure. But measurements corrupted by rain are well detected by other altimeter parameter criteria. Then, threshold criteria are applied on altimeter, radiometer and geophysical parameters and are described in the table 7. Except for the dual frequency ionosphere correction, only Ku-band measurements are used in this editing procedure, as they mainly represent the end user dataset. Moreover, a spline criterion is applied to remove the remaining spurious data. For each criterion, the cycle per cycle percentage of edited measurements has been monitored. This allows detection of anomalies in the number of removed data, which could come from instrumental, geophysical or algorithmic changes.

Parameter	Min thresholds	Max thresholds	mean edited
Sea surface height	$-130\,m$	$100\,m$	0.77%
Sea level anomaly	$-10\,m$	$10.0\,m$	1.07%
Number measurements of range	10	*Not applicable*	1.04%
Standard deviation of range	0	$0.2\,m$	1.40%
Squared off-nadir angle	$-0.2\,deg^2$	$0.64\,deg^2$	0.59%
Dry troposphere correction	$-2.5\,m$	$-1.9\,m$	0.00%
Inverted barometer correction	$-2.0\,m$	$2.0\,m$	0.00%
AMR wet troposphere correction	$-0.5m$	$-0.001\,m$	0.26%
Ionosphere correction	$-0.4\,m$	$0.04\,m$	1.18%
Significant wave height	$0.0\,m$	$11.0\,m$	0.65%
Sea State Bias	$-0.5\,m$	$0.0\,m$	0.62%
Number measurements of Ku-band Sigma0	10	*Not applicable*	1.03%
Standard deviation of Ku-band Sigma0	0	$1.0\,dB$	1.94%
Ku-band Sigma0 [1]	$7.0\,dB$	$30.0\,dB$	0.60%
Ocean tide	$-5.0\,m$	$5.0\,m$	0.01%
Equilibrium tide	$-0.5\,m$	$0.5\,m$	0.00%
Earth tide	$-1.0\,m$	$1.0\,m$	0.00%
Pole tide	$-15.0\,m$	$15.0\,m$	0.00%
Altimeter wind speed	$0\,m.s^{-1}$	$30.0\,m.s^{-1}$	1.02%
All together	-	-	3.29%

Table 7: *E*diting criteria

3.2.2. Selection of measurements over ocean and lakes

In order to remove data over land, a land-water mask is used. Only measurements over ocean or lakes are kept. This allows to keep data near the coasts and so to detect potential anomalies in these areas. Furthermore, there is no impact on global performance estimations since the most significant results are derived from analyzes in deep ocean areas. Figure 4 shows the cycle per

[1] The thresholds used for the Ku-band Sigma0 are the same than for Jason-1 and T/P, but the same sigma0 bias as between Jason-1 and T/P (about 2.4 dB) is applied.

cycle percentage of measurements eliminated by this selection. The signal shows mainly a seasonal cycle, due to changing properties of land reflection. But it also reveals the impact of the different altimeter tracking modes: SGT (split gate tracking), Median and DIODE/DEM (digital elevation model). SGT mode, the nominal mode for Jason-1, was used for Jason-2 during cycle 0 and half of cycle 1. This mode does not perform very well over land (as also depicted on right side of figure 2), therefore a comparable small percentage of measurements are edited over land for cycle 1 (approximately 24%). Most of Jason-2 cycles (cycles 2, 4, 6, 8 to 33, and onwards from cycle 35) were operated in Median mode (also used by Envisat). This mode is more adapted for tracking over land than SGT and provides therefore more measurements over land (as also seen on left side of figure 2) and so more measurements are edited (between 25.5% and 27% depending on season) due to the ocean/land criteria. A new tracking mode, DEM, was used during cycles 3, 5, 7, and 34. It has been designed to provide more data over inland water surfaces and coastal areas. It provides a continuous data set over land but some are not meaningful (in areas where the DEM is not accurate enough like in the major mountains). Therefore during these cycles, almost 29% of measurements are removed by the selection. Since 10th of December, 2008 the onbord altimeter configuration was modified to correct for the low signal tracking anomaly, which led to a more strict control of acquisition gain loop (to avoid the tracking of low signal anomalies). This explains the quite steep decrease of land measurements edited around cycle 16 (section **??**).

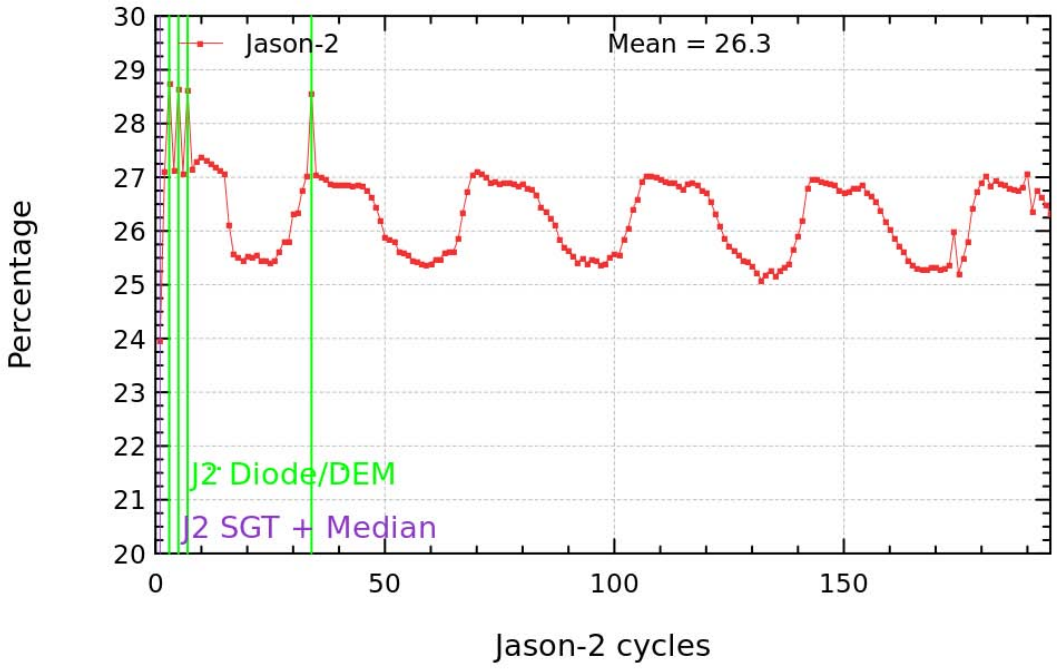

Figure 4: *Cycle per cycle percentage of eliminated measurements during selection of ocean/lake measurements.*

3.2.3. Flagging quality criteria: Ice flag

The ice flag is used to remove the sea ice data. Figure 5 shows the cycle per cycle percentage of measurements edited by this criterion. Over the shown period, no anomalous trend is detected (figure 5 left) but the nominal annual cycle is visible. Indeed, the maximum number of points over ice is reached during the southern winter (ie. July - September). As Jason-2 takes measurements between 66° north and south, it does not detect thawing of sea ice (due to global warming), which takes place especially in northern hemisphere over 66°N. The percentage of measurements edited by ice flag is plotted in the right of figure 5 for a period of 1 year.

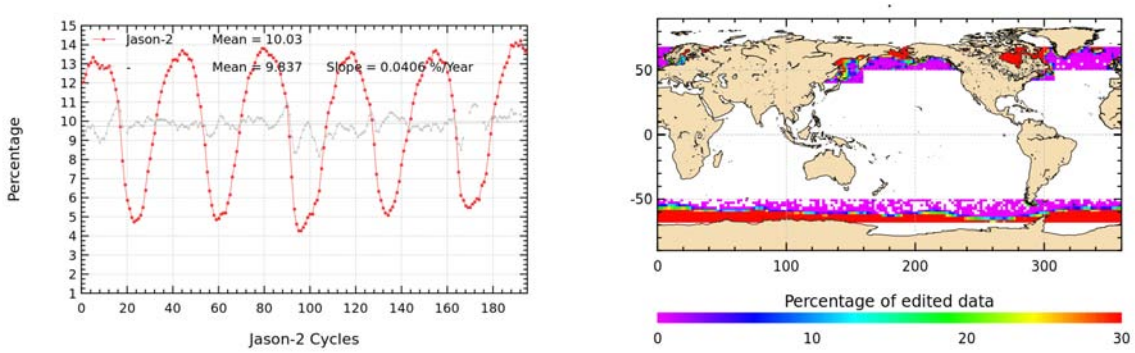

Figure 5: *Percentage of edited measurements by ice flag criterion. Left: Cycle per cycle monitoring. The gray curve shows the trend of edited measurements after adjusting for annual and semi-annual signals. Right: Map over a one year period (cycles 159 to 195).*

3.2.4. Flagging quality criteria: Rain flag

Though the altimeter rain flag is now present in GDR-D release, it is not used hereafter during the editing procedure. The percentage of rain edited measurements is plotted in figure 6 over cycles 159 to 195 (covering 12 months). It shows that measurements are especially edited near coasts, but also in the equatorial zone and open ocean. The altimeter rain flag seems to be slightly too strict, using it would lead to edit 6.7% of additional measurements.

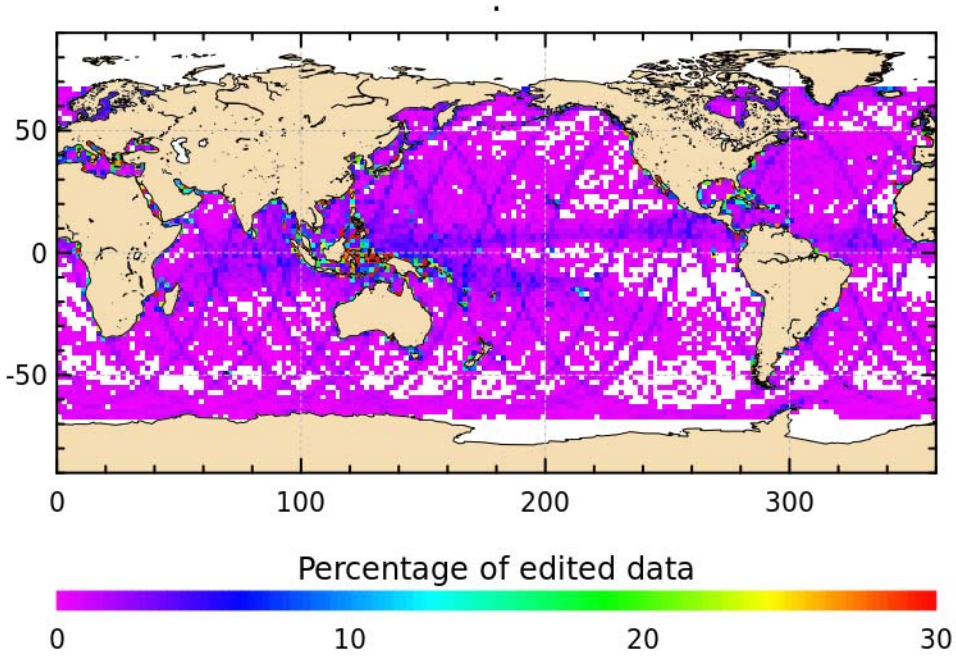

Figure 6: *Percentage of edited measurements by altimeter rain flag criterion. Map over a one year period (cycles 159 to 195).*

3.2.5. Threshold criteria: Global

Instrumental parameters have also been analyzed from comparison with thresholds, after having selected only ocean/lakes measurements and applied flagging quality criteria (ice flag). Therefore measurements appear not as edited by thresholds, when they were already edited by land or sea ice flag. Note that no measurement is edited by the following corrections : dry troposphere correction, inverted barometer correction (including DAC), equilibrium tide, earth and pole tide. Indeed these parameters are only verified in order to detect data at default values, which might happen during a processing anomaly.
The percentage of measurements edited using each criterion is monitored on a cycle per cycle basis (figure 7). The mean percentage of edited measurements is about 3.3%. A small annual cycle is visible. The high percentage of edited measurements of cycles 019, 168 and 169 are explained by an AMR anomaly, which resulted in defaulted radiometer values during several passes. Concerning cycles 174 and 191, it is explained by the time lag between the altimeter restart and the radiometer restart after safe hold modes.

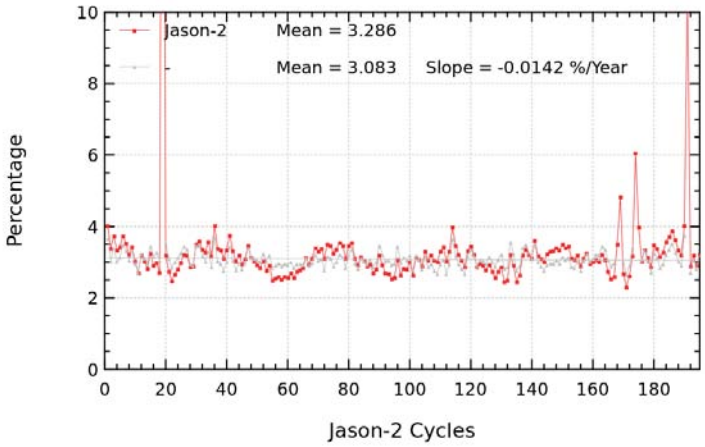

Figure 7: *Cycle per cycle percentage of edited measurements by threshold criteria. The gray curve shows the trend of edited measurements after adjusting for annual and semi-annual signals.*

3.2.6. Threshold criteria: 20-Hz measurements number

The percentage of edited measurements because of a too low number of 20-Hz measurements is represented on left side of figure 8. No trend neither any anomaly has been detected.
The map of measurements edited by 20-Hz measurements number criterion is plotted on right side of figure 8 and shows correlation with heavy rain and wet areas (in general regions with disturbed sea state). Indeed waveforms are distorted by rain cells, which makes them often meaningless for SSH calculation. As a consequence, edited measurements due to several altimetric criteria are often correlated with wet areas.

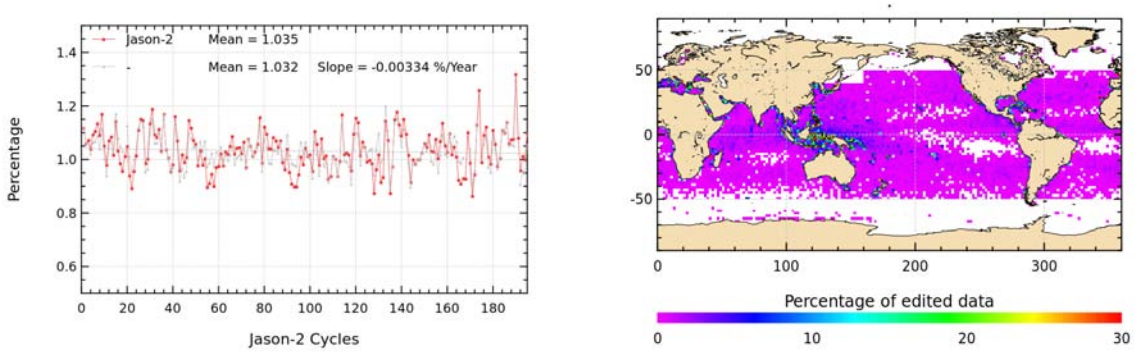

Figure 8: *Percentage of edited measurements by 20-Hz measurements number criterion. Left: Cycle per cycle monitoring. The gray curve shows the trend of edited measurements after adjusting for annual and semi-annual signals. Right: Map over a one year period (cycles 159 to 195).*

3.2.7. Threshold criteria: 20-Hz measurements standard deviation

The percentage of edited measurements due to 20-Hz measurements standard deviation criterion is shown in figure 9 (left). During cycle 1, slightly more measurements are edited by 20-Hz measurements standard deviation criterion than during other cycles. This is likely due to low signal tracking anomaly which impacted especially this cycle. The right side of figure 9 shows a map of measurements edited by the 20-Hz measurements standard deviation criterion. As in section 3.2.6., edited measurements are correlated with wet areas.

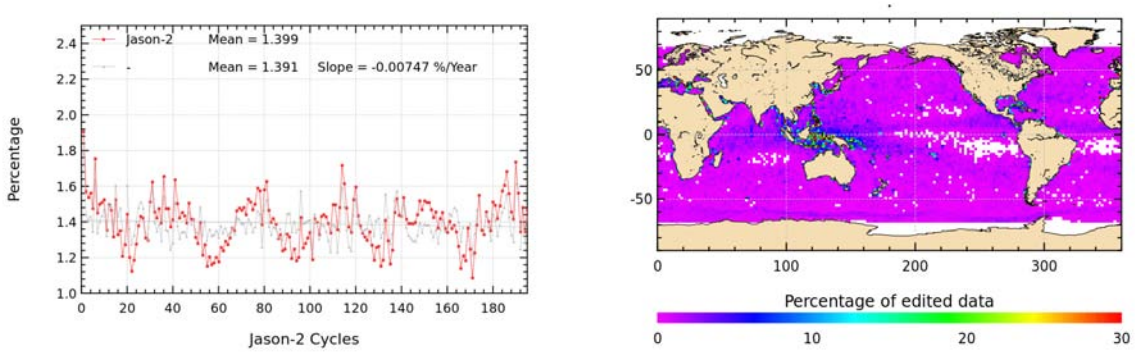

Figure 9: *Percentage of edited measurements by 20-Hz measurements standard deviation criterion. Left: Cycle per cycle monitoring. The gray curve shows the trend of edited measurements after adjusting for annual and semi-annual signals. Right: Map over a one year period (cycles 159 to 195).*

3.2.8. Threshold criteria: Significant wave height

The percentage of edited measurements due to significant wave height criterion is represented in figure 10. It is about 0.65%. In the beginning of the mission, the curve of measurements edited by SWH threshold criterion is quite irregular, as low signal tracking anomalies occurred during SGT and Median tracking modes, whereas there are no low signal tracking anomalies during DEM tracking modes (cycles 3, 5, and 7). Indeed during periods of low signal tracking anomaly, parameters like significant wave height, backscattering coefficient and squared off-nadir angle from waveforms are out of thresholds and therefore edited (see section **??**). Figure 10 (right part) shows that measurements edited by SWH criterion are especially found near coasts in the equatorial regions and in the Mediterranean Sea.

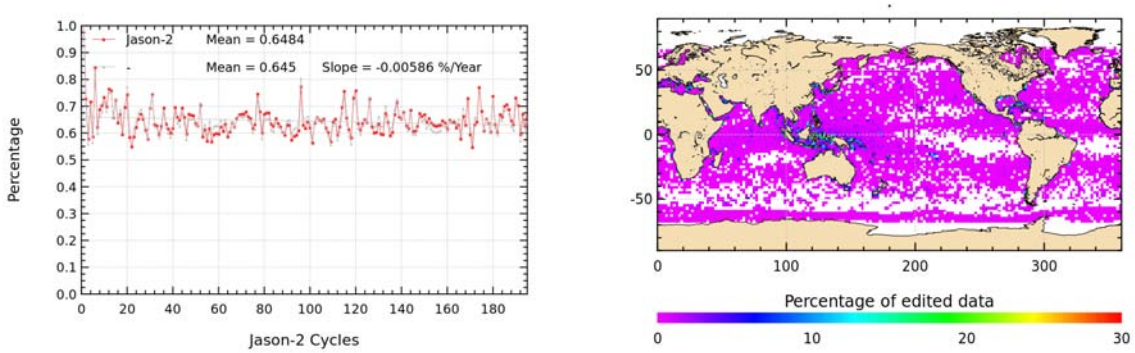

Figure 10: *Percentage of edited measurements by SWH criterion. Left: Cycle per cycle monitoring. The gray curve shows the trend of edited measurements after adjusting for annual and semi-annual signals. Right: Map over a one year period (cycles 159 to 195).*

3.2.9. Backscatter coefficient

The percentage of edited measurements due to backscatter coefficient criterion is represented in figure 11. It is about 0.60% It is also impacted by low signal tracking anomalies, especially during cycle 1. The right part of figure 11 shows that measurements edited by backscatter coefficient criterion are especially found near coasts in the equatorial regions and enclosed sea (Mediterranean).

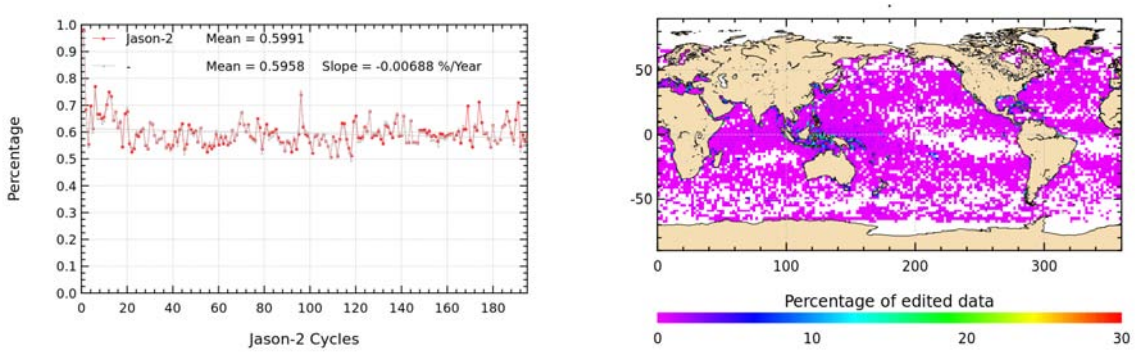

Figure 11: *Percentage of edited measurements by Sigma0 criterion. Left: Cycle per cycle monitoring. The gray curve shows the trend of edited measurements after adjusting for annual and semi-annual signals. Right: Map over a one year period (cycles 159 to 195).*

3.2.10. Backscatter coefficient: 20 Hz standard deviation

The percentage of edited measurements due to 20 Hz backscatter coefficient standard deviation criterion is represented in figure 12. It is about 1.9%. The right part of figure 11 shows that measurements edited by 20 Hz backscatter coefficient standard deviation criterion are especially found in regions with disturbed waveforms.

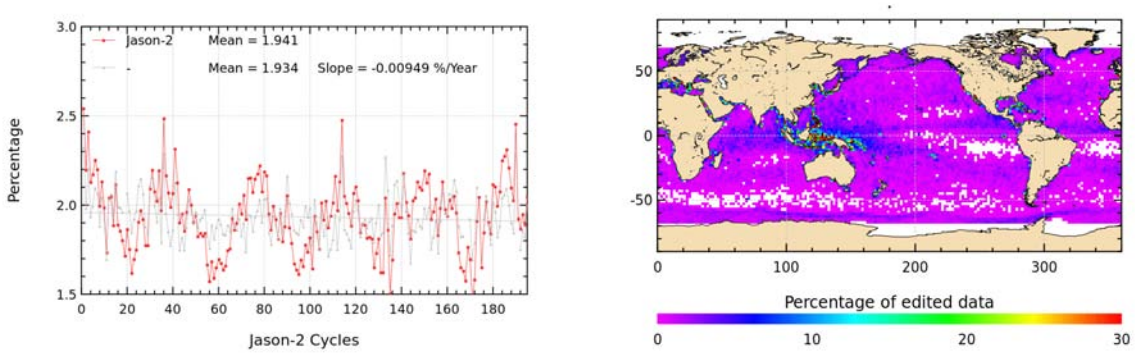

Figure 12: *Percentage of edited measurements by 20 Hz Sigma0 standard deviation criterion. Left: Cycle per cycle monitoring. The gray curve shows the trend of edited measurements after adjusting for annual and semi-annual signals. Right: Map over a one year period (cycles 159 to 195).*

3.2.11. Radiometer wet troposphere correction

The percentage of edited measurements due to radiometer wet troposphere correction criterion is represented in figure 13. It is about 0.3%. When removing cycles which experienced problems, percentage of edited measurements drops to about 0.1%. For somme cycles the percentage of edited measurements is higher than usual. This is linked to radiometer wet troposphere correction at default value due to AMR unavailability in case of cycle 19, AMR reset in case of cycles 168 and 169, and gap between altimeter restart and radiometer restart after safe hold modes in case of cycles 174, 175 and 191.

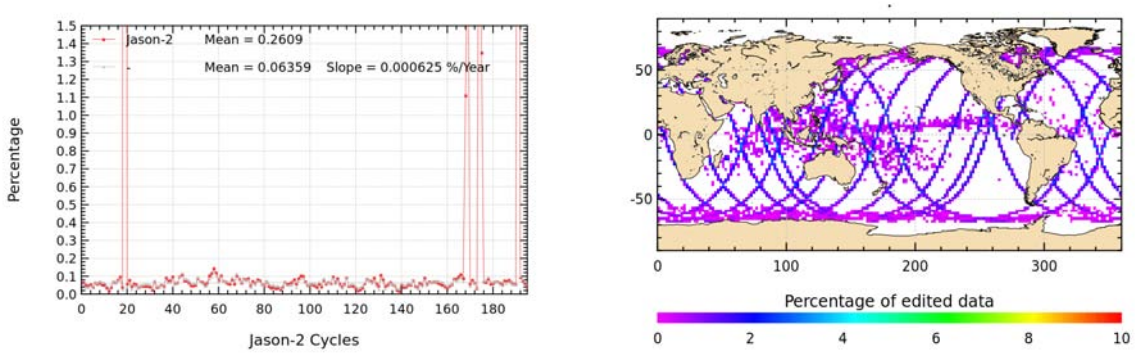

Figure 13: *Percentage of edited measurements by radiometer wet troposphere criterion. Left: Cycle per cycle monitoring. The gray curve shows the trend of edited measurements after adjusting for annual and semi-annual signals. Right: Map over a one year period (cycles 159 to 195).*

3.2.12. Dual frequency ionosphere correction

The percentage of edited measurements due to dual frequency ionosphere correction criterion is represented in figure 14. It is about 1.2% and shows no drift. The map 14 shows that measurements edited by dual frequency ionosphere correction are mostly found in equatorial regions, but also near sea ice.

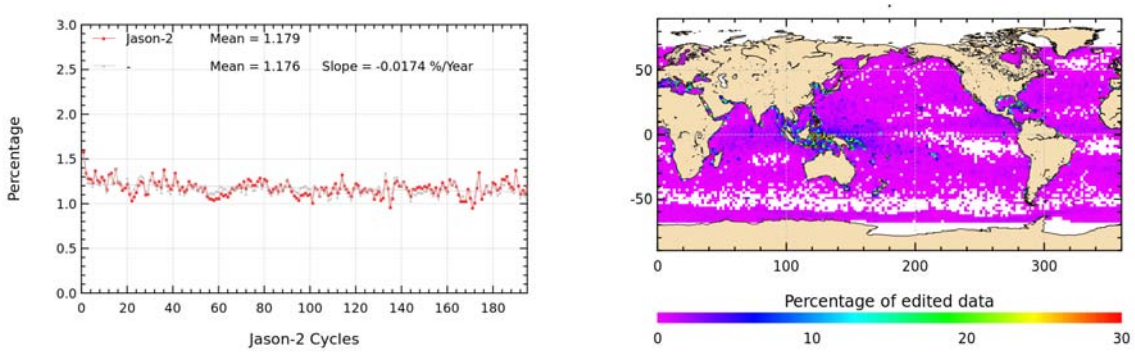

Figure 14: *Percentage of edited measurements by dual frequency ionosphere criterion. Left: Cycle per cycle monitoring. The gray curve shows the trend of edited measurements after adjusting for annual and semi-annual signals. Right: Map over a one year period (cycles 159 to 195).*

3.2.13. Square off-nadir angle

The percentage of edited measurements due to square off-nadir angle criterion is represented in figure 15. It is about 0.6%. As for other parameters, impact of low signal tracking anomalies is visible in general for the first 16 cycles and especially for cycle 1. The map 15 shows that edited measurements are mostly found in coastal regions and regions with disturbed waveforms.

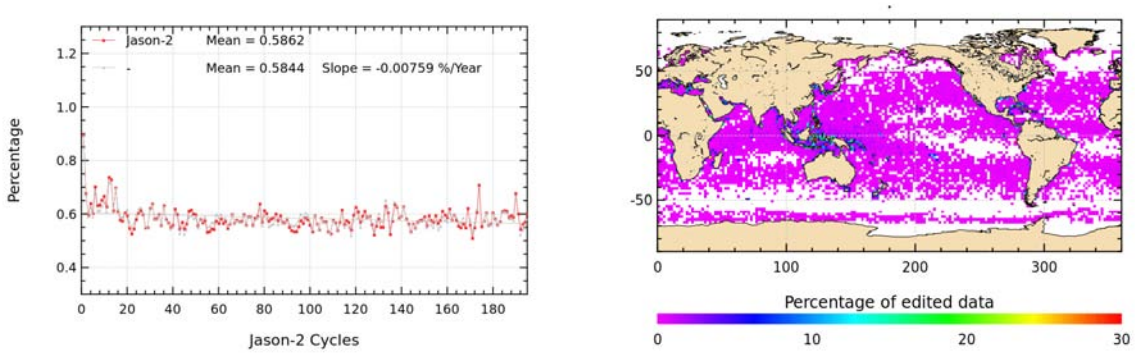

Figure 15: *Percentage of edited measurements by square off-nadir angle criterion. Left: Cycle per cycle monitoring. The gray curve shows the trend of edited measurements after adjusting for annual and semi-annual signals. Right: Map over a one year period (cycles 159 to 195).*

3.2.14. Sea state bias correction

The percentage of edited measurements due to sea state bias correction criterion is represented in figure 16. The percentage of edited measurements is about 0.6% and shows no drift.
The map 16 shows that edited measurements are mostly found in equatorial regions near coasts.

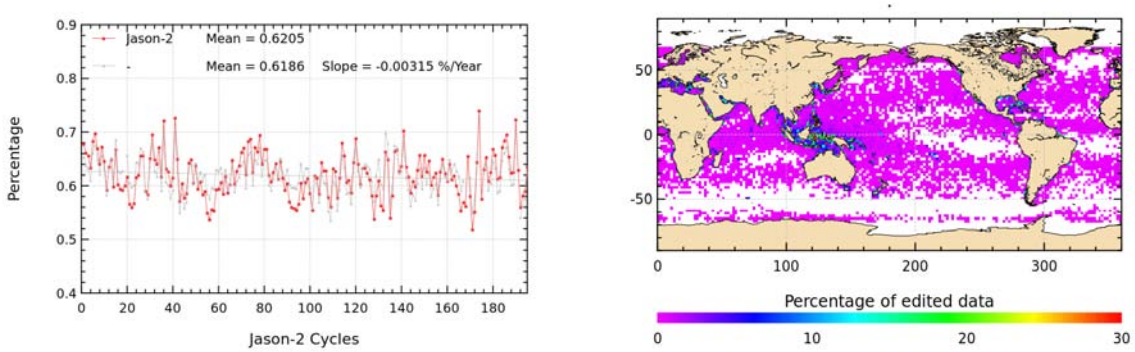

Figure 16: *Cycle per cycle percentage of edited measurements by sea state bias criterion (left). The gray curve shows the trend of edited measurements after adjusting for annual and semi-annual signals. Right: Map of percentage of edited measurements by sea state bias criterion over a one year period (cycles 159 to 195).*

3.2.15. Altimeter wind speed

The percentage of edited measurements due to altimeter wind speed criterion is represented in figure 17. It is about 1.0%. The measurements are edited, because they have default values. This is the case when sigma0 itself is at default value, or when it shows very high values (higher than 25 dB), which occur during sigma bloom and also over sea ice. Indeed, the wind speed algorithm (which uses backscattering coefficient and significant wave height) can not retrieve values for sigma0 higher than 25 dB.
Wind speed is also edited, when it has negative values, which can occur in GDR products. Nevertheless, sea state bias is available even for negative wind speed values. Therefore, the percentage of edited altimeter wind speed is higher than that of edited sea state bias.

The map 17 showing percentage of measurements edited by altimeter wind speed criterion is correlated with maps 16 and 10.

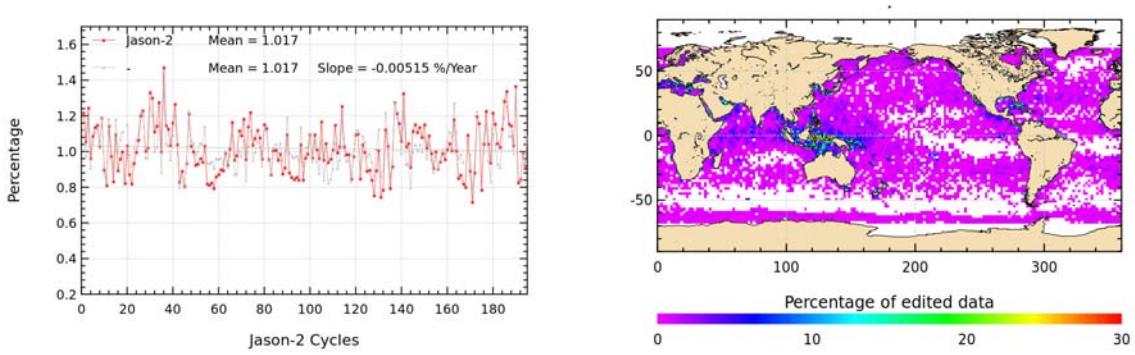

Figure 17: *Percentage of edited measurements by altimeter wind speed criterion. Left: Cycle per cycle monitoring.The gray curve shows the trend of edited measurements after adjusting for annual and semi-annual signals. Right: Map over a one year period (cycles 159 to 195).*

3.2.16. Ocean tide correction

The percentage of edited measurements due to ocean tide correction criterion is represented in figure 18. It is less than 0.01% and is very stable. The ocean tide correction is a model output, there should therefore be no edited measurements. Indeed there are no measurements edited in open ocean areas, but only very few near coasts (Alaska, Kamchatka, Labrador). These measurements are mostly at default values. The percentage of measurement increases for cycle 174 and 175 (2013 safe hold mode).

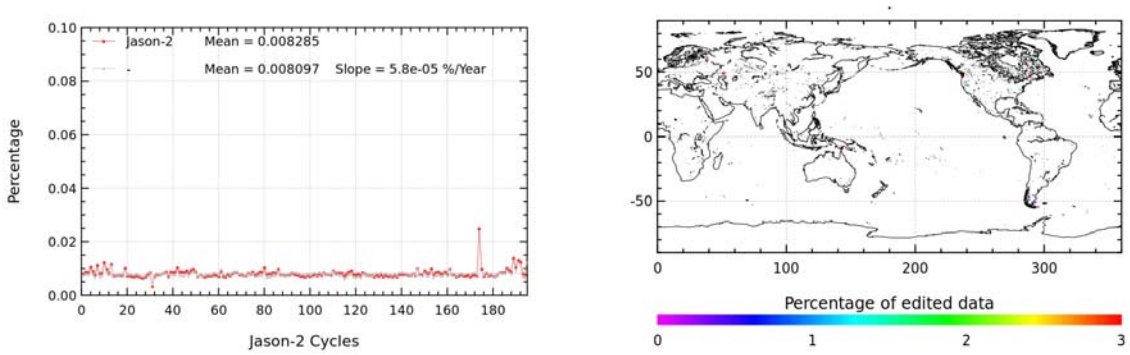

Figure 18: *Percentage of edited measurements by ocean tide criterion. Left: Cycle per cycle monitoring. The gray curve shows the trend of edited measurements after adjusting for annual and semi-annual signals. Right: Map over a one year period (cycles 159 to 195).*

3.2.17. Sea surface height

The percentage of edited measurements due to sea surface height (orbit - ku-band range) criterion is represented in figure 19. It is about 0.77% and shows no drift. The measurements edited by sea surface height criterion are mostly found near coasts in equatorial regions (see map 19). The majority of the edited measurements has defaulted range values.

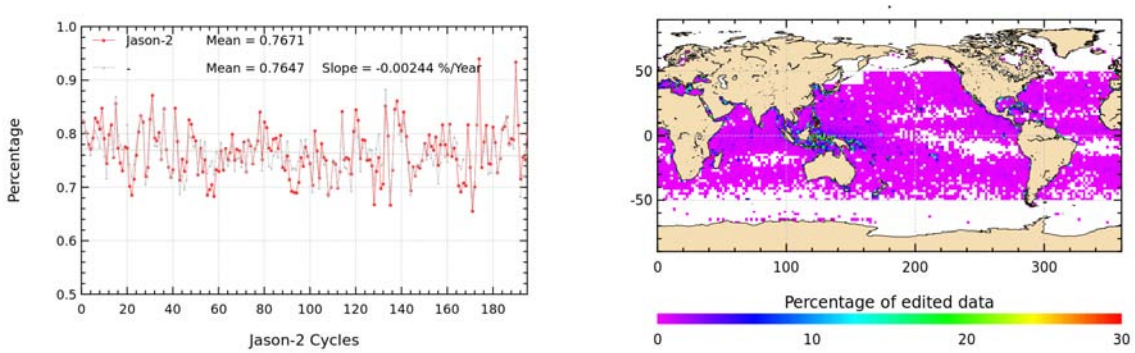

Figure 19: *Percentage of edited measurements by sea surface height criterion. Left: Cycle per cycle monitoring. The gray curve shows the trend of edited measurements after adjusting for annual and semi-annual signals. Right: Map over a one year period (cycles 159 to 195).*

3.2.18. Sea level anomaly

The percentage of edited measurements due to sea level anomaly criterion is represented in figure 20. It is about 1.1% (0.9% without cycles 19,168,169,174,175,191) and shows no drift. The peaks are related to AMR unavailabilities (see figure 13 (showing the percentage of measurements edited by AMR)), as the SLA clip contains, among other parameters, the radiometer wet troposphere correction.
Whereas the map in figure 20 allows us to plot the measurements edited due to sea level anomaly out of thresholds (after applying all other threshold criteria). There are only very few measurements, principally located in Caspian Sea.

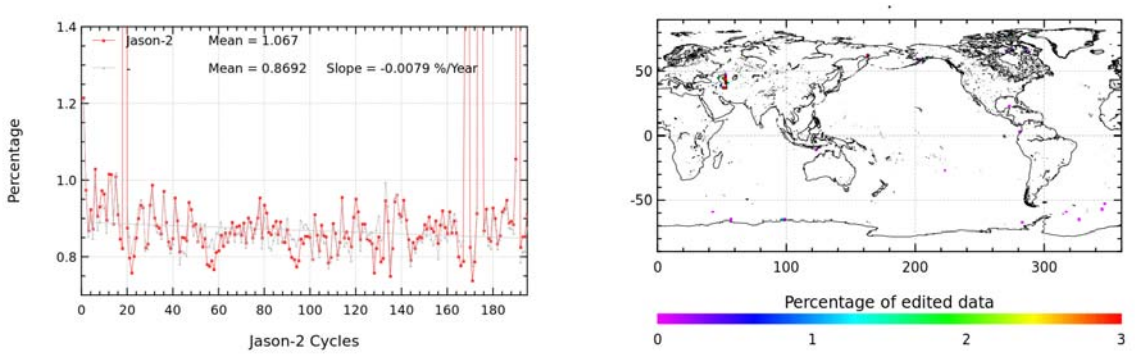

Figure 20: *Percentage of edited measurements by sea level anomaly criterion. Left: Cycle per cycle monitoring. The gray curve shows the trend of edited measurements after adjusting for annual and semi-annual signals. Right: Map over a one year period (cycles 159 to 195).*

4. Monitoring of altimeter and radiometer parameters

4.1. Methodology

Both mean and standard deviation of the main parameters of Jason-2 (GDR-D) have been monitored since the beginning of the mission. Moreover, a comparison with Jason-1 parameters has been performed: it allows us to monitor the bias between the parameters of the 2 missions. Two different methods have been used to compute the bias:

- Till Jason-2 cycle 20, Jason-2 and Jason-1 are on the same ground track and are spaced out about 1 minute apart. The mean of the Jason-1 - Jason-2 differences can be computed using a point by point repeat track analysis.
- From Jason-2 cycle 21 (Jason-1 cycle 260), a maneuver sequence was conducted (from 26th of January to 14th of February 2009) to move Jason-1 to the new tandem mission orbit. Jason-1 has a repeat ground-track which is interleaved with Jason-2. It is the same ground-track as already used by Topex/Poseidon during its tandem phase with Jason-1, but there is a time shift of 5 days. Geographical variations are then too strong to directly compare Jason-2 and Jason-1 parameters on a point by point basis. Therefore day per day global differences have been carried out to monitor differences between the two missions. A filter over 11 days was applied. Nevertheless the differences are still quite noisy, especially for corrections which vary rapidly in time and space. Therefore occasional small jumps might be covered by the noise of the differences. Nevertheless it should be possible to detect drifts and permanent jumps. Jason-2 and Jason-1 were in this tandem phase from Jason-2 cycles 22 to 135 (Jason-1 cycles 262 to 374).

In February and March of 2012, Jason-1 experienced severals safe holds (anomaly on gyro3, double EDAC error in RAM memory). It was decided to move Jason-1 to a geodetic orbit (more about the Jason-1 geodetic mission can be found in [7]). Science data on the geodetic orbit are available from 7th of May 2012 onwards. Note that the first cycle on the geodetic orbit starts with cycle 500 (this corresponds to end of Jason-2 cycle 141). The last (incomplete) cycle of Jason-1 on the repeat ground-track was cycle 374. As during the tandem phase, day per day global differences of the parameters have been carried out to monitor differences between the two missions.
finally, after loss of telemetry on 21 June 2013 (during cycle 537), Jason-1 was passivated and decommissioned on 01 July 2013, with the last command sent at 16:37:40 UTC.

Note that differences are done over Jason-2 cycles 1 to 183, corresponding to Jason-1 cycles 240 to 537.

4.2. 20 Hz Measurements

The monitoring of the number and standard deviation of 20 Hz elementary range measurements used to derive 1 Hz data is presented here. These two parameters are computed during the altimeter ground processing. For both Jason-1 and Jason-2, before performing a regression to derive the 1 Hz range from 20 Hz data, a MQE (mean quadratic error) criterion is used to select valid 20 Hz measurements. This first step of selection consists in verifying that the 20 Hz waveforms can be approximated by a Brown echo model (Brown, 1977 [23]) (Thibaut et al. 2002 [61]). Then, through an iterative regression process, elementary ranges too far from the regression line are dis-

carded until convergence is reached. Thus, monitoring the number of 20 Hz range measurements and the standard deviation computed among them is likely to reveal changes at instrumental level. The Jason-1 MQE threshold are not applicable to Jason-2, using those thresholds would edit more measurements than necessary. Therefore, for the first GDR release of Jason-2 (GDR-T), the MQE threshold had been set to default, leading to no editing based on MQE values. Note that for Jason-2 data in version GDR-D, specific Jason-2 MQE thresholds were computed and are applied.

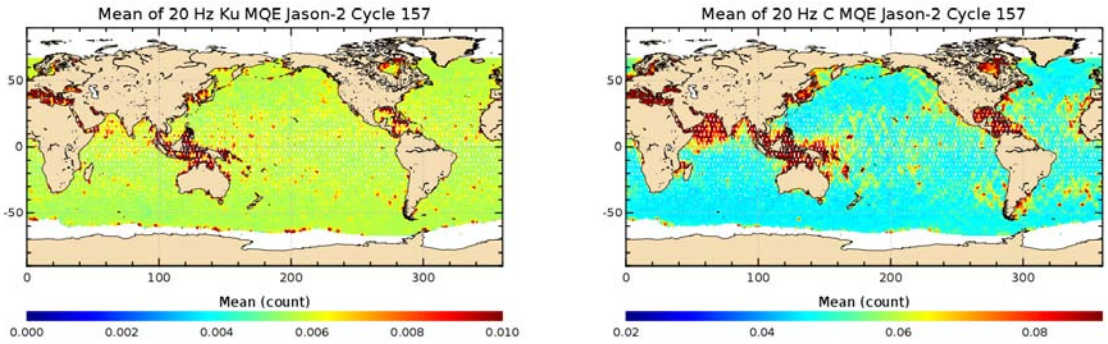

Figure 21: *Map of 20 Hz Ku-band (left) and C-band (right) MQE for Jason-2 cycle 157. Note that the color scales are different for the two maps.*

4.2.1. 20 Hz measurements number in Ku-Band and C-Band

GDR-D Jason-2 number of elementary 20 Hz range mesurements is very similar to Jason-1's (especially for C-band) with an average of 19.61 for Ku-band and 19.25 for C-band as shown on figure 22. For both satellites a slight annual signal is visible (especially for C-band). Figures 23 and 24 show on the left the daily monitoring of the mean and standard deviation of Jason-1 - Jason-2 differences of 20-Hz measurements number in Ku-Band and C-band during the formation flight phase. Besides a slight variation, they are quite stable and do not show any anomaly. Number of 20 Hz Ku-band range measurements is slightly higher for Jason-2 than for Jason-1, since mean of Jason-1 - Jason-2 difference is slightly negatif (-0.07 for Ku-band), whereas the difference for C-band is close to zero. The regions where Jason-1 has less elementary Ku-band range measurements are especially located around Indonesia, as shown on map of Jason-1 - Jason-2 differences (right side of figures 23). Indeed in regions of sigma bloom or rain, using a MQE criterion during the regression to derive 1Hz from 20Hz data, discards 20 Hz measurements and therefore reduces the value of number of the 20 Hz measurements used for the 1 Hz data. It is possible that differences in the tuning of the MQE criterion for Jason-1 and Jason-2 Ku-band explain what is observed on the right side of figure 23.

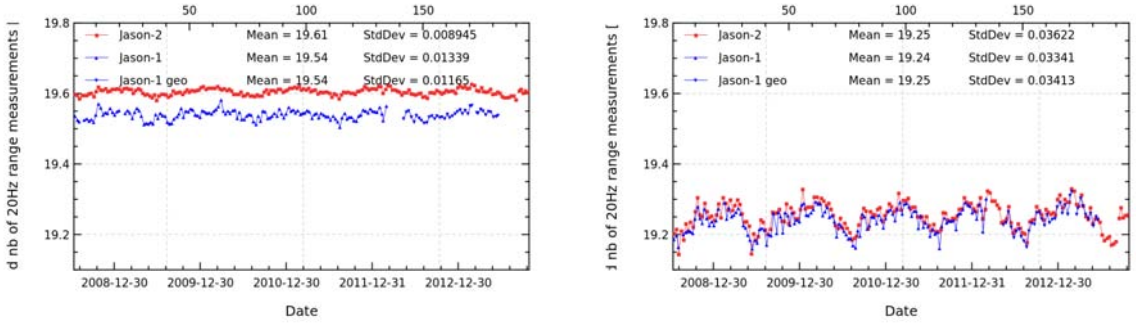

Figure 22: *Cyclic monitoring of number of elementary 20 Hz range measurements for Jason-1 and Jason-2 for Ku-band (left) and C-band (right).*

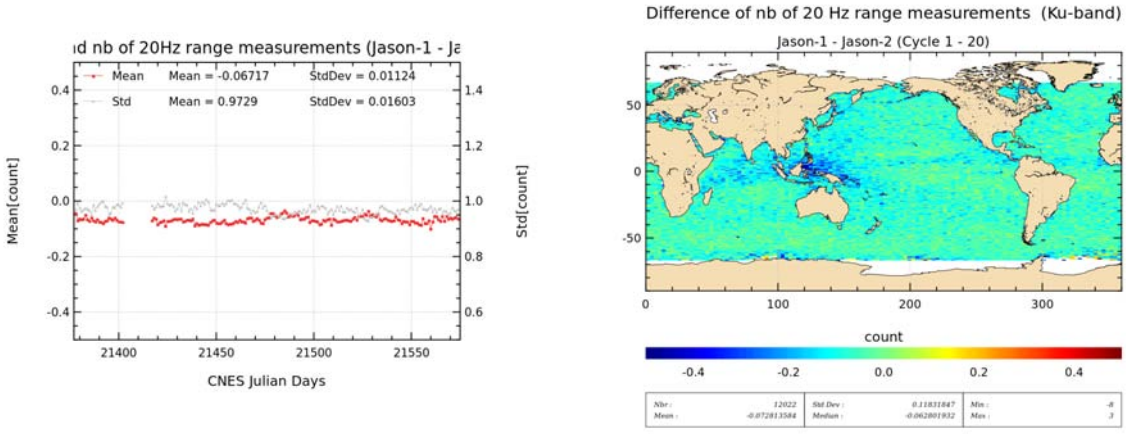

Figure 23: *Daily monitoring of mean and standard deviation of Jason-1 - Jason-2 differences for number of elementary 20 Hz Ku-band range measurements (left) and map showing mean of Jason-1 - Jason-2 differences over cycles 1 to 20.*

4.2.2. 20 Hz measurements standard deviation in Ku-Band and C-Band

Jason-2 standard deviation of the 20 Hz measurements is 8.0 cm for Ku-Band and 17.3 cm for C-Band (figure 25). It is very similar to Jason-1 data. Figure 26 and 27, showing daily monitoring of Jason-1 - Jason-2 difference of standard deviation of the 20 Hz measurements in Ku-Band and C-Band (on the left), reveal no trend neither anomaly. C-Band standard deviation of the 20 Hz measurements rms is noisier than those of Ku-Band. This is directly linked to the C-band standard deviation which is higher than the Ku, as the onboard averaging is performed over less waveforms (6 Ku for 1 C) leading to an increased noise.

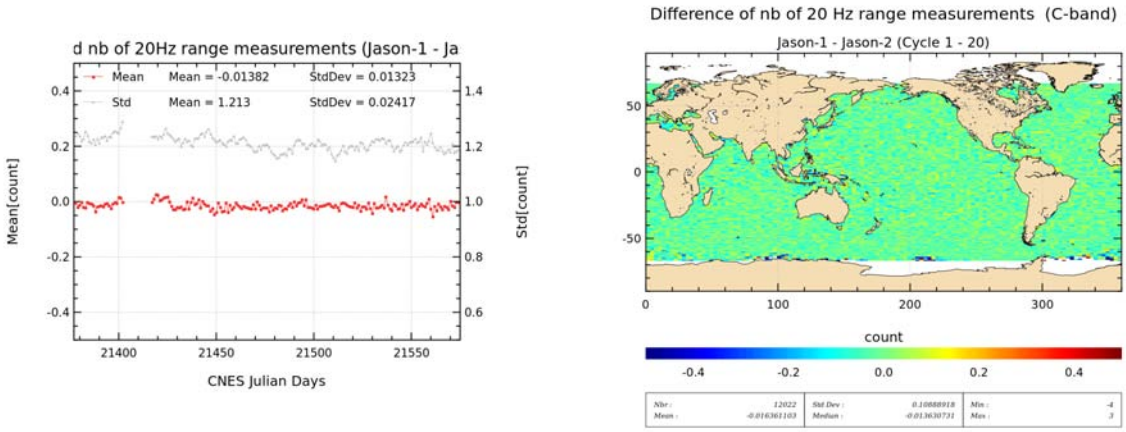

Figure 24: *Daily monitoring of mean and standard deviation of Jason-1 - Jason-2 differences for number of elementary 20 Hz C-band range measurements (left) and map showing mean of Jason-1 - Jason-2 differences over cycles 1 to 20.*

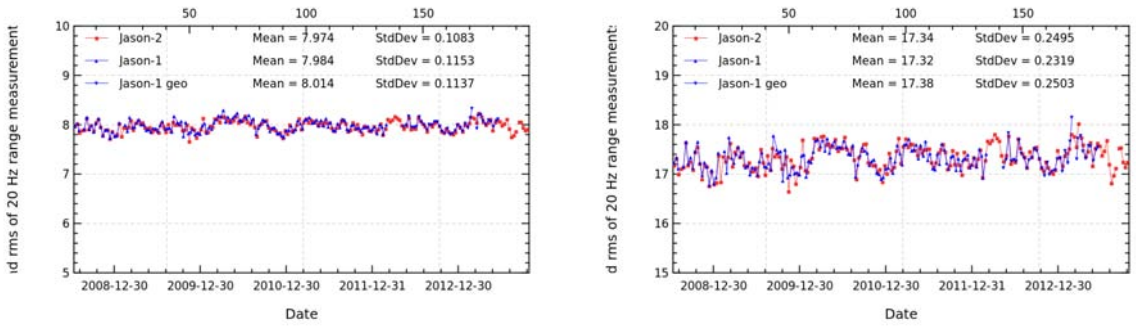

Figure 25: *Cyclic monitoring of rms of elementary 20 Hz range measurements for Jason-1 and Jason-2 for Ku-band (left) and C-band (right).*

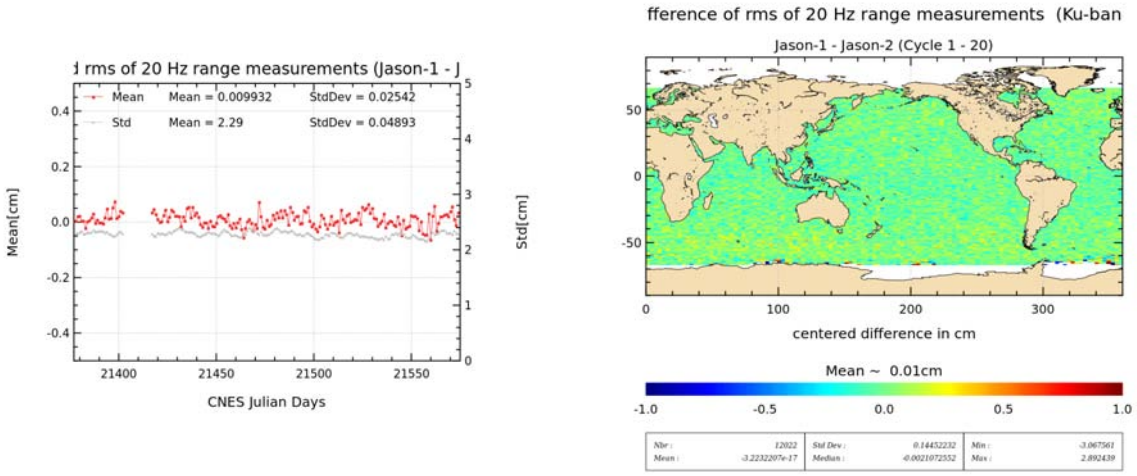

Figure 26: *Daily monitoring of mean and standard deviation of Jason-1 - Jason-2 differences for the rms of elementary 20 Hz Ku-band range measurements (left) and map showing mean of Jason-1 - Jason-2 differences over cycles 1 to 20 (right).*

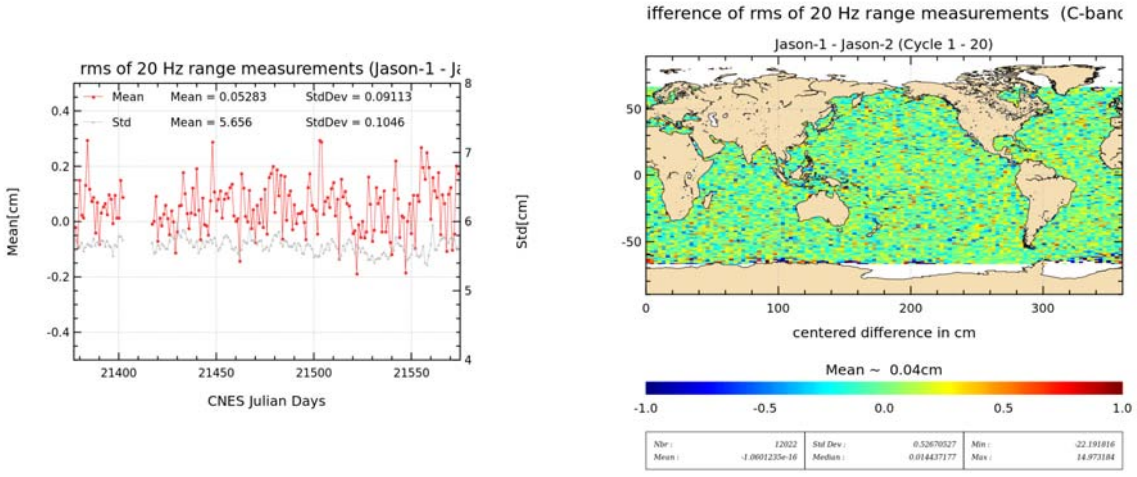

Figure 27: *Daily monitoring of mean and standard deviation of Jason-1 - Jason-2 differences for rms of elementary 20 Hz C-band range measurements (left) and map showing mean of Jason-1 - Jason-2 differences over cycles 1 to 20 (right).*

4.3. Off-Nadir Angle from waveforms

The off-nadir angle is estimated from the waveform shape during the altimeter processing. The square of the off-nadir angle, averaged on a daily basis, has been plotted for Jason-1 and Jason-2 on the left side of figure 28, whereas the right side shows the histograms over one cycle. For GDR-D Jason-2 the mispointing is very stable and very close to zero (though very slightly negative). Whereas Jason-1 may show higher values (related to the reduced tracking performance of both star trackers, especially during fixed-yaw). Jason-1 experienced especially during 2010 very high mispointing values, for more information see Jason-1 validation report [71]. Jason-1 mispointing situation has been highly improved since end of 2010.
Jason-2 GDR-T mispointing was slightly positive (see also reprocessing report ([11])), which was related to the antenna aperture values used for data processing (1.26° for GDR-T, 1.29° for GDR-D). Indeed [63] shows, that retracking with different values of antenna aperture, changes the mean value of Jason-2 mispointing (see figure 29). Note that for Jason-1 1.28° is used for the antenna aperture.

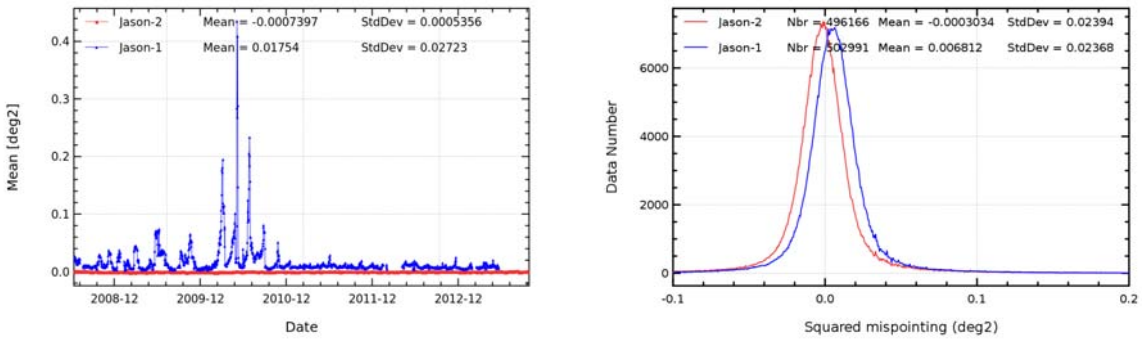

Figure 28: *Square of the off-nadir angle deduced from waveforms (deg^2) for Jason-1 and Jason-2: Daily monitoring (left), histograms for Jason-2 cycle 157 (Jason-1 cycle 513/514).*

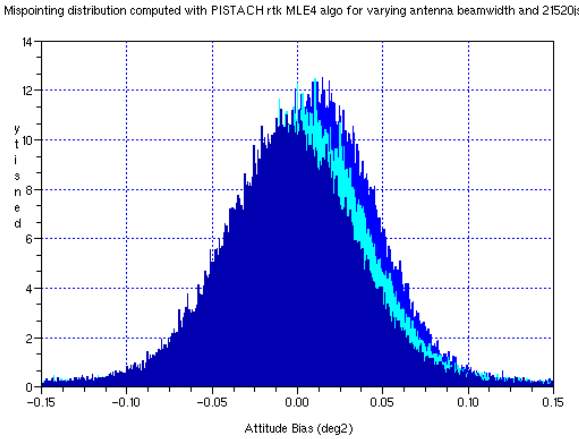

Figure 29: *Histograms of Jason-2 mispointing after retracking with different antenna beamwidth (from [63]): 1.26° (blue), 1.28° (light blue), 1.30° (dark blue).*

4.4. Backscatter coefficient

The Jason-2 Ku-band and C-band backscattering coefficient shows good agreement with Jason-1 as visible for cyclic monitoring in figure 30 (top left and right). Left sides of figures 31 and 32 show daily monitoring of mean differences during the formation flight phase. For Ku-band, a bias close to 0.3 dB is detected, it varies slightly (+/- 0.05 dB). This slight variation (± 0.05 dB) is related to Jason-1 backscattering coefficient which is slightly impacted by the higher off-nadir angles (due to low star tracker availability). Note that backscattering coefficients include instrumental corrections, which include also atmospheric attenuation which comes from the radiometer. Therefore differences between backscattering coefficients can also be partly due to differences between the atmospheric attenuation algorithms of Jason-1 and Jason-2. The main reasons for the differences (between Jason-1 and Jason-2 backscattering coefficients) are related to the antenna calibrations and to the internal calibrations of the altimeters (steps of numerical gain control).
The average standard deviation of both Sigma0 differences (measurement by measurement) is also very low around 0.15 dB rms. C-Band sigma0 differences indicate a small bias close to 0.17 dB. In the meantime, the map of mean differences (right side of figures 31 and 32) highlights very small differences. During the tandem phase (from Jason-2 cycle 21 onwards), mean differences continue to be calculated but comparing only the global day per day statistics (see bottom of figure 30). Although the statistic is calculated less accurately, a similar bias is observed as during the formation flight phase, and no significant drift is detected between both missions.

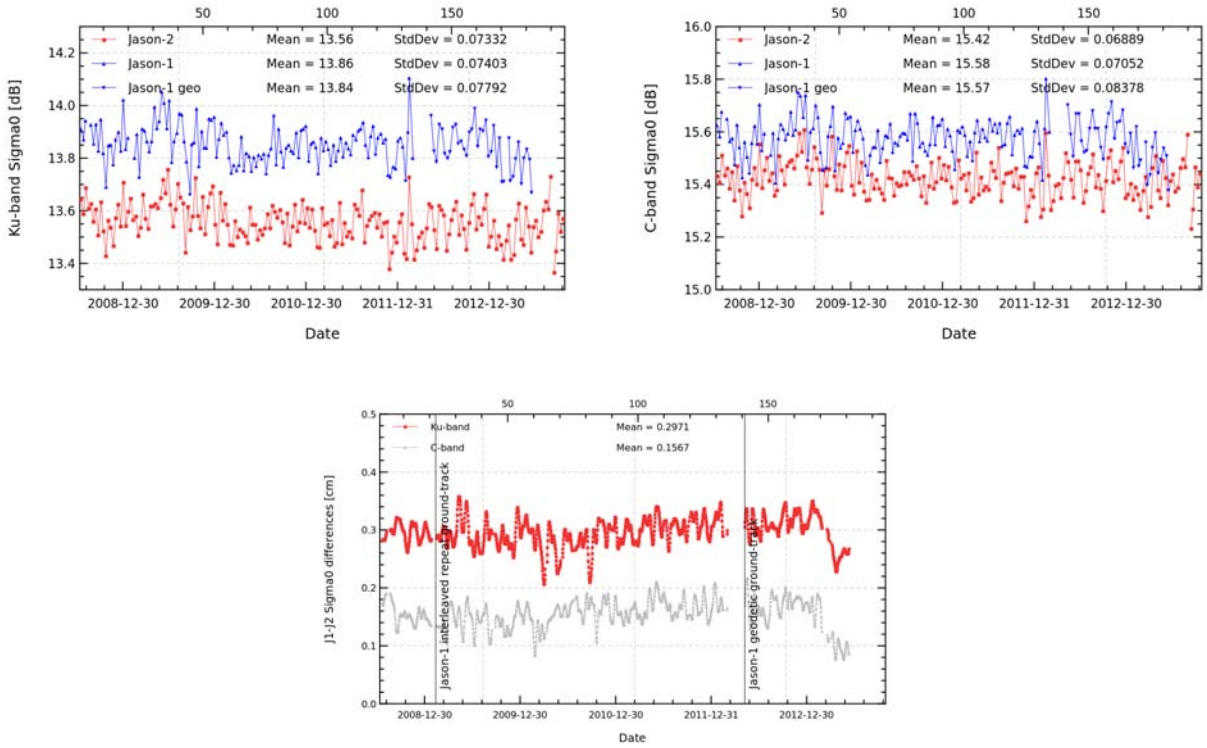

Figure 30: *Cyclic monitoring of Sigma0 for Jason-1 and Jason-2 for Ku-band (left) and C-band (right). Daily monitoring of Jason-1 - Jason-2 differences (bottom), a 10 day filter is applied.*

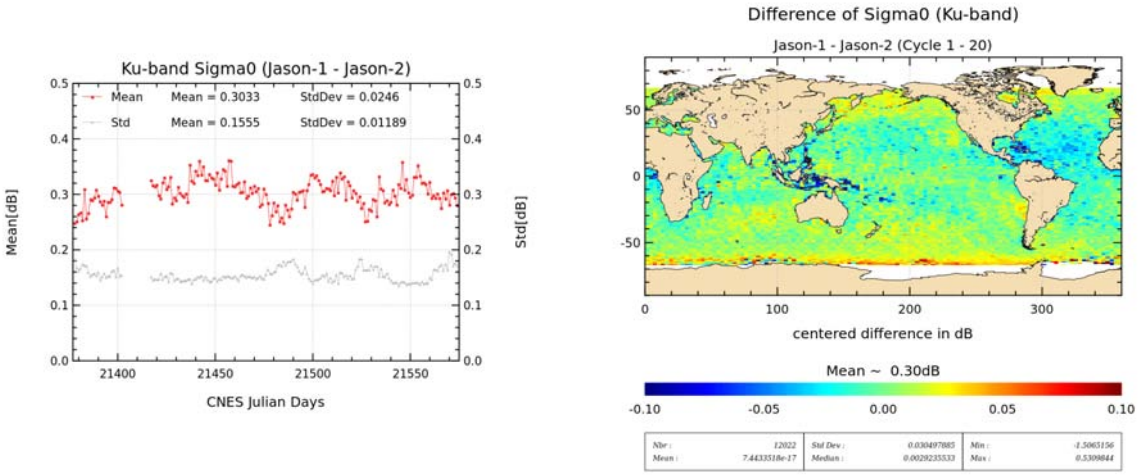

Figure 31: *Daily monitoring of mean and standard deviation of Jason-1 - Jason-2 differences for Ku-band Sigma0 (left) and map showing mean of Jason-1 - Jason-2 differences over cycles 1 to 20.*

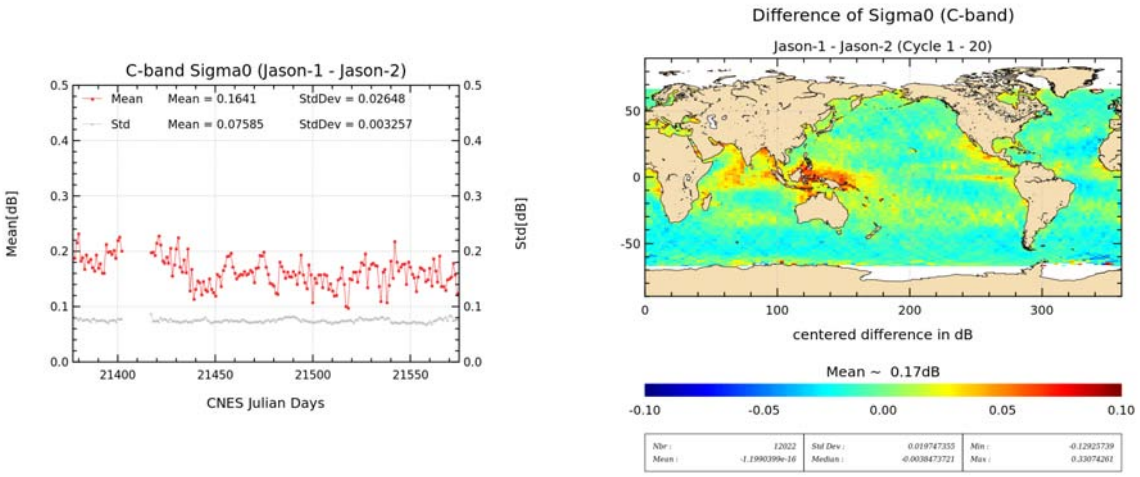

Figure 32: *Daily monitoring of mean and standard deviation of Jason-1 - Jason-2 differences for C-band Sigma0 (left) and map showing mean of Jason-1 - Jason-2 differences over cycles 1 to 20.*

4.5. Significant wave height

As for Sigma0 parameter, a very good consistency between both significant wave height is shown (see top left and right of figure 33). A small bias close to around -1.3 cm is calculated over the formation flight phase. It is close to -1.7 cm in C-band (see left side of figures 34 and 35). It is stable in time and space (see map of differences in right side of figures 34 and 35). These differences are too weak to impact scientific applications. They are probably due to ground processing differences between both missions. Differences are noisier for C-band. As previously, extending the monitoring of SWH bias during the tandem phase (bottom of figure 33) highlights larger variations since both satellites do not measure the same SWH. However bias is still stable and no drift is detected.

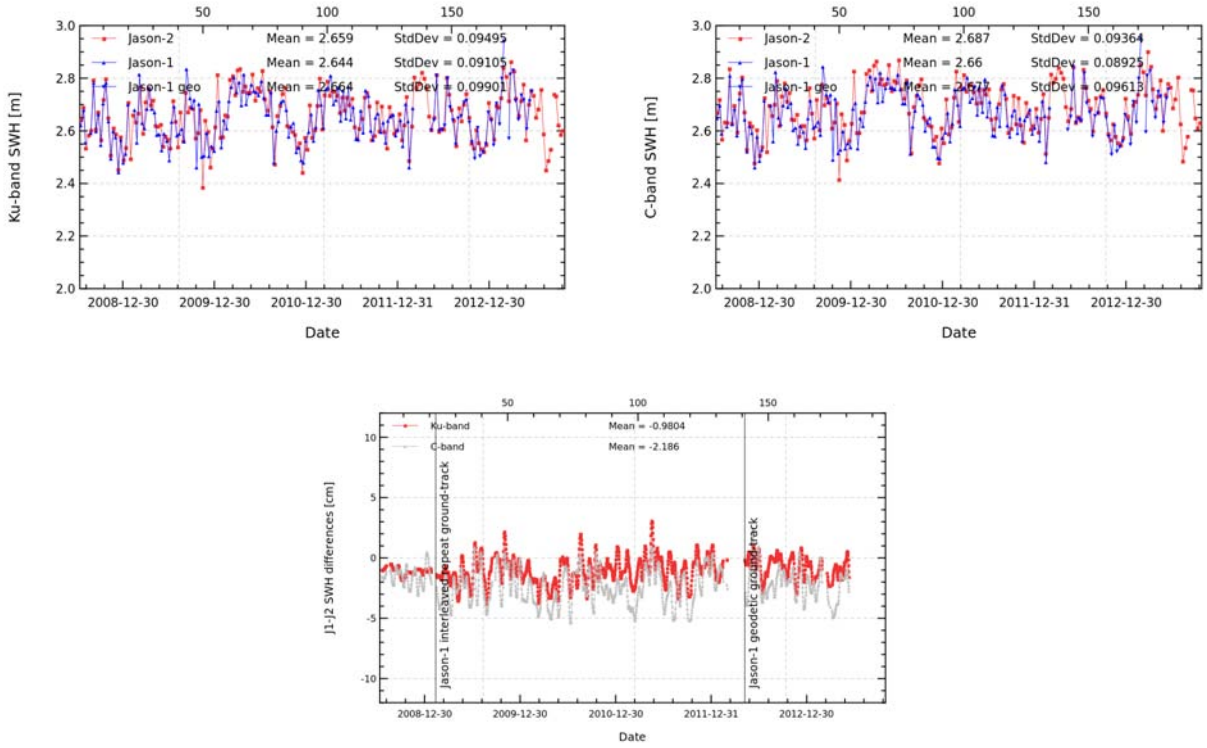

Figure 33: *Cyclic monitoring of SWH for Jason-1 and Jason-2 for Ku-band (left) and C-band (right). Daily monitoring of Jason-1 - Jason-2 differences (bottom), a 10 day filter is applied.*

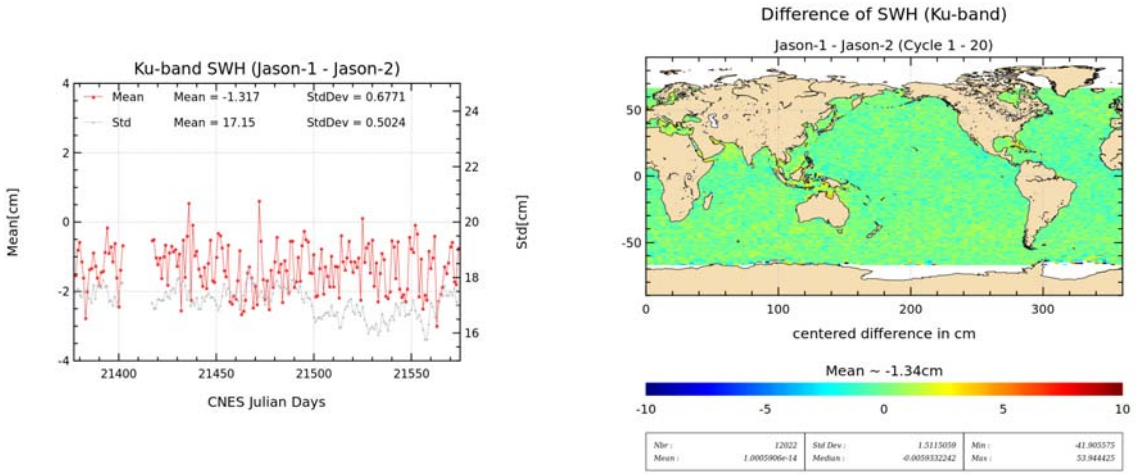

Figure 34: *Daily monitoring of mean and standard deviation of Jason-1 - Jason-2 differences for Ku-band SWH (left) and map showing mean of Jason-1 - Jason-2 differences over cycles 1 to 20.*

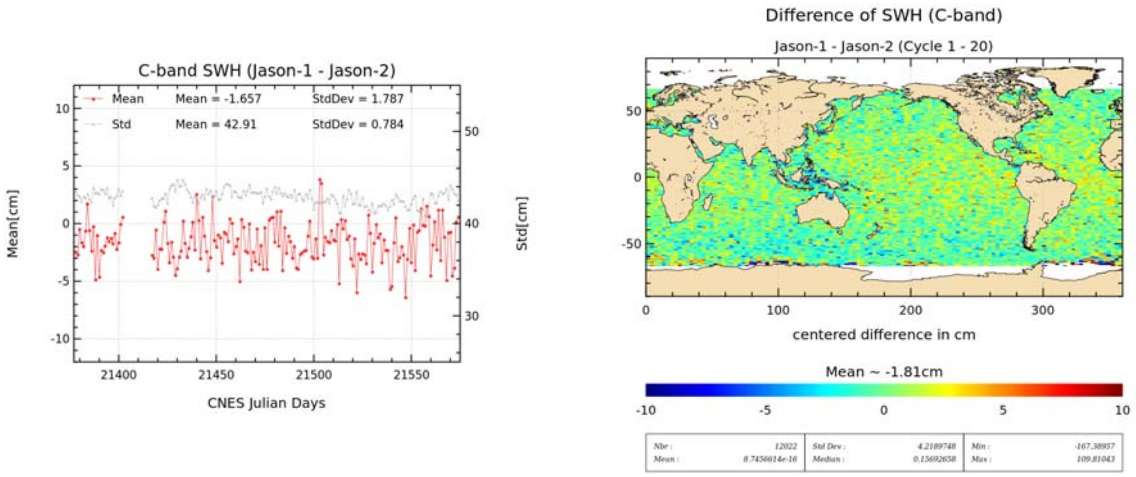

Figure 35: *Daily monitoring of mean and standard deviation of Jason-1 - Jason-2 differences for C-band SWH (left) and map showing mean of Jason-1 - Jason-2 differences over cycles 1 to 20.*

4.6. Dual-frequency ionosphere correction

The dual frequency ionosphere corrections derived from the Jason-2 and Jason-1 altimeters show a mean difference of about -0.3 cm (figure 36 (left)), with cycle to cycle variations lower than 1 mm. This bias is due to the relative Ku-band (-7.0 cm) and C-band (-2.2 cm) range difference between Jason-1 and Jason-2, as well as the relative Ku-band (-2.8 cm) and C-band (-6.0 cm) sea state difference between Jason-1 and Jason-2. As the dual-frequency ionosphere correction is derived from a combination of Ku and C band ranges (corrected for the corresponding sea state bias), a bias of -3 mm between Jason-1 and Jason-2 ionospheric corrections results. Apart from this bias, the two corrections are very similar and vary according to the solar activity. The map of local differences (figure 36 right) shows small regional differences.

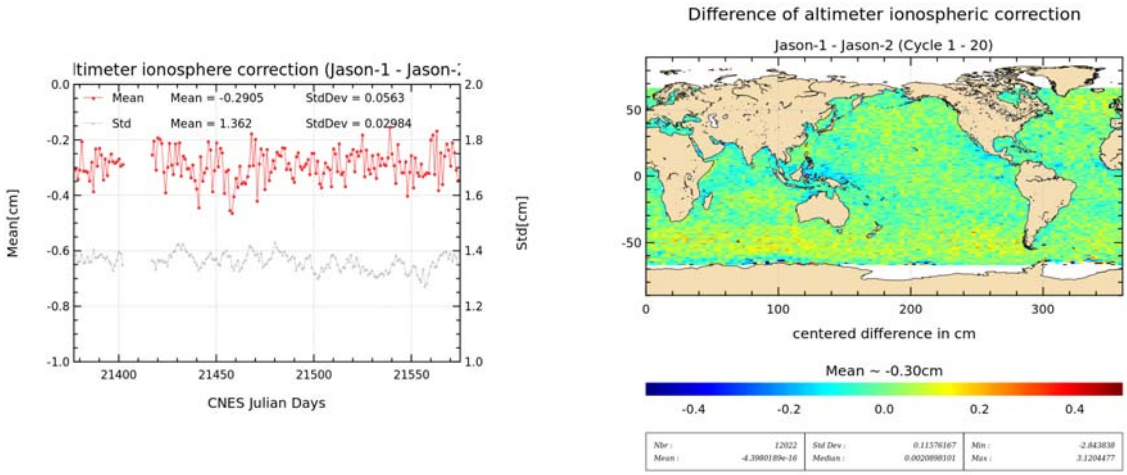

Figure 36: *Daily monitoring of mean and standard deviation of Jason-1 - Jason-2 differences for dual-frequency ionospheric correction (left) and map showing mean of Jason-1 - Jason-2 differences over cycles 1 to 20.*

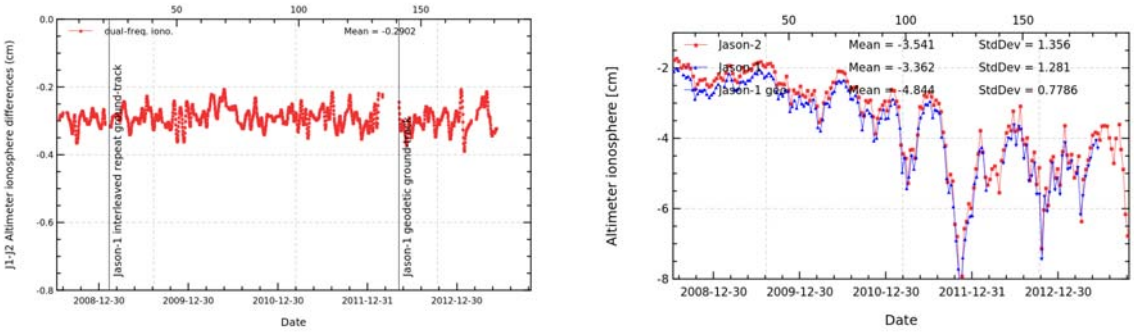

Figure 37: *Cyclic monitoring of dual-frequency ionosphere for Jason-1 and Jason-2 (right). Daily monitoring of Jason-1 - Jason-2 differences (left), a 10 day filter is applied.*

Notice that, as for TOPEX and Jason-1 (Le Traon et al. 1994 [47], Imel 1994 [45], Zlotnicky

1994 [72]), it is recommended to filter the Jason-2 dual frequency ionosphere correction before using it as a SSH geophysical correction (Chambers et al. 2002 [29]). A low-pass filter has thus been used to remove the noise of the correction in all SSH results presented in the following sections. Plotting difference of non-filtered ionospheric correction between Jason-1 and Jason-2 versus Jason-2 ionospheric correction shows an apparent scale error, which disappears when using filtered data (see figure 38). As in the beginning of the Jason-2 mission, ionosphere correction was very low, the ionosphere noise is of the same order of magnitude as the ionosphere correction itself. Therefore plotting the difference of non-filtered dual-frequency ionospheric correction versus dual-frequency ionospheric correction induces an apparent scale error.

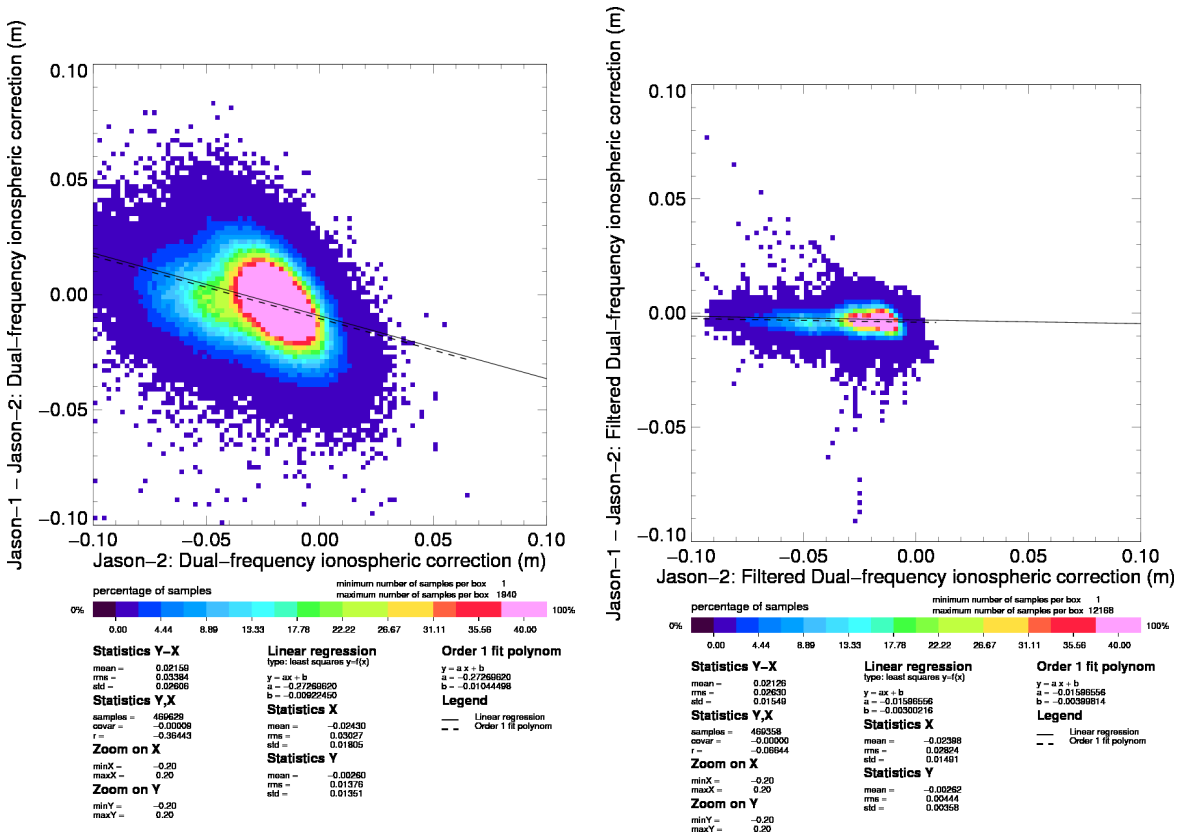

Figure 38: *Diagram of dispersion of Jason-1 - Jason-2 versus Jason-2 dual-frequency ionosphere correction for Jason-2 cycle 15. Left: non-filtered, right: filtered.*

During 2011, solar activity has increased and therefore also the absolute value of ionosphere correction (right part of figure 37).
When comparing altimeter ionosphere correction to GIM correction (figure 39), mean as well as standard deviation of this difference increases over 2011. This concerns both Jason missions. Figure 40 shows the mean difference between altimeter ionosphere and GIM correction after a one-year smooth for slots of local hours. Ionosphere differences between altimeter and GIM are higher for day time measurements than for night time measurements.

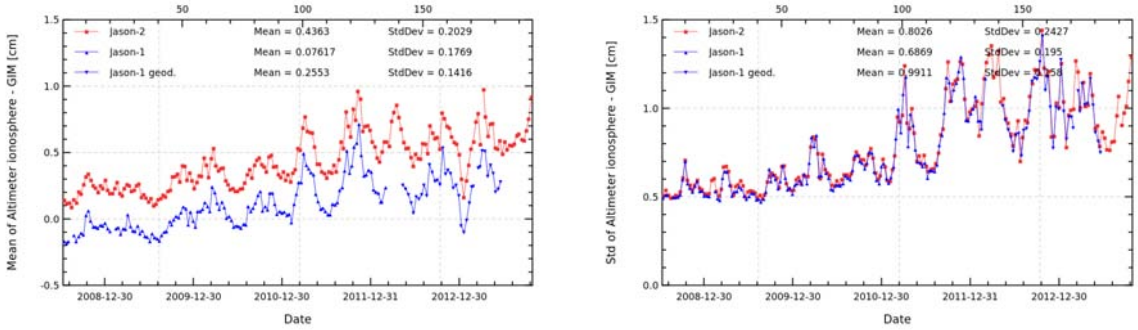

Figure 39: *Cycle per cycle monitoring of filtered altimeter ionosphere correction minus GIM ionosphere correction for Jason-1 and Jason-2. Left: Mean, right: standard deviation.*

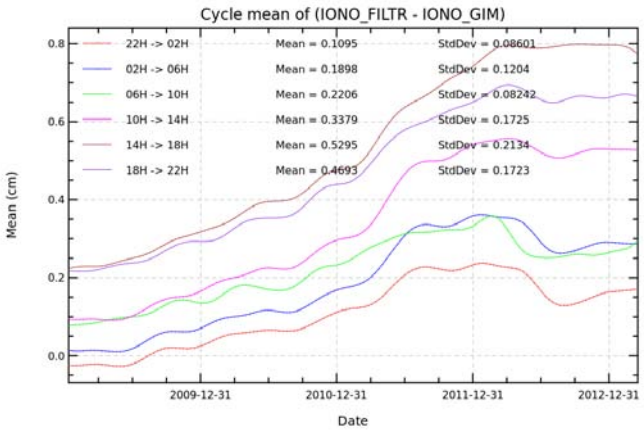

Figure 40: *Cycle per cycle monitoring of filtered altimeter ionosphere minus GIM correction computed per local hour time intervals. A one-year smooth is applied.*

4.7. AMR Wet troposphere correction

4.7.1. Overview

The Jason-2 radiometer wet troposphere correction available contains an improved retrieval algorithm near coasts ([26]). Note that the product AMR radiometer wet troposphere correction has (according to S. Brown) several level of calibration:

- Cycles 1-113 - Climate data record quality calibration Cycles
- 114-140 - Intermediate quality calibration (somewhere between climate quality and operational(ARCS) quality)
- Cycle 141 onward - Operational(ARCS) quality calibration

Figure 41 shows on the left side the daily monitoring of the difference of radiometer wet troposphere correction between the two missions (JMR - AMR) during the formation flight phase. Note that for Jason-1 the JMR replacement product (which was available for cycles 228 to 259) was used. This corrects for stability problems of JMR which occured after the safehold in August 2008. For the other cycles the correction available in Jason-1 GDR-C is used. AMR is globally slightly dryer than JMR (-0.09 cm). But locally, especially near coasts (right side of figure 41), AMR is wetter than JMR. This is related to the fact that the Jason-2 correction uses improved retrieval algorithm in coastal areas, whereas this is not the case for Jason-1. The daily monitoring is very stable, except for julian day 21556 (2009-01-07), where the difference between the two radiometers shows a drop of 3 mm. This is related to the JMR replacement, which is for this day about 3 mm wetter than usually.

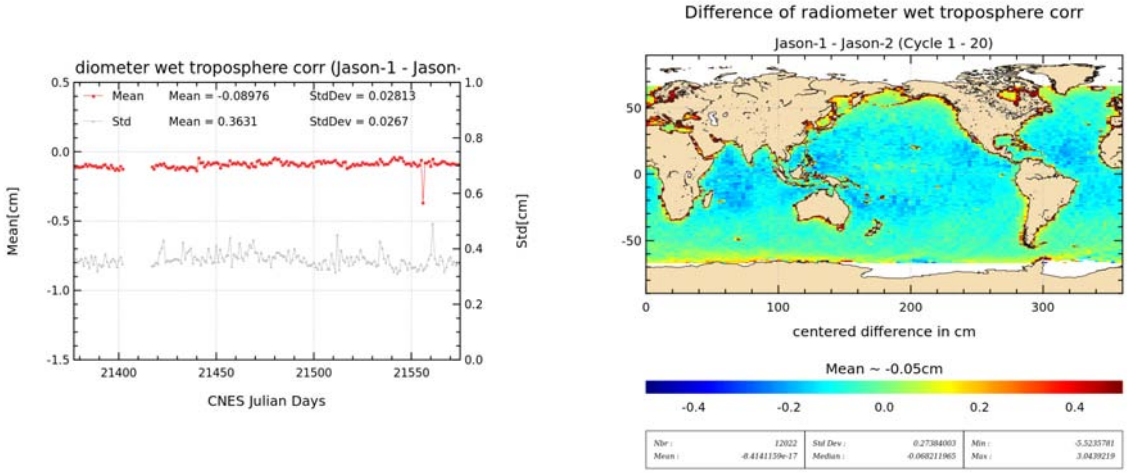

Figure 41: *Daily monitoring of mean and standard deviation (left) of Jason-1 - Jason-2 radiometer wet troposphere correction. Map showing mean of Jason-1 - Jason-2 differences over cycles 1 to 20.*

4.7.2. Comparison with the ECMWF model

The ECMWF wet troposphere correction has been used to check the Jason-1 and Jason-2 radiometer corrections. Daily differences are calculated and plotted in figure 43. It clearly appears (on left side of figure 43) that Jason-2 radiometer correction (AMR) from GDR products is much more stable than for Jason-1 (JMR), especially at the beginning of Jason-2 period where large oscillations (up to 7mm) are observed between JMR (from GDR-C product) and model. Indeed after the safe-hold mode of Jason-1 in August 2008 (corresponding to Jason-2 cycle 4), JMR experienced some thermal instability. In addition, small differences linked to yaw-dependent effects (as also observed on TOPEX radiometer (Dorandeu et al., 2004, [37])) are visible (yaw maneuvers are indicated as gray lines on left side of figure 43). In order to take into account these effects, new JMR calibration coefficients are provided and updated at each Jason-1 GDR reprocessing campaign. Using the JMR replacement product (available for Jason-1 cycles 228 to 259) corrects for the instabilities during August 2008 (Brown et al. 2009, [25]). Now, thanks to the new ARCS (Autonomous Radiometer Calibration System) (Brown et al. 2009, [25]) calibration system set up for Jason-2, AMR radiometer correction is calibrated at each GDR cycle and the calibration coefficients are modified if necessary. On right side of figure 43 the black lines indicate, each time a modification of the calibration coefficients were necessary. The lines are only drawn from cycle 114 onwards.
During 2011, the frequency of application of new calibration coefficients has increased, especially during summer 2011. The AMR wet troposphere correction shows jumps and drifts in the IGDRs. The calibrations applied for the GDRs correct most of these anomalies, nevertheless small jumps persist. There are also small drifts visible within a cycle (for exemple cycle 111 and 112), as the ARCS corrections apply a discret value to correct a drift. Furthermore, the AMR comparison with model highlights also long-term signals with Jason-2 not clearly observed with Jason-1. As a result of a poor confidence in stability of just one radiometer, Envisat wet troposphere correction (MWR) is also compared to the ECMWF model in the same figure 43 (left side). Sometimes MWR and JMR show similar differences, sometimes AMR and JMR show similar differences. For AMR, there might be a risk that real geophysical signals are absorbed by the calibration method used. Finally, the cross-comparison between all radiometers and models available is necessary to analyze the stability of each wet troposphere correction. An overview of the wet troposphere correction importance for mean sea level is given in Obligis et al. [49].

Figure 42 shows mean and standard deviation for cycle per cycle differences between Jason-2 radiometer and ECMWF model wet troposphere corrections for several data types. Over year 2013, OGDR, IGDR and GDR radiometer data were less subject to drifts and jumps. The mean of IGDR and GDR wet troposphere differences are similar as no change of coefficient was needed between cycle 156 and 195. The standard deviation of OGDR and IGDR wet troposphere differences is higher for OGDR than for IGDR, as OGDR contain predicted model fields instead of analysed model field (for IGDR and GDR products).

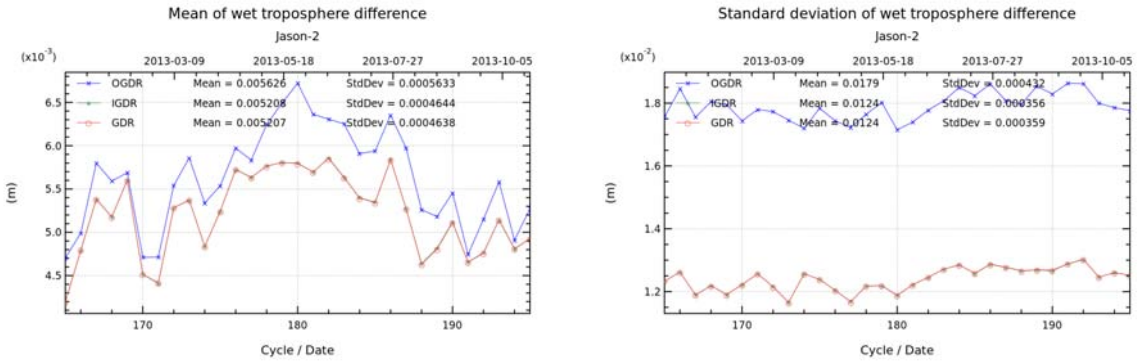

Figure 42: *Cycle per cycle monitoring of mean (left) and standard deviation (right) of radiometer minus ECMWF model wet troposphere correction over 2013 (until cycle 195) for Jason-2 O/I/GDR.*

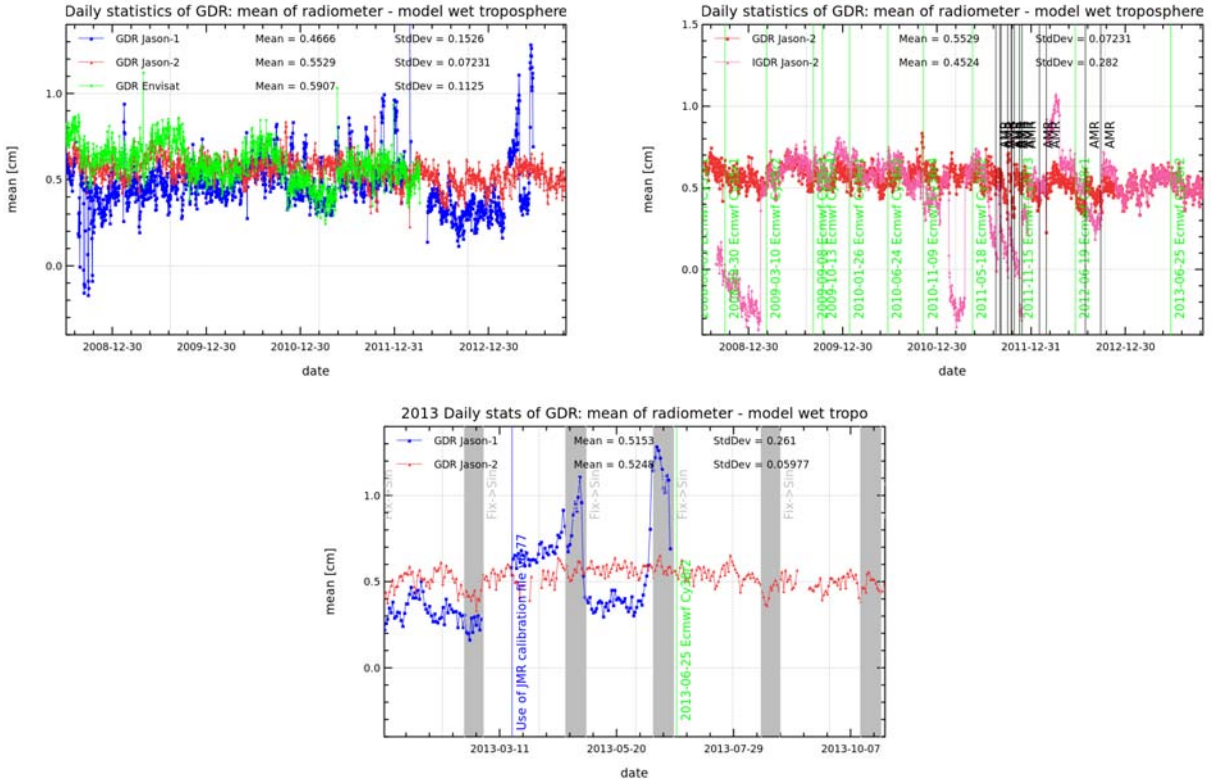

Figure 43: *Daily monitoring of radiometer and ECMWF model wet troposphere correction differences for Jason-1 (blue), Jason-2 (red) and Envisat (green) limited to 66° latitude. Vertical gray lines correspond to yaw maneuvers on Jason-2. Right: daily monitoring for Jason-2 GDRs (red) and IGDRs (pink). Vertical green lines correspond to ECMWF model version changes, black lines correspond to AMR calibration coefficients changes on GDR products also impacting IGDR product (but latter). Bottom: Daily monitoring for Jason-2 GDRs (red) and IGDRs (pink), as well as Jason-1 GDRs (blue) for 2013. Vertical green lines correspond to ECMWF model version changes, black lines correspond to AMR calibration coefficients changes on GDR products. They impact also IGDR products (but later).*

4.8. Altimeter wind speed

Figure 44 shows on the left side the daily monitoring of the difference of altimeter wind speed between the two missions. Before the Jason-2 reprocessing, there was a difference of about -0.4 m/s between Jason-1 and Jason-2. Note that the histograms of Jason-2 GDR-T and Jason-1 had different shapes. Using GDR-D data, the mean difference between Jason-1 and Jason-2 altimeter wind speed is reduced to 0.05 m/s, and the shapes of the histograms (figure 45) are also much more closer. Finally the regional differences are also reduced. Locally (right side of figure 44), altimeter wind speed from Jason-1 is higher than from Jason-2. The signal visible on daily monitoring, is anti-correlated to the signal visible on daily monitoring of backscattering coefficient (see figure 31), as wind speed computation uses principally backscattering coefficient. This signal is related to events of high mispointing of Jason-1.

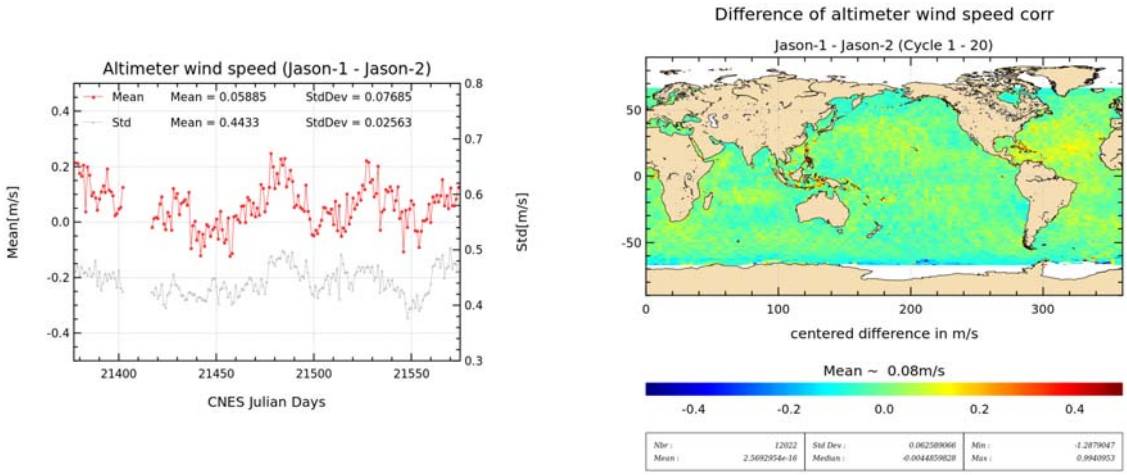

Figure 44: *Daily monitoring of mean and standard deviation (left) of Jason-1 - Jason-2 altimeter wind speed. Map showing mean of Jason-1 - Jason-2 differences over cycles 1 to 20.*

For Jason-1 Gdr-C release, the wind speed is calculated with an algorithm based on ([41]), fitted on Jason-1 Sigma0 (Collard algorithm). It is the same algorithm applied for Jason-2 now. As there is a bias between Jason-1 and Jason-2 Ku-band backscattering coefficients, prior to the altimeter wind speed computation of GDR-D, a calibration bias of 0.32 dB has been added to the Ku-band backscattering coefficient.
Thanks to the altimetry standard improvements since Jason-1 launch ([55], [31]), the error budget of SSH calculation has been reduced. Through the sea state bias correction, the Sigma0 bias uncertainty has thus become not inconsiderable as shown in recent study ([65], [2]). Indeed an error of 0.1 dB on the backscattering coefficient has an impact of about 0.5 m/s on the altimeter wind speed, which in turn has an impact of about 1.6 mm on the sea state bias correction.

Figure 46 shows mean and standard deviation for cycle per cycle altimeter wind speed for several data types of Jason-2. The altimeter wind speed of the different data types is coherent.

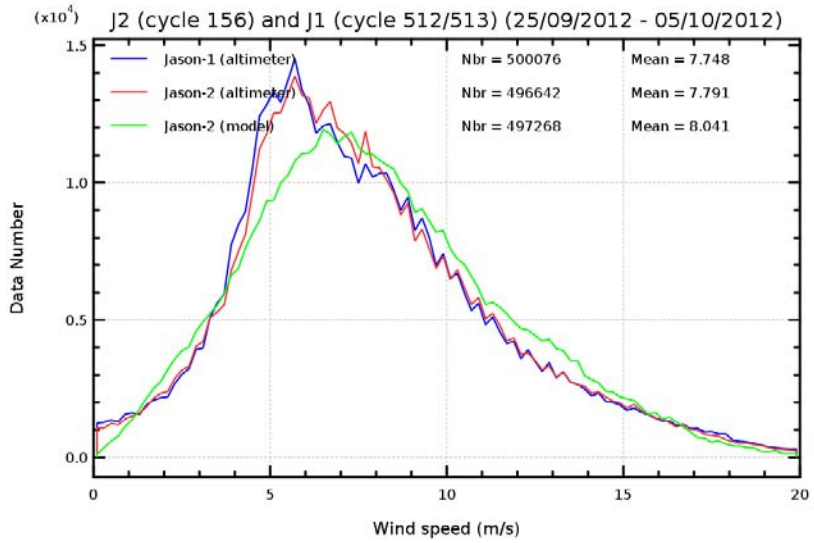

Figure 45: *Histogram of altimeter (Jason-1 in blue, Jason-2 in red) and model wind speed (green) for a 10 day period.*

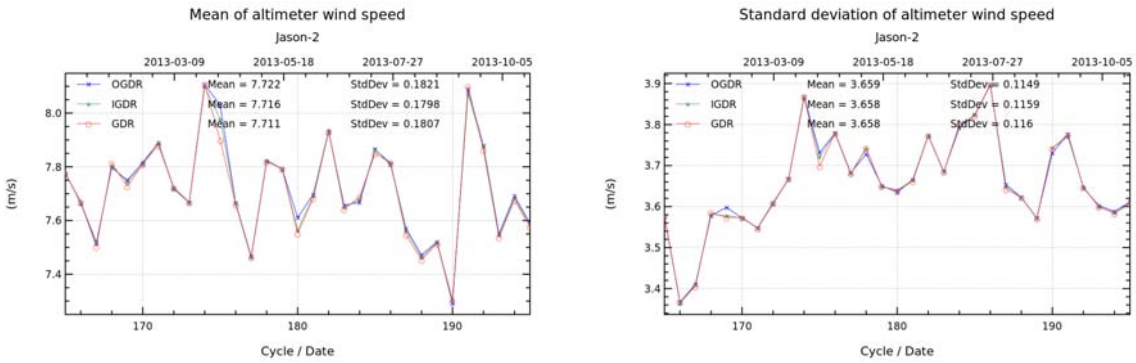

Figure 46: *Cycle per cycle monitoring of mean (left) and standard deviation (right) of altimeter wind speed over 2013 (until cycle 195) for Jason-2 O/I/GDR.*

4.9. Sea state bias

The sea state bias look-up table used for GDR-D was computed using Jason-2 data from internal reprocessing which were as close as possible to the GDR-D standards. Differences between Jason-1 and Jason-2 are about -3 cm (left of figure 47).

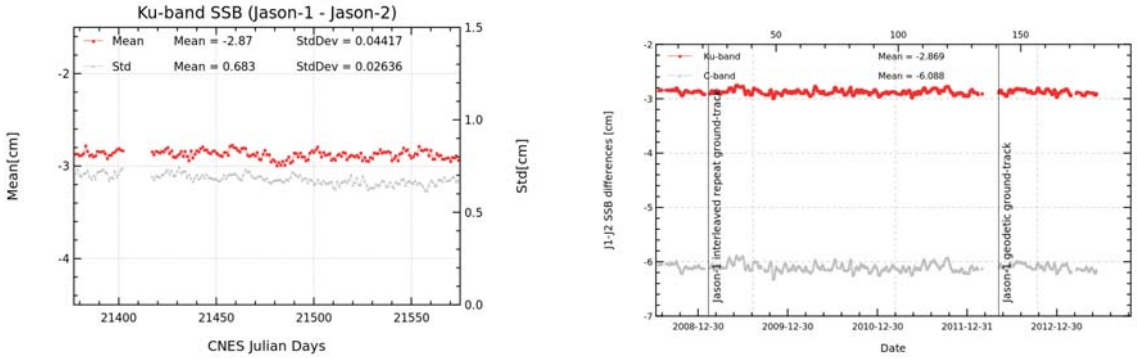

Figure 47: *Daily monitoring of mean and standard deviation (left) of Jason-1 - Jason-2 sea state bias over cycles 1 to 20. Daily monitoring of Jason-1 - Jason-2 differences (right), a 10 day filter is applied.*

This difference is not a bias, as can be seen from the maps of the Jason-1 - Jason-2 sea state bias difference (figure 48). Differences between Jason-1 and Jason-2 sea state bias increase using Jason-2 GdrD (top of figure 48), as the methods (as well as data) used for the SSB model computation are different.

In the case of top left side of figure 48, the method for Jason-1 and Jason-2 are different (the new method used in case of Jason-2 is explained in (see [65]) and the input values (wind, wave) for Jason-2 are those of standard D version. Indeed, GDR-D sea state model is calculated with a different approach of low sea states. In these areas, the editing method has changed so that differences are mainly observed here.

On the top right, the Tran 2012 sea state bias model is used for Jason-2. At OSTST 2012 meeting, Tran et al. [67] presented a new SSB model computed using one year of GDR-D data. This model seems better than the SSB model used for the GDR-D product. Though the SSB model used for the GDR-D products was computed on Jason-2 data from an internal reprocessing which was as close as possible to the GDR-D standard, there were nevertheless some differences with the GDR-D data. Indeed, the wind speed (necessary for SSB computation) from the internal reprocessing was tuned with a preliminary bias on sigma0, whereas the wind speed of the GDR-D product uses a fine-tuned bias (takes into account additionally a correction from LTM and corrected atmospheric correction from S. Brown in sigma0).

When using the updated sea state bias proposed by Tran et al. [67] for both missions, the Jason-1 minus Jason-2 differences are much more homogeneous (see bottom of figure 48). Note that this homogenization is mainly due to the updated Jason-2 SSB and to a lesser extent due to the updated Jason-1 SSB.

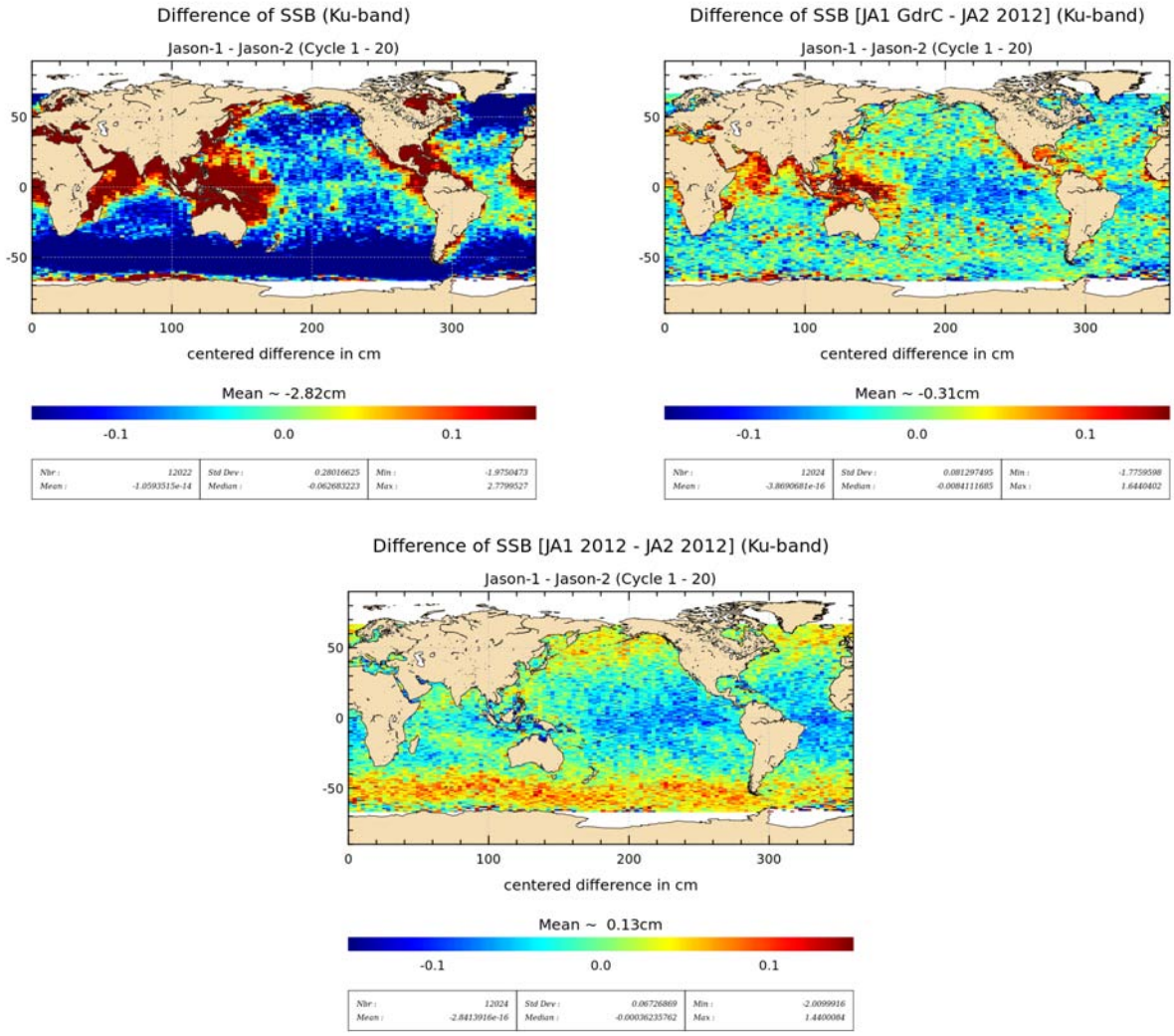

Figure 48: *Map showing mean of Jason-1 - Jason-2 sea state bias differences over cycles 1 to 20.* ***Top left:*** *using SSB from Jason-1 GDR-C and Jason-2 GDR-D (map centered around -2.82 cm).* ***Top right:*** *using SSB from Jason-1 GDR-C and updated (2012) SSB for Jason-2 (map centered around -0.31 cm).* ***Bottom:*** *using updated (2012) SSB for both Jason-1 and Jason-2 (map centered around 0.13 cm).*

5. SSH crossover analysis

5.1. Overview

SSH crossover differences are the main tool to analyze the whole altimetry system performances. They allow us to analyze the SSH consistency between ascending and descending passes. However in order to reduce the impact of oceanic variability, we select crossovers with a maximum time lag of 10 days. Mean and standard deviation of SSH crossover differences are computed from the valid data set to perform maps or a cycle by cycle monitoring over all the altimeter period. In order to monitor the performances over stable surfaces, additional editing is applied to remove shallow waters (bathymetry above -1000m), areas of high ocean variability (variability above 20 cm rms) and high latitudes ($> |50|deg$). SSH performances are then always estimated with equivalent conditions.
The main SSH calculation for Jason-2 and Jason-1 are defined below.

$$SSH = Orbit - Altimeter\ Range - \sum_{i=1}^{n} Correction_i$$

with $Jason-1/Jason-2\ Orbit = CNES\ orbit$ for GDR products, and

$$\begin{aligned}\sum_{i=1}^{n} Correction_i &= Dry\ troposphere\ correction \\ &+ Dynamical\ atmospheric\ correction \\ &+ Radiometer\ wet\ troposphere\ correction \\ &+ Dual\ frequency\ ionospheric\ correction\ (filter\ 250\ km) \\ &+ Non\ parametric\ sea\ state\ bias\ correction \\ &+ Ocean\ tide\ correction\ (including\ loading\ tide) \\ &+ Earth\ tide\ height \\ &+ Pole\ tide\ height\end{aligned}$$

In order to allow better comparisons between Jason-1 and Jason-2, some standards of Jason-1 GDR-C were updated.

Parameter	Jason-1 GDR-C	Jason-1 GDR-C with updates
Orbit	CNES POE-C	CNES POE-D
radiometer wet troposphere correction	JMR	JMR replacement product for period which corresponds to Jason-2 cycles 001 to 020
		.../...

Parameter	Jason-1 GDR-C	Jason-1 GDR-C with updates
Global ocean tide	GOT00V2	GOT 4.8
Mean Sea Surface	CLS_2001	CNES_CLS_2011

Table 8: *u*pdated standards of Jason-1 for comparison with Jason-2

Note that from 7th of May 2012 (Jason-1 cycle 500, which corresponds to end of Jason-2 cycle 141) and until the end of the Jason-1 mission (21st of June 2013, during Jason-2 cycle 183), Jason-1 was on a geodetic ground-track. The Jason-1 GDR-C product contains from cycle 500 onwards already the POE-D solution and the MSS CNES_CLS_2011.

5.2. Mean of SSH crossover differences

The cycle by cycle mean of SSH differences is plotted in figure 49 for Jason-2 and Jason-1 (using standards from Jason-1 GDR-C products and updated standards). The curves are very similar and do not highlight any anomaly. However, a small 120 day signal is visible for Jason-2 data. It is increased for updated Jason-1 products (compared to Jason-1 GDR-C products). The map of mean SSH crossover differences plotted in left side of figure 49 was calculated using Jason-2 GDR products, no great geographically correlated patterns are detected.

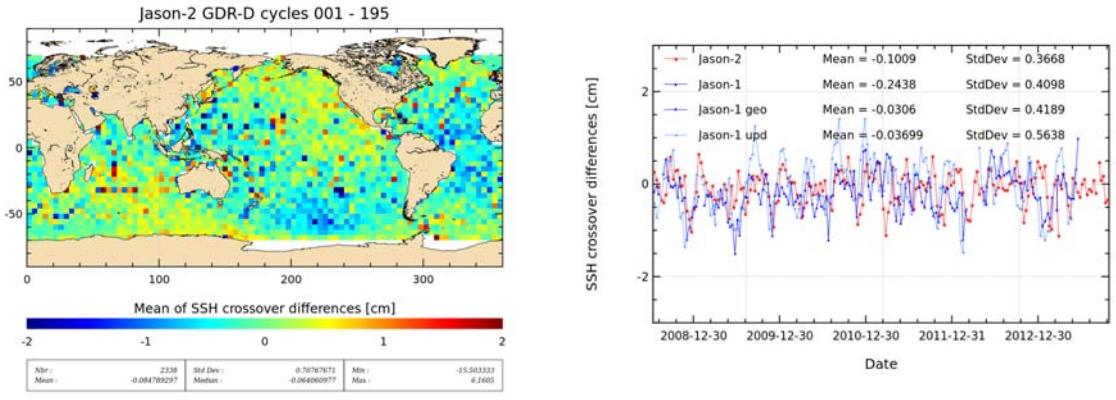

Figure 49: *Map of mean of SSH crossovers differences for Jason-2 cycle 1 to 195on the left. Monitoring of mean of SSH crossover differences for Jason-2 and Jason-1 using Jason-2 (red), Jason-1 GdrC (blue), Jason-1 GdrC Upd with GOT4V8 + POE-D + JMR replacement (light blue) on the right.*

Mean of SSH differences at crossovers for Jason-2 IGDR products (using MOE orbits) has noticeable negative values in average (-0.62cm over the last year versus -0.11cm in case of GDR), as can be seen on figure 50. In addition, the IGDR data monitoring shows a 120 day signal that is reduced in case of GDR.

SSH differences of OGDR products (using Doris/Diode navigator orbit) show slightly stronger variations, but since the use of the Doris version 11 (from 2012-09-19 onwards), the mean of OGDR

SSH crossover differences is much more homogeneous (negative in average too).

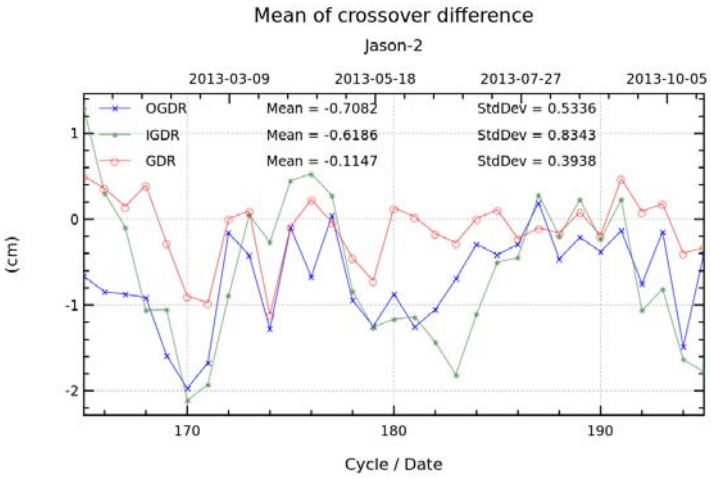

Figure 50: *Monitoring over 2013 of mean of SSH crossover differences for different data types of Jason-2: OGDR (blue), IGDR (green), GDR (red).*

5.3. Mean of SSH crossover differences between Jason-2 and other missions

Dual-mission crossover performances are computed between Jason-2 and Jason-1, as well as Jason-2 and Envisat. Jason-1 GDR-C data were used with updated standards (see table 8). Mean SSH differences at Jason-2/Jason-1 crossovers (shown on left side of figure 51) have a bias of about 10 cm (JA1-JA2). This bias is mostly due to the range differences between the two satellites, but also due to different sea state bias models. The map shows small regional structures of about ±1 cm, especially in southern Pacific, but also around Indonesia and in the Mediterranean Sea. These structures are stronger than those observed between Jason-2 GDR-T and Jason-1 GDR-C (see Jason-2 annual report 2011 [[9]]). This difference comes mainly from the different sea state biases used for Jason-1 GDR-C and Jason-2 GDR-D (see also chapter 4.9.). Using updated sea state bias (presented at 2012 OSTST by Tran et al. [[67]]) for both Jason-2 and Jason-1 data, reduces most of the geographical pattern (right of figure 51). A small pattern remains. This structure was also seen during the flight formation phase, when differences without applying geophysical corrections were possible. It is dependant on orbit solutions, as it is strongly reduced when using GSFC orbit solutions for both missions ([4], see also bottom of figure 56).

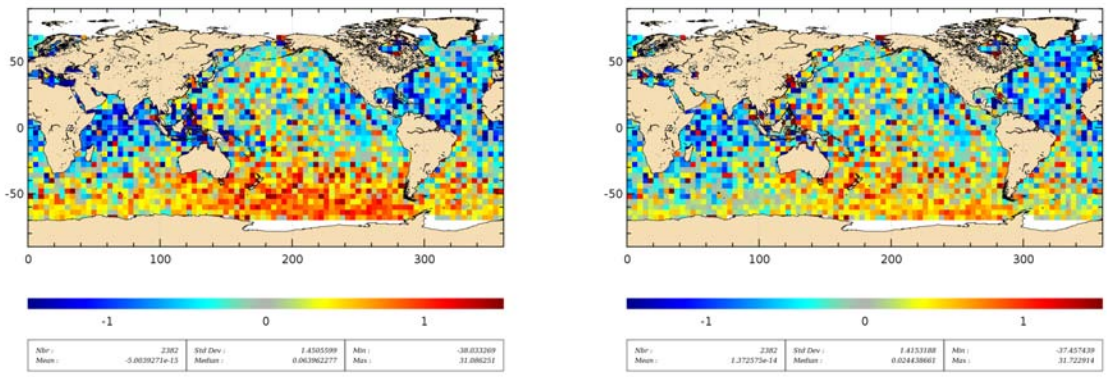

Figure 51: *Map of mean of SSH crossovers differences between Jason-2 and Jason-1 (JA1-JA2) for 2011 using POE-D orbit (left). The map is centered around the mean (10.06 cm). Right: same as left, but using 2012 sea state biais for both satellites. The map is centered around the mean (7.09 cm).*

For comparisons with Envisat, reprocessed V2.1 Envisat data were used, in addition GOT4.8 global ocean tide was updated. Though Jason-2 GDR-T and Envisat V2.1 are using CNES produced POE (POE-C standard), a large east/west bias is observed on the left side of figure 52, see also [36]. This is also seen on Jason-1/Envisat crossovers, especially since 2007 (see [39]). This behaviour is related to the gravity field used during orbit computation. When using Jason-2 GDR-D, as well as POE-D for Envisat (POE-D is based on EIGEN-GRGS_RL02bis_MEAN-FIELD gravity fiels), this east/west biased disappears, as shown on right side of figure 52 (see also annual report of Envisat 2011 [52]). The remaining structure is partly due to the different SSB models, especially in South Pacific and Mediterranean Sea, as these differences are decreased using OSTST 2012 sea state model for both satellites (as shown on bottom of figure 52). The remaining differences could be due to the ionosphere correction (as the dual-frequency ionosphere correction is no longer available for this period on Envisat) or other differences.

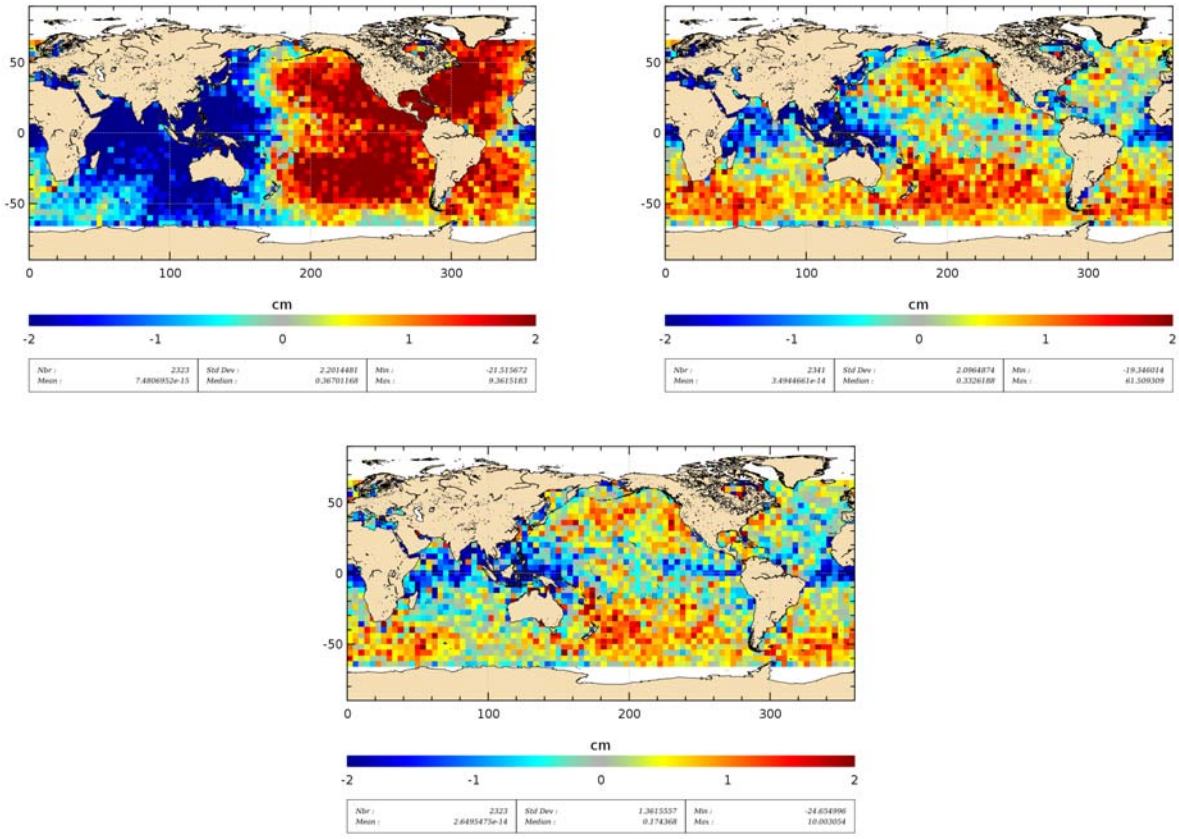

Figure 52: *Map of mean of SSH crossovers differences between Jason-2 and Envisat (EN-JA2) for 2011 using model wet troposphere correction. Left: Jason-2 GdrT (POE-C already included) and Envisat V2.1 data (POE-C already included). The map is centered around the mean of 28.64 cm. Right: Jason-2 GdrD (POE-D already included) and Envisat V2.1 data + POE-D standard. The map is centered around the mean of 46.18 cm. Bottom: Jason-2 GdrD and Envisat V2.1 data + POE-D standard + OSTST 2012 sea state bias (for both missions). The map is centered around 44.74 cm.*

5.4. Standard deviation of SSH crossover differences

The cycle by cycle standard deviation of SSH crossovers differences are plotted for Jason-2 and Jason-1 in figure 53 after applying geographical criteria (bathymetry, latitude, oceanic variability) as defined previously (chapter 5.1.). Both missions show very good performances, very similar and stable in time. No anomaly is detected (the value above 6 cm for Jason-1 is related to degraded orbit quality due to several inclination maneuvers during Jason-1 cycle 315). The average figure is 5.1 cm rms for Jason-1, 5.0 for updated Jason-1, and 4.9 cm rms for Jason-2 data. Keeping in mind that during the Jason-1/TOPEX formation flight phase in 2002, the same statistic using Jason-1 GDR-A products was close to 6.15 cm (see [37]). This illustrates the improvements performed in the altimetry ground processing since the Jason-1 launch especially thanks to new retracking algorithms, new geophysical corrections (oceanic tidal, dynamic atmospheric correction, ...) and new orbit calculations implemented first in GDR-B and later in GDR-C release (see [55] concerning impact of GDR-B/GDR-A, [31] concerning impact of GDR-C/GDR-B). The reprocessing of Jason-

2 in GDR-D also improved the performance at crossover points. The variance of SSH crossover differences was reduced by 1.7 cm2 when switching from GDR-T to GDR-D standards, as shown on [8]. The main contributors to this improvement are the POE-D orbit standard and the GOT4.8 global ocean tide. Though Jason-1 and Jason-2 show very good performances and are within the mission specifications, their standard deviation of SSH differences at crossovers is sometimes higher than usual.

When comparing the performances of the different Jason-2 data types (OGDR, IGDR, GDR) over 2013 (right of figure 53), OGDR have the highest standard deviation with 6.3 cm, though this value is already extremely good considering that OGDR have a latency of about 3h, recalling that Jason-1 GDR-A products had a standard deviation of 6.15 cm. IGDR data have a standard deviation of 5.1 cm over 2013.

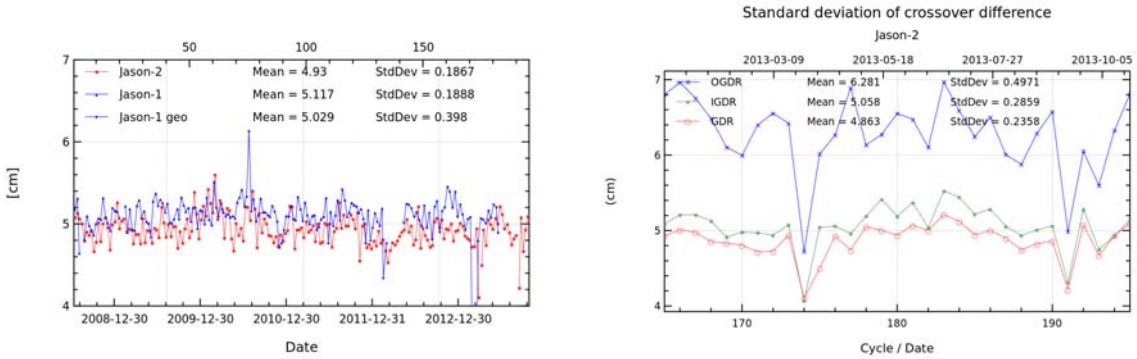

Figure 53: *Cycle by cycle standard deviation of SSH crossover differences for Jason-2 and Jason-1. Only data with abs(latitude) < 50°, bathymetry < -1000m and low oceanic variability were selected.*

5.5. Estimation of pseudo time-tag bias

The pseudo time tag bias (α) is found by computing at SSH crossovers a regression between SSH and orbital altitude rate ($\dot{H}$), also called satellite radial speed:

$$SSH = \alpha \dot{H}$$

This empirical method allows us to estimate the potential real time tag bias but it can also absorb other errors correlated with $\dot{H}$. Therefore it is called "pseudo" time tag bias. The monitoring of this coefficient estimated at each cycle is performed for Jason-1 and Jason-2 in figure 54. Both curves are very similar highlighting an almost 59-day signal with almost no bias (close to 0.01 ms for Jason-1 and -0.02 ms for Jason-2). Investigations are ongoing about the impact of the ocean tide solution on this signal.
Before the Jason-2 reprocessing the GDR-T showed a bias of -0.29 ms. The origin of this pseudo time tag bias was found by CNES [22] and so corrected in the GDR-D product, nevertheless the 59 day-signal is still unexplained. The constant part of the datation bias is corrected in the Jason-2 GDR release (see also the Jason-2 handbook [42]). Therefore the datation of Jason-2 GDR-T and GDR-D is not the same. For Jason-1 GDR-C products ([3], an empirical correction containing $\alpha \dot{H}$ has been already added to improve the Jason-1 SSH calculation.

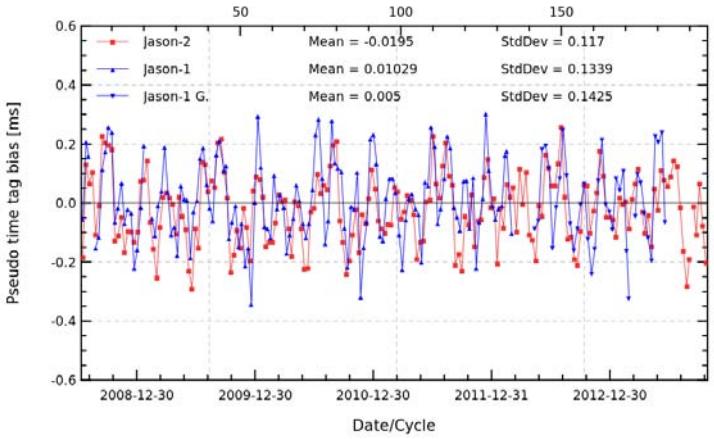

Figure 54: *Monitoring of pseudo time-tag bias estimated cycle by cycle from GDR products for Jason-2 and Jason-1*

6. Sea Level Anomalies (SLA) Along-track analysis

6.1. Overview

The Sea Level Anomalies (SLA) are computed along track from the SSH minus the mean sea surface with the SSH calculated as defined in previous section 5.1. :

$$SLA = SSH - MSS(CNES/CLS2011)$$

Note that Jason-2 GDR-D products contain MSS_CNES_CLS_2011. For better comparison with Jason-1, in this study MSS 2011 was also updated on Jason-1 data (in addition to the other updates: POE-D, GOT4.8, JMR replacement product).

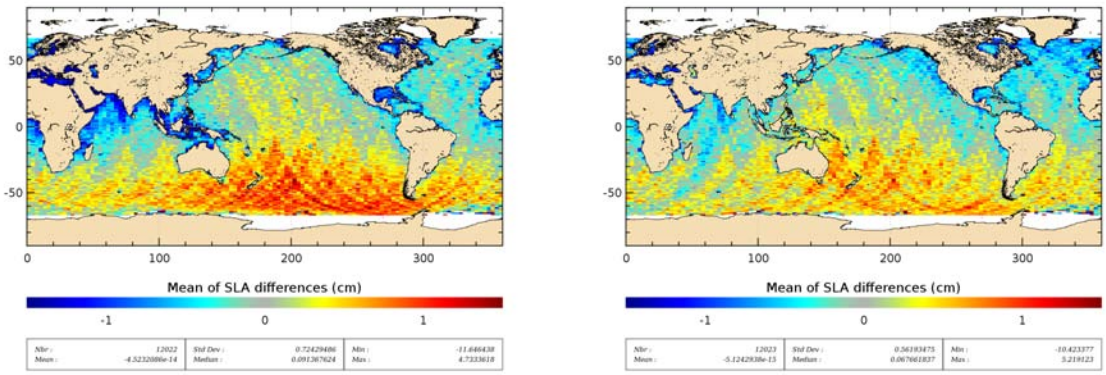

Figure 55: *Maps of SLA (orbit - range - geophysical corrections - MSS2011) mean differences between Jason-1 and Jason-2 during formation flight phase (cycles 1 to 20). Top left: using Jason-2 GDR-D and Jason-1 updated GDR-C (the map is centered around the mean of 10.24 cm). Top right: same as left, but in addition using for both satellites OSTST 2012 sea state bias (the map is centered around the mean of 7.26 cm).*

SLA analysis is a complementary indicator to estimate the altimetry system performances. It allows us to study the evolution of SLA mean (detection of jump, abnormal trend or geographical correlated biases), and also the evolution of the SLA variance highlighting the long-term stability of the altimetry system performances. In order to take advantage of the Jason-2/Jason-1 formation flight phase (cycles 1 to 20), we performed direct SLA comparisons between both missions during this period.

There are geographically correlated structures of up to ± 1.5 cm amplitude between Jason-2 GDR-D and updated Jason-1 GDR-C data (see left of figure 55). This is particularly the case for regions with low, but also high significant wave height. Most of this difference comes from the still different sea state bias models used on both satellites (see also chapter 4.9.). Updating both satellites with the OSTST 2012 sea state bias strongly reduces the differences, as shown on right side of figure 55. The remaining differences are due to orbit differences (though for both POE-D orbit standard was used), as shown on figure 56.

Corrections applied in SSH calculation are theoretically the same for Jason-1 and Jason-2 since both satellites measure the same ocean. Thus, it is possible to not apply them in order to obtain directly information on the altimeter range and the orbit calculation differences. However, as the stability of both ground passes is not exact (the ground track is maintained within a window of $\pm$ 1 km across-track distance from the theoretical ground track), SLA measurements have to be projected and interpolated over the Jason/TOPEX theoretical ground pass after applying the MSS in order to take into account cross-track effects on SSH.

$$\Delta SLA_{J1-J2} = [(Range_{Ku} - Orbite - MSS)_{J1}]_{\bar{T}} - [(Range_{Ku} - Orbite - MSS)_{J2}]_{\bar{T}}$$

This allows us also to select the intersection of both datasets and compare exactly the same data. After Jason-1 ground track change to its interleaved ground track, direct SLA comparisons are no more possible. Thus, global statistics computed cycle by cycle are just basically compared.

6.2. Mean of SLA differences between Jason-2 and updated Jason-1

Spatial uncorrected SLA (orbit - range - MSS) differences (only during the Jason-1/Jason-2 formation flight phase) between both missions as plotted in left side of figure 56 show a weak hemispheric bias lower than 1 cm. In addition, positive differences are stronger in South Pacific and negative differences are stronger in North Atlantic. These differences are in relationship with orbit calculation differences. Though for both satellites POE-D was used, there are some differences between Jason-1 POE-D and Jason-2 POE-D, for Jason-1 orbit computation the GPS data are no longer available, whereas they are used for the Jason-2 POE computation. Jason-2 POE-D is therefore based on three orbit determination techniques (Doris, GPS, Laser), whereas Jason-1 POE (over the Jason-2 period) is only based on two orbit determination techniques (Doris and Laser). On the right of figure 56 the difference between Jason-1 and Jason-2 uncorrected SLA is shown using for Jason-2 also a Doris/Laser orbit (instead of an Doris/GPS/Laser orbit, see also part *"Towards a nex Jason-1 orbit solution for climate studies"* in [17]). The hemispheric differences seems to be more homogeneous, but are still present. When using GSFC std 0905 orbits for both satellites (bottom of figure 56) the hemispheric bias disappears (the same result has been found using GSFC std 1204 orbit solution, but it is not shown here).

The cycle by cycle monitoring of mean SLA differences between updated Jason-1 data and Jason-2 is plotted in figure 57 over all the Jason-2 period. During the formation flight phase, the SSH bias is computed with and without the SSH corrections. During this period, both types of curves are very similar and stable in time with variations close to 1 mm rms. They are spaced out by a 3.3 cm bias (3.2 cm when using ECMWF model wet troposphere correction) resulting from differences between Jason-1 and Jason-2 sea state bias model used, and to a small amount due to ionosphere correction differences. The global average SSH bias is close to 10.3 cm using SSH corrections (10.2 cm when using ECMWF instead of radiometer wet troposphere correction) and 7.1 cm without. The differences between Jason-1 and Jason-2 are related to a small bias due to troncated altimeter PRF (-0.316 cm) before the geodetic ground track, the characterization file (-11.7 cm) and the antenna reference point (+18.09 cm), which sums up to a difference of 6.1 cm (see [57]). This is quite close to the curently observed value of 7.1 cm. These biases are present in Jason-1 data only as they were corrected in Jason-2 GDR-D data thanks to the 2012 reprocessing (see [11]), the correction will be applied to Jason-1 data during the 2014 reprocessing. However, the more crucial point for scientific applications is to insure that there is no drift between both missions,

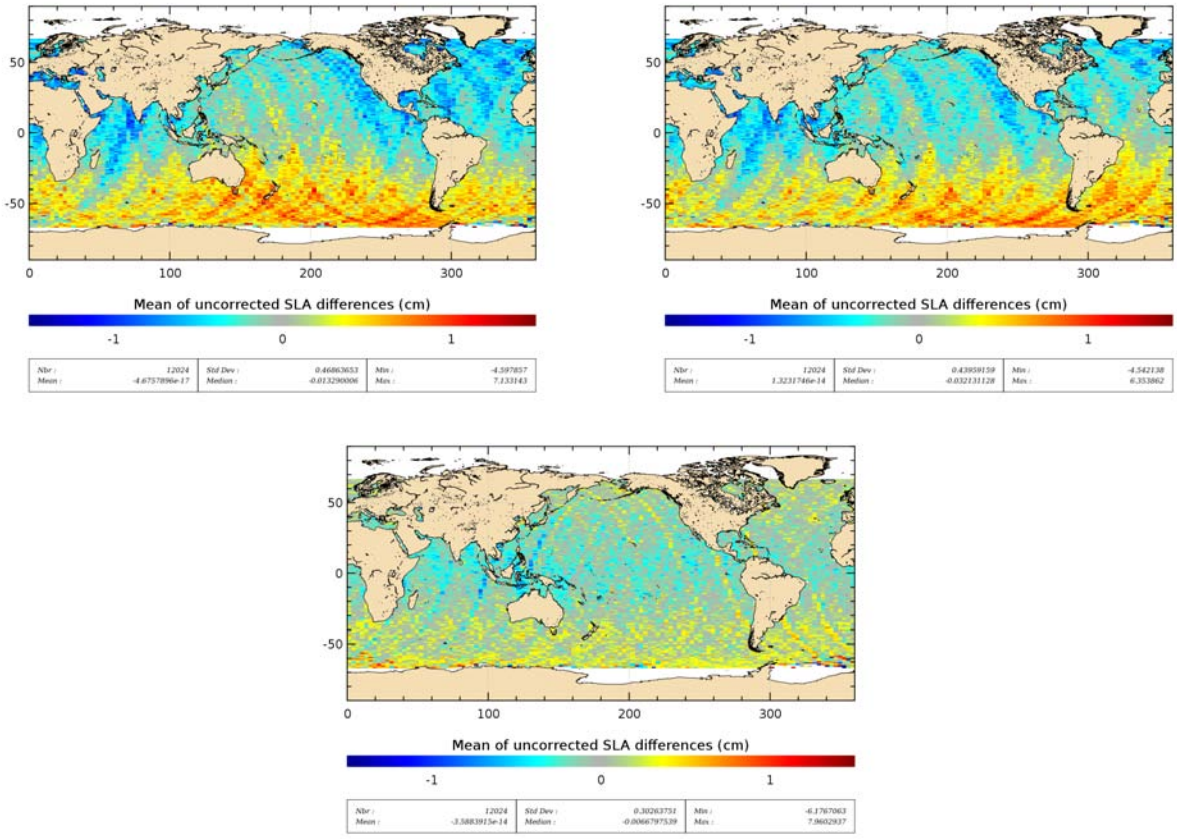

Figure 56: *Maps of SLA (orbit - range - MSS2011) mean differences between Jason-1 and Jason-2 during formation flight phase (cycles 1 to 20). Top left: using POE-D orbits. Top right: using POE-D orbit for Jason-1 and Doris/Laser POE-D orbit for Jason-2. Bottom: using GSFC09 orbits.*

since the global bias can be easily corrected a fortiori. The extension of the monitoring of the SSH bias after the Jason-1 ground track change is precisely a good way to check the long-term Jason-1 and Jason-2 stability. It is plotted over 195 cycles in figure 57. The curve using radiometer wet troposphere correction seems to show a small drift before the end of the Jason-1 repeat mission. This is not the case when using ECMWF model wet troposphere correction.
When Jason-1 was moved to a geodetic ground track, a jump is visible. It is slightly smaller when using ECMWF model wet troposphere correction than when using radiometer wet troposphere correction. Indeed from Jason-1 cycle 500 (geodetic ground-track) to cycle 527, a different JMR calibration file was used, accounting for a bias of 1 to 2 mm (a new JMR calibration file was also used after Jason-1 safe hold mode, from Jason-1 cycle 528 to 537, which can explain another smaller jump in March 2013). Furthermore, since the geodetic ground-track, Jason-1 PRF is no longer truncated (as it was previously). This accounts for a bias of 3.16 mm. Nevertheless a small part of the jump remains unexplained.

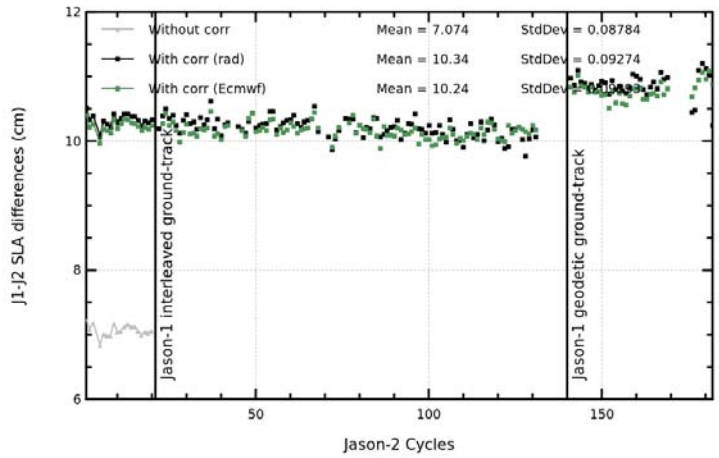

Figure 57: *Cycle by cycle monitoring of SSH bias between Jason-1 and Jason-2 before and after Jason-1 ground-track change (black curve and dots) and SSH bias without applying corrections in SSH calculation for both missions only during the formation flight phase (gray curve).*

6.3. Standard deviation of SLA differences between Jason-2 and Jason-1

The monitoring of SLA standard deviation has been computed for both missions, as well as updated Jason-1 standards over the whole data set (plotted in figure 58). The curves are very well correlated during the formation flight phase, as well as after Jason-1 moved to the geodetic ground-track. For the geodetic ground-track Jason-1 GDR-C contain the MSS CNES/CLS 2011 which is improved compared to the 2001 MSS ([43]) especially for ground-tracks outside the historical T/P-Jason ground track. During the Jason-1 interleaved repetitive ground-track (from Jason-2 cycle 21 to 134), Jason-1 standard deviation increases by 3 mm rms in average: 11.0 cm rms for Jason-1 instead of 10.6 cm rms for Jason-2. Similar feature was observed comparing Jason-1 and TOPEX performances after T/P satellite was moved on its new ground track in August 2002 ([37]). The new MSS CNES/CLS 2011 ([59]), using all the satellite tracks including the interleaved T/P and Jason-1 ground tracks - which was computed in the frame of the SLOOP project ([38]) - improves the SLA calculation also for the interleaved ground tracks. Cartography of standard deviation of spatial Jason-1 minus Jason-2 SLA differences (not shown here) does not show any anomaly. It varies indeed in function of noise on measurements, which is dependant on significant wave height. Therefore, standard deviation of SLA differences is higher in regions with important significant wave heights.
In addition to these results, a special investigation on SLA with 500km filtering is detailed in part 8.2..

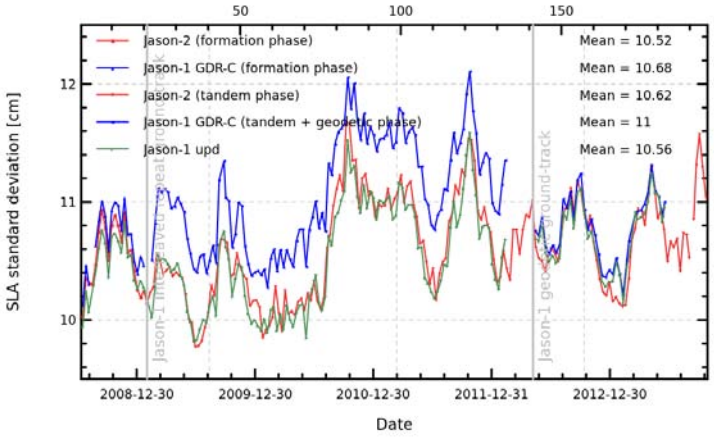

Figure 58: *Cycle by cycle monitoring of SLA standard deviation for Jason-1 and Jason-2.*

7. Mean Sea Level (MSL) calculation

7.1. Altimeter Mean Sea Level evolution

7.1.1. Mean sea level (MSL) calculation of reference time serie

The global mean level of the oceans is one of the most important indicators of climate change. Precise monitoring of changes in the mean level of the oceans, particularly through the use of altimetry satellites, is vitally important, for understanding not just the climate but also the socioeconomic consequences of any rise in sea level. Thanks to the T/P, Jason-1 and now Jason-2 altimetry missions, the global MSL has been calculated on a continual basis since January 1993 (figure 59) highlighting a trend of 3.16 mm/yr (see http://www.aviso.oceanobs.com/msl). We connect Topex/Poseidon and Jason-1 at Jason-1's cycle 11 (May 2002) by applying a bias of 8.45 cm to Jason-1's MSL. We replaced Jason-1 by Jason-2 in the MSL time data series at Jason-2 cycle 11 (October 2008) applying a SSH bias between both missions of -10.67 cm as calculated previously (in addition to the bias between Jason-1 and Topex/Poseidon). The altimeter standards used are described on Aviso website (http://www.aviso.oceanobs.com/en/news/ocean-indicators/mean-sea-level/processing-corrections.html). Note that Jason-2 GDR-D data and Jason-1 GDR-C data (only updated for GOT4.7 and JMR replacement product (cycles 228 to 259)) were used. To calculate a precise MSL rate, it is essential to link accurately time data series together. A study ([1]) showed the uncertainty on the global MSL trend resulting from the impact of MSL bias uncertainties between TOPEX-A and TOPEX-B (due to altimeter change in February 1999) and between TOPEX-B and Jason-1 (in May 2002) is close to 0.2 mm/yr from 1993 onwards. As we showed just previously, the SSH consistency between Jason-1 and Jason-2 is very good in space and stable in time during the formation flight phase, the SSH bias uncertainty is consequently very weak and close to 0.5 mm. It is lower than between T/P and Jason-1 (estimated close to 1 mm ([1])). Its impact on global MSL trend error budget is thus very weak: lower than 0.05 mm/yr.
Notice, that MSL decreased in 2010/2011, similar, but much stronger to what was already observed in 2007. According to Boening et al. ([20] and [21]) the global mean sea level drop of 5 mm between beginning 2010 and mid-2011 is due to a decline of ocean mass coinciding with an equivalent increase in terrestrial water storage (primary over Australia, northern South America and Southeast Asia). The authors write, that this temporally shift of water from ocean to land is closely related to the transition from El Niño conditions in 2009/2010 to a strong 2010/2011 La Niña which affected precipitation patterns world wide. As these terrestrial water mass are not directly linked to the ocean (thanks to rivers for example), they can only return to ocean thanks to evaporation. This process is long, which could explain the rise in GMSL in 2012.

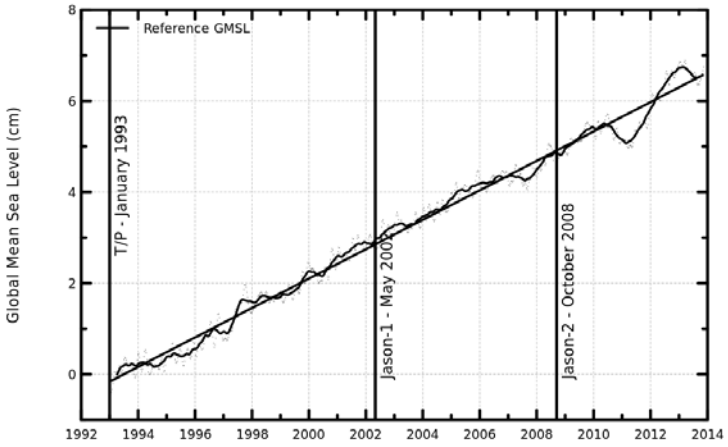

Figure 59: *MSL evolution calculated from T/P, Jason-1 and using Jason-2 data from october 2008 onwards. GIA (-0.3 mm/yr, [54]) is applied.*

7.1.2. Regional and global mean sea level trend for Jason-2

Although, 5 years of Jason-2 is still a short time period for MSL trend calculation, it is possible to compute a MSL trend. Nevertheless, slope values are to be taken with caution and are rather used to compare between several standards. Due to the short period, slope values change much when passing from one period to another period. Using radiometer wet troposphere correction increases for Jason-2 data the slope by around 0.3 mm/yr (left side of figure 60). Separating in ascending and descending passes, shows very similar slopes thanks to the POE-D standard (see right of figure 60). The amplitude of the MSL curve computed from descending passes is higher than for ascending passes. The difference between ascending and descending passes shows a signal of a period around 120 days (see also chapter 5.2.), and difference of MSL slopes (MSL ascending passes - MSL descending passes) for Jason-2 is under 0.1mm/yr.

The regional MSL trends over the Jason-2 period (figure 61) show a small increase in western tropical pacific and a small decrease in eastern tropical pacific. This is probably influenced by the La Niña or neutral conditions which occured before mid-2009 and after mid-2010 ([68],[69]).

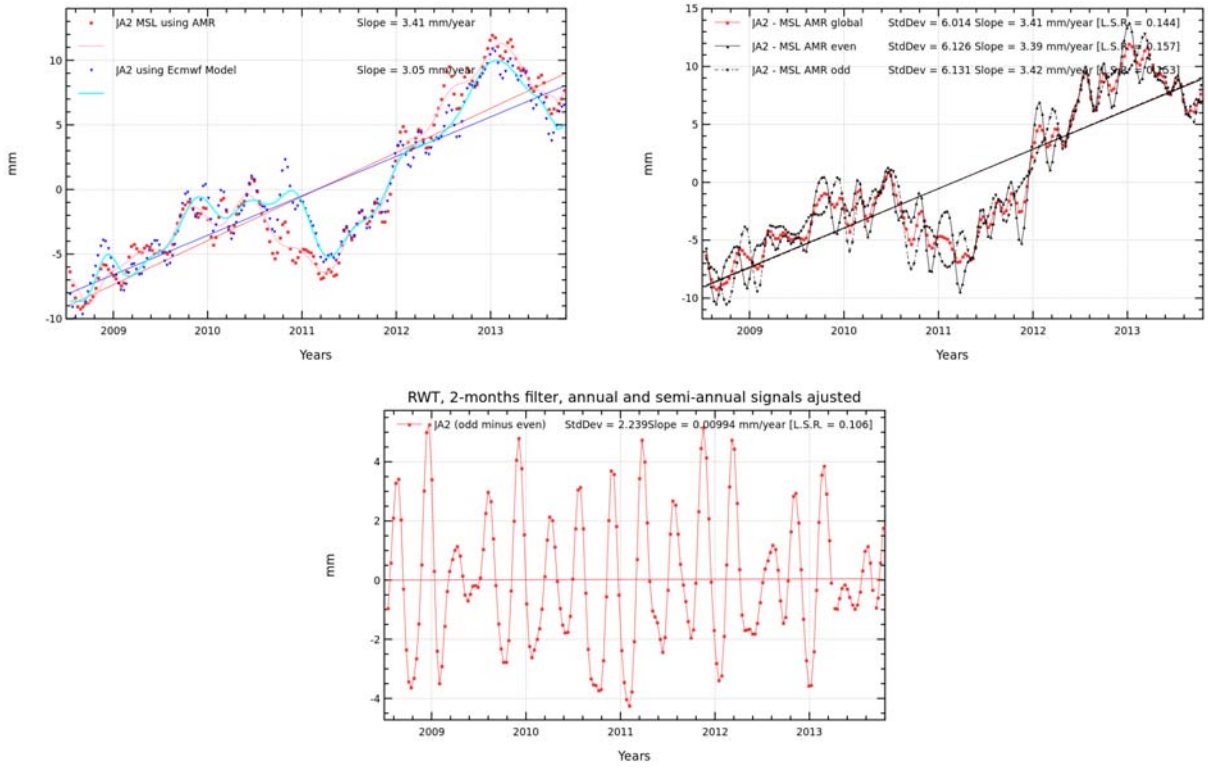

Figure 60: *Global MSL trend evolution calculated for Jason-2 (left). MSL trend evolution when separating in ascending and descending passes (right) , Seasonal signal (annual and semi-annual) is adjusted for top figures. Difference of MSL slopes (MSL ascending passes - MSL descending passes) for Jason-2. Slopes are computed for 2 month filtered data. GIA correction is not applied.*

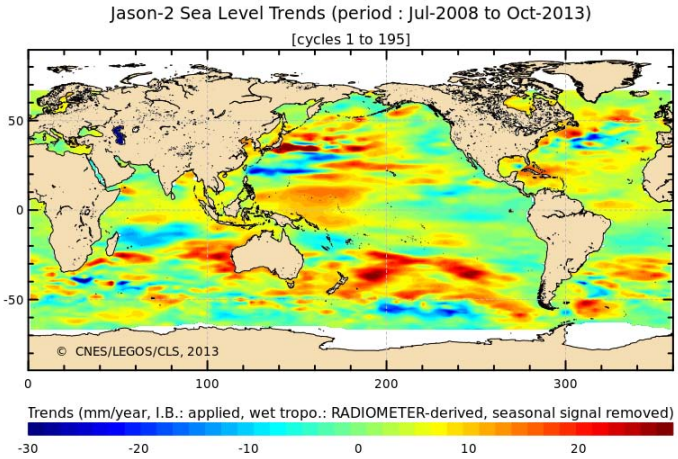

Figure 61: *Maps of regional MSL slopes for Jason-2 cycles 1 to 195, seasonal signal removed.*

7.1.3. Comparison to Jason-1

Global Mean Sea Level computed over common period of Jason-1 and Jason-2 (this study has been computed over about 4.5 years from July 2008 to February 2013) shows differences of about 0.7 mm/yr with radiometer wet troposphere correction (the bias between JA1 repetitive and JA1 geodetic has been corrected as described in [17]).

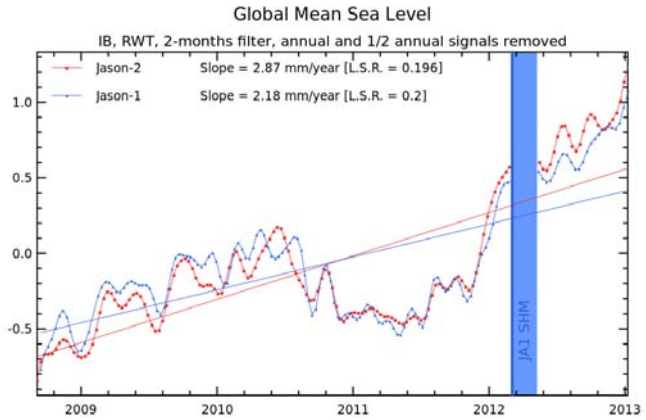

Figure 62: *Global Mean Sea Level using Jason-1 or Jason-2 data (with 2-months filter, with adjustment of the annual and semi-annual signals, no GIA applied*

To update Jason-1 data toward an homogeneous to Jason-2 solution allows to reduce the difference in GMSL trends between Jason-1 and Jason-2 (reduction of the difference of about 0.1mm/yr, see top right of figure 63). The radiometer drift between JMR and AMR explain 0.4mm/yr in the difference that remains (a difference of about 0.2 mm/yr is still unexplained between the two monomission GMSL when using a model wet troposphere correction, see bottom of figure 63).

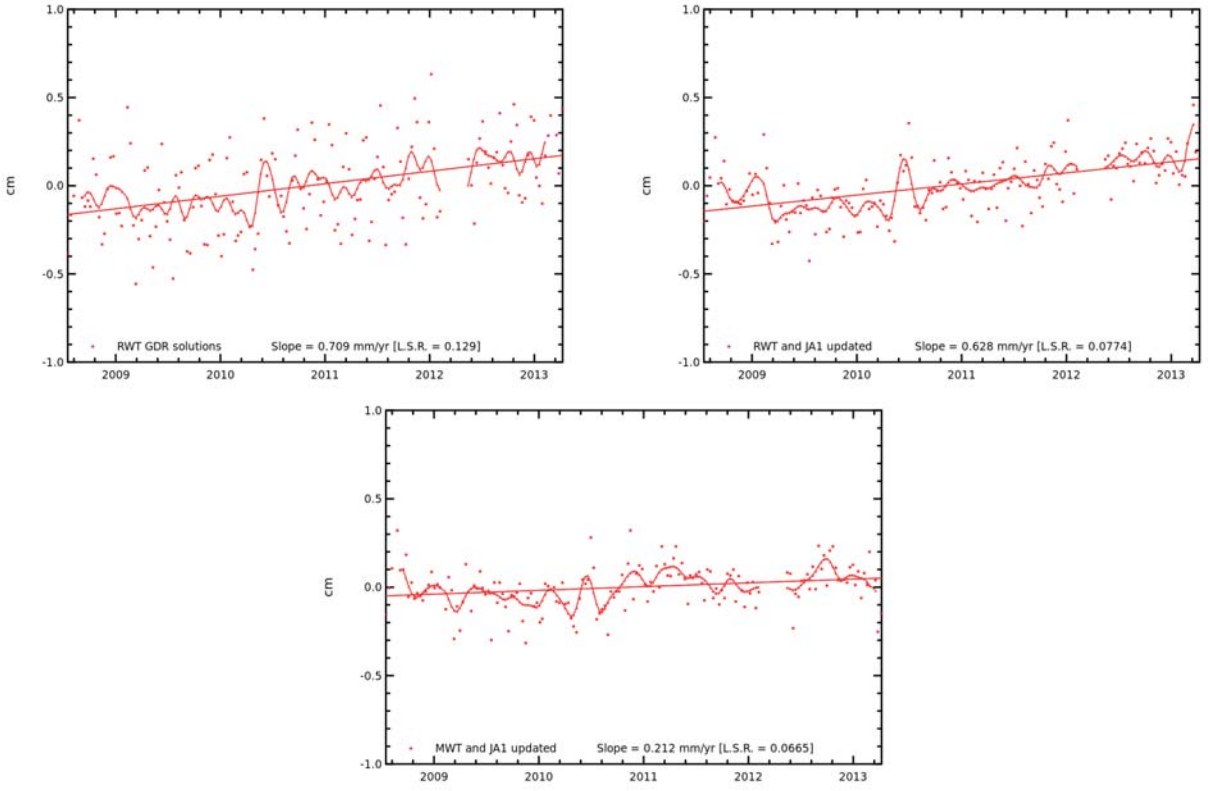

Figure 63: *Difference of Jason-2 GMSL – Jason-1 GMSL computed over Jason-2 cycles. Top left: with radiometer wet troposphere. Top right: with radiometer wet troposphere and Jason-1 updates. Bottom:with model wet troposphere and Jason-1 updates. (Jason-1 updates= homogeneous POE-D orbit, GOT4.8 tide, and MSS 2011*

7.2. External data comparisons

In order to assess the global MSL trend, comparisons to independent in-situ datasets are of great interest. Two methods have been developed in the frame of in-situ Calval studies and thoroughly described in annual reports ([15] and [16]).

7.2.1. Comparison with tide gauges

Firstly, Jason-2 altimeter data is compared with tide gauge measurements thanks to a dedicated method which aims at detecting potential drifts in sea surface heights (SSH). The tide gauge network processed is the GLOSS/CLIVAR "fast" sea level database, formerly known as the WOCE network. For more information on the method and more detailed results, please refer to the 2013 report of comparison between altimeter data and tide gauges ([15]).

From these comparison methods, SSH bias monitorings has been computed and is shown on figure 64. The comparison with tide gauges measurements provides consistent long-term trend differences (0.2 mm/year for Jason-1, 0.1 mm/year for Jason-2), with a low formal adjustment error, close to 0.1 mm/yr. The coherence with in-situ measurements along coastal areas is pretty good, and rms differences are lower than 4 cm. An annual signal appears, the origin of such annual signal in the time series of the differences is still unknown, see [15] for more explanation.

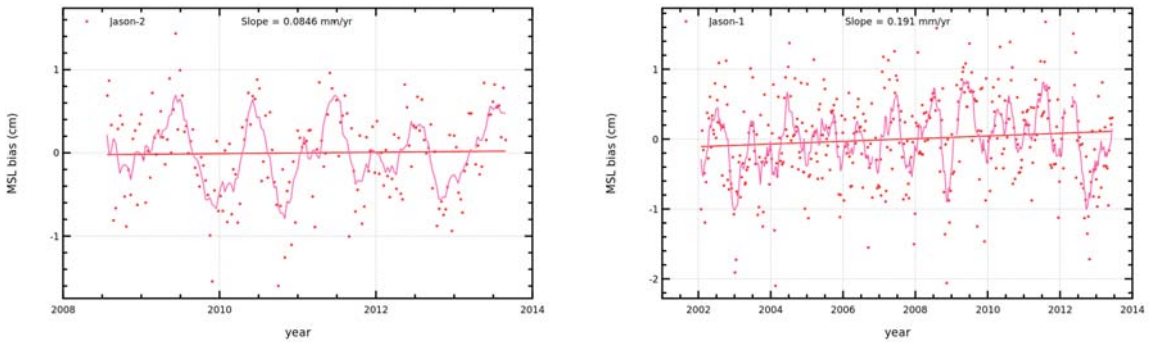

Figure 64: *Jason-2 and Jason-1 altimeter (with radiometer wet troposphere) MSL drift compared with tide gauges measurements*

7.2.2. Inter annual evolution of the altimeter residuals compared with Argo T/S profiles

Major improvements have been achieved in 2013 in order to improve the validation of altimeter data compared with Argo in-situ steric dynamic heights and the mass contribution. In particular, strong efforts have been made to better estimate the uncertainty of the method. Sensitivity studies have been performed in order to estimate the impact of the pre processsing of altimeter data, the varying length of the time series, the spatial sampling of Argo data and also the reference depth of integration of the in-situ steric dynamic heights. A new GRACE dataset (GRGS V2) has been taken into account to estimate the mass contribution to the sea level in order to improve the global comparison with altimeter measurements. Together with the steric in-situ dynamic heights from

Argo, it provides sea level estimations with the same physical content as the altimeter measurements and allow to reduce the uncertainty associated with the estimation of the absolute altimeter drift. The use of this GRACE dataset has required a correction of the Glacial Isostatic Adjustment to take into account the response of the solid Earth to the last deglaciation and thus compare altimetry and GRACE homogeneously. New tools and diagnoses have been integrated in order to improve the understanding of the signals at varying temporal ans spatial scales and improve the confidence in the results. As for the data processing, the reference period used to compute sea level anomalies has been increased to the 2003-2011 period and a new version of the processing chain has been developed so that it is more efficient and it automatically provides diagnoses in the context of systematic Cal/Val analyses. This work is performed in an operationnal framework which is essential to make this activity durable. For more details, see [16].
Figure 65 (left) presents the mean differences between altimetry and Argo+mass (GRGS V2) for Jason-1 (red), Envisat (blue) and Jason-2 (green) missions. As mentionned in the former section, a GIA correction is applied on these trends. An 0.7 mm/yr drift is observed for Jason-1 and 2.2 mm/yr for Envisat over 2005-2012.5 period. Concerning Jason-2, a 1.9 mm/yr drift is observed over its shorter period. When using SSALTO/DUACS altimeter merged products, a 1.1 mm/yr drift is observed over the 2005-2012.5 period (see [16]). The 1 mm/yr remaining drift of altimetry compared with Argo and GRACE measurements could have several origins:

- The reference level of integration used to compute steric dynamic heights. Indeed, as discussed in [16], this residual trend is affected by a change of reference depth of the steric heights.
- A leakage effect of the GRACE data around areas of strong continental ice loss (mainly Greenland but also Patagonia and Antarctic peninsula). A selection of data only at coastal distance greater than 500 km could help to assess whether this leakage effect has an impact on the residual altimeter drift.

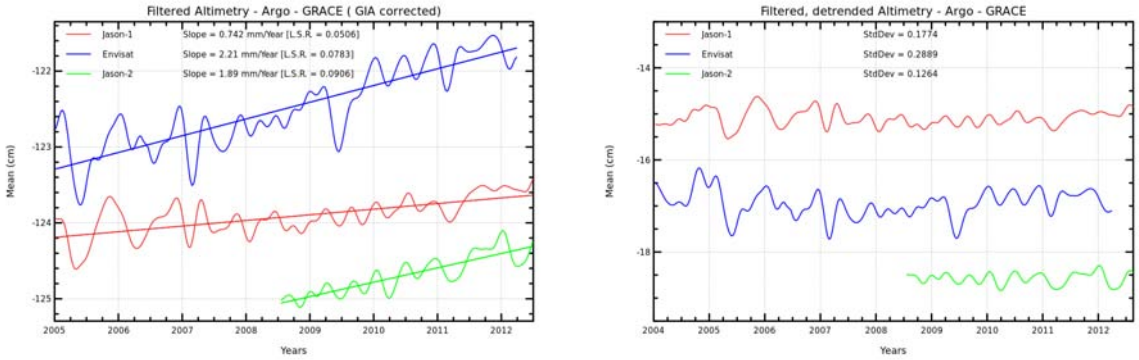

Figure 65: *Left: 3-months filtered mean differences between altimetry and Argo+mass (GRGS V2) for Jason-1 (red), Envisat (blue) and Jason-2 (green) missions with the GIA effects included. Right: idem after removing the trend.*

The analysis of the inter annual signals is made thanks to the detrended time series of the mean differences (figure 65, right). Over the total period, the standard deviation of the filtered time series is significantly higher for the Envisat mission than for Jason-1 (0.29 cm and 0.18 cm respectively). The difference of altimeter standards contributes to this difference. The value associated with Jason-2 over its shorter period (0.13 cm) is slightly reduced compared with Jason-1. At inter annual time scales, higher variability is observed both for Jason-1 (red) and Envisat (green) in 2005 and at the beginning of 2007. A drop of the Envisat signal is observed in 2009 but it is not detected with other altimeter missions.

8. Particular Investigations

This sections contains some particular investigations led on Jason-2 data during 2013.

8.1. 2013 Jason-2 safe hold modes

Jason-2 entered safe hold mode (SHM) by three times in 2013. Each time the first data after restart are particularly analysed in order to detect any anomaly due to SHM event.

8.1.1. The first two Safe hold modes for Jason2

The Jason-2 mission was interrupted two times in two weeks in March and April. Missing measurements due to the first Safe Hold Mode occured from 25 March at 02:42 UT to 29 March 2013 at 17:53 UT, impacting 174 cycle. Missing measurements due to the second SHM occured from 30 March at 21:57 UT to 05 April 2013 at 14:19 UT, impacting 174 and 175 cycles. After the second SHM, Jason-2 was switched from payload module A to payload module B.

Jason-2 OGDR, IGDR and GDR data comparison for significant altimetric fields were studied just after restart. When comparing Jason-2 pass statistics before and just after the safehold events, no noticeable differences can be found, except for mispointing, which seems slightly more centered around zero just after the second safehold mode and less centered around zero since the routine daily LTM calculation had been resumed (see figure 66). The differences observed (for mispointing, backscatter coefficient and altimeter wind) between Igdr and Ogdr data on 09/04/2013 can be explained as the old LTM (calculated from 24/03/2013) were used to compute the data for days 05, 06, 07 and 08 of April whereas the 09 of April results were computed with the LTM calculated from 08/04/2013 only for Igdr data.

8.1.2. A third safe hold mode event in september 2013

The Jason-2 mission was interrupted on 05 September 2013 at 09:26, during cycle 190 (last measurement 07:44:17). Jason-2 payload science instruments were returned to operation on 12/09/2013 with a first data at 12:25 for POSEIDON and at 21:54 for AMR. Pass and daily statistics on Jason-2 OGDR and IGDR data were studied. *Please note that daily statistics for julian day 23265 (2013-09-12) are not relevant as there are computed with only two entire passes with valid data on this day because of no AMR data.*

Ku-band Significant Wave Height, dual-frequency ionosphere correction, Ku-band backscatter coefficient, Altimeter Wind speed, standard deviation of range, radiometer and SLA were analysed, but not shown here. All seem not to be impacted by SHM event. The daily evolution are coherent with what is observed thanks to other missions.
The SHM event had little impact on the mispointing, tough mispointing values were slightly more negative just after the SHM (see 67).

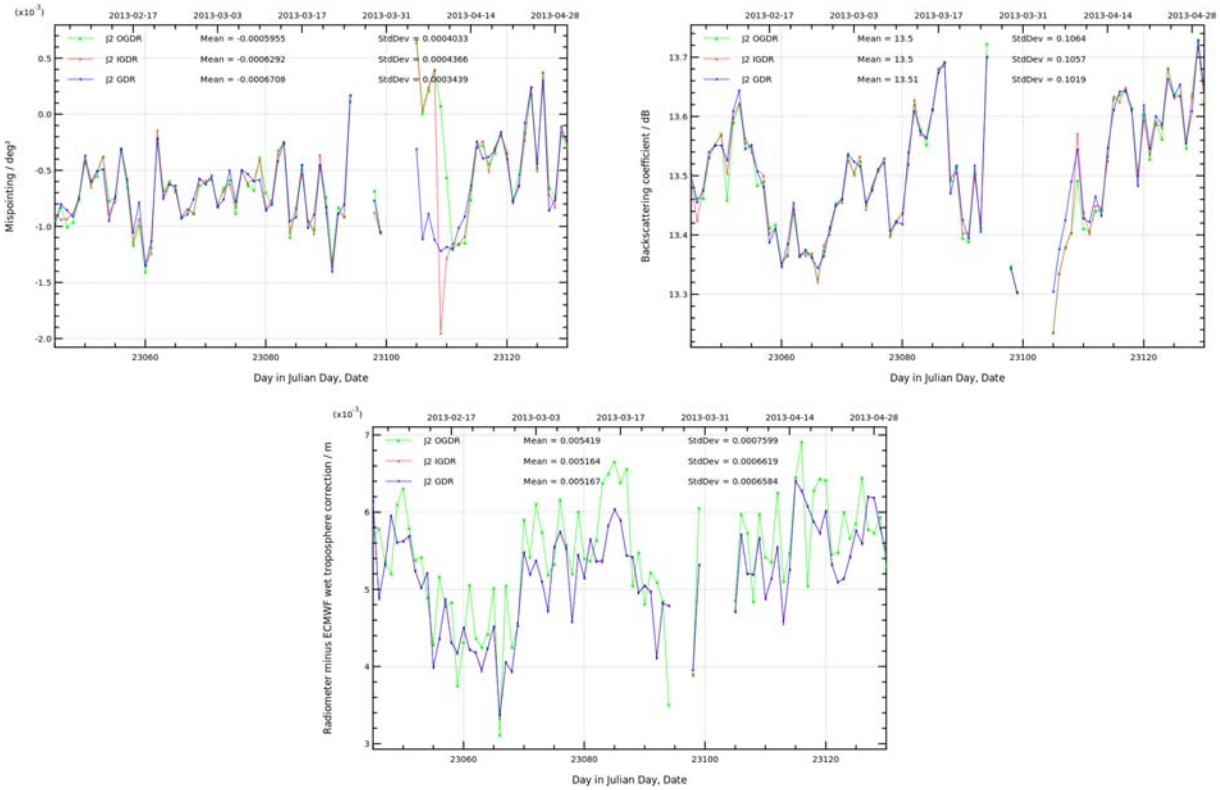

Figure 66: *Monitoring per day of mispointing (top left), backscattering coefficient (top right) and Radiometer minus ECMWF wet troposphere correction (bottom) during safe hold mode periods in March and April 2013.*

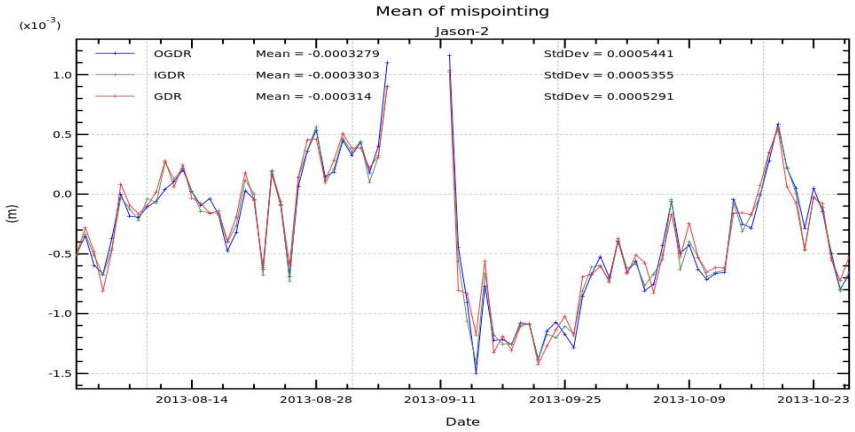

Figure 67: *Monitoring per day of mispointing around safe hold mode periods in September 2013.*

8.2. Standard deviation of along-track SLA for Jason1 and Jason2

In this part, the impact of selection (on latitude, bathymetry and ocean variability) and filtering (wavelengh of 500km) on SLA are studied. The results are shown on figure 68 in terms of standard deviation of Jason-1 and Jason-2 SLA after along track filtering.

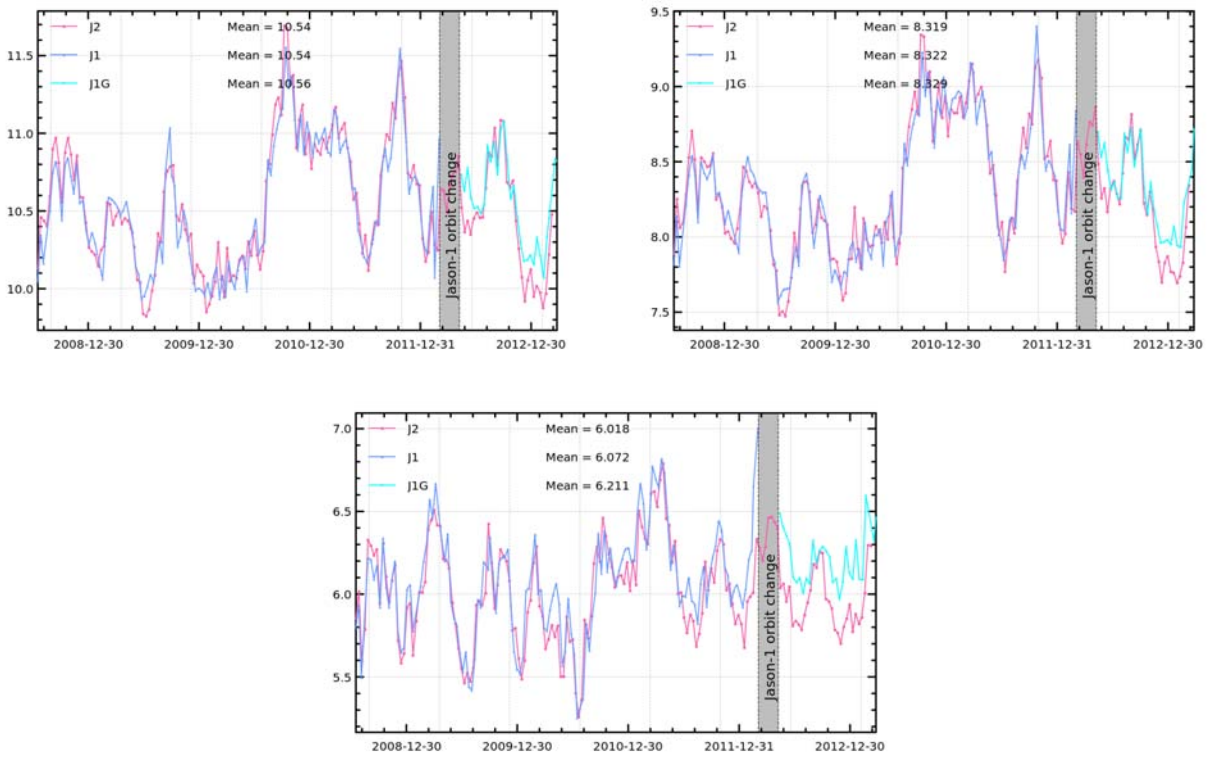

Figure 68: *Standard deviation of along-track SLA differences for Jason-1 and Jason-2, depending on different selection : without any filtering (top left), only considering wave-lengths lower than 500 km (top right), only considering wave-lengths lower than 500 km with latitude defined in [-50°,+50°] interval, bathymetry lower than -1000m and ocean variability lower than 0.1m (bottom)*

This comparison has been performed computing SLA relative to CNES/CLS11 Mean Sea Surface. The CNES/CLS11 MSS is dertermined from seven satellite missions (Topex, ERS1, ERS2, Jason1, Topex interleaved mission, GFO and Envisat) whereas Jason2 data were not inclused because the data set used for the determination of this MSS comes from work done in 2009 using data validated up to 2008.

The monitoring of Jason-1 and Jason-2 SLA standard deviation removing also wavelengths lower than 50 km are not shown on figure 68 but only for wavelenghts from 0 to 500 km, nevertheless they were computed and the results show no significant differences to be noted in our study case. Without any filtering or selection, standard deviation average around 10.5 cm for both missions (top left). The main part can be found with 500km filtered SLA (about 8.3 cm on the figure on top right). Finally, removing water areas with $|latitude|$ higher than 50°, bathymetry above -1000m and high oceanic variability, the standard deviation of SLA decreases to 6.0 to 6.1 cm.
The standard deviation curves obtained for Jason-1 and Jason-2 are similar when the two satellites are flying on the same orbit (during the repetitive phase for Jason-1), so before the Jason-1 orbit

change (move to the geodetic one). There is no impact of a selection done on latitude, bathymetry and ocean variability on the period when Jason-1 is on its repetitive phase. However, differences are more significant between both missions after the Jason-1 orbit move to geodetic phase and more stronger with selection active on latitude, bathymetry and ocean variability. During the geodetic Jason1 period, the signature of MSS errors appears in all graphs of figure 68 even if no filtering and no selection are used. The main difference come from the ground track move of Jason1 and must be taken into account in the next MSS computation.

8.3. Study of a doris only solution for Jason-2 and Jason-1 (in order to analyse remaining geographical biases)

The consistency between Jason-1 and Jason-2 during the flight formation phase is very good. Using CNES POE_D solutions for the orbit, a fine North/South signature is visible yet, with impact on the long term trend estimation at regional scales when connecting the two consecutive missions (it can be corrected empirically afterwards but datasets without this regional differences are preferable for climate studies). Those fine North/South descrepencies are observed using CNES GDR-D solutions but not with GSFC_0905 solutions neither with GSFC_1204 solutions, which are based on Doris/Laser data.
CNES POD team computes routinously, besides the official POE-D solutions, also Doris only solutions for Jason-2. In order to evaluate the impact of the way data from Doris system are included in orbit computation, this Doris only solution has been used in comparisons with different solutions for the Jason-1 orbit. The detailed results are presented in [17].

8.4. Impact of orbits based on the last gravity field: GFZ-GRGS EIGEN6S2

Thanks to analysis of SSH differences at Jason-1/Envisat crossovers, a residual from the time gravity model was found in the GDR-D orbits. These orbits include the gravity field named EIGEN-GRGS_RL02bis_MEAN-FIELD and are a linear fit over the GRACE period (see OSTST 2012 presentation by Luca Cerri). A new orbit solution has been computed and analysed this year, using the new gravity field named EIGEN6S2 (linear interpolation per piece over one year interval and includes interannual variability). For more information on this new gravity field consideration, please refer to http//grgs.obs-mip.fr/grace/variable-models-grace-lageos/mean_fields.
The two solutions are compared to a GRACE10days solution, based on Grace only measured every 10 days without any model applied and that constitute a very stochastic reference. The detailed results are presented in [19]. As a result, this study shows that taking into account the new gravity field in the POE is better to restitute the interannual variability of the signal. Jason-1 and Jaon-2 are less sensitive to the gravity than Envisat due to their altitude and weight, so that this effect is less important (but noticeable) on these missions. The impact of the EIGEN6S2 gravity field compared to GRD-D is negligible on global MSL and considered as small, but not negligible, on interannual signals for Jason missions (see left of figure 69). The standard deviation of the difference is also higher at the end of the period for the three altimetric missions, due to the fact that GDR-D gravity field was built on GRACE data for a period going from 2002 to 2011 only (see right of figure 69).
The impact on mesoscale (10 days crossovers variance) is estimated, and the error made at mesoscale is comparable to the one obtained with the POE-D solution.
As a conclusion, using the EIGEN6S2 gravity field instead of EIGEN-GRGS_RL02bis_MEAN-FIELD as in GDR-D standards

- has a negligible impact to restitude mesoscale,
- is not significant to change the global MSL
- but improves the long term evolution of regional mean sea level (see Jason-1/Envisat comparisons in [17]).

Its use is recommended for Envisat and Jason-1 for climate oriented studies.

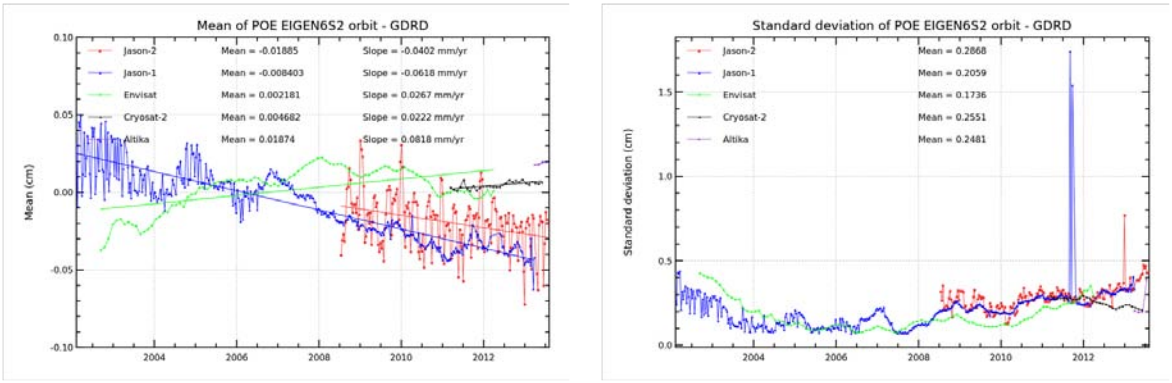

Figure 69: *Mean and standard deviation of difference EIGEN6S2/GDR-D for altimetrics missions*

8.5. Error budget of the Jason-2 mission

8.5.1. Introduction

The objective of this part is to provide an estimation of the global error budget of Jason-2 altimeter level 2 products: OGDR, IGDR, GDR (the naming convention of these products is JA2_(O/I/G)PN). Please note that the results presented here have been obtained using GDR data version D. The main goal is to provide a synthetic table with all the global errors estimated versus each level-2 products. The global errors have been estimated for several instrumental parameters but also geophysical corrections. In order to clarify and explain how each error has been calculated, dedicated sections have been performed with illustrations for all the errors described in the table. It is also very important to mention that the errors described here do not take into account long-term errors impacting climate implications as long-term drift, periodic signals (annual, semi-annual or 60-day signals) and isolated jumps for instance. We also do not describe the spatial repartition of errors but only the mean error at global scale. For most of the parameters presented in Table 70, the errors have been averaged spatially and temporally over a short period (∼10 days).

8.5.2. Description of the error content

Several types of errors can be defined in order to describe the error of altimetry measurements. These errors are depending on time and spatial scales. For time scales, the following errors are defined:

- White noise: this error is uncorrelated on time and is due most of the time to the instrumental measurements (altimeter).
- Short-time temporal error (< 10 days) : these errors includes all the error uncorrelated and correlated on time for time scales lower than 10 days. It is important to define these errors for oceanographic applications in relationship with mesoscale or sub-mesoscale studies.
- Medium temporal errors (2 months – 1year) : these errors include all correlated temporal errors at medium scales such as for instance periodic signals (annual, semi-annual,..). The description of these errors is useful for climate application.
- Long-term errors (> 1 year) : these errors include inter-annual and drift. It is the most important for climate applications as the global mean sea level evolution.

The purpose of this document is not to describe all these errors although it would be very useful. On the one hand, currently, we are not able to describe the errors at all these temporal scales and on the other hand there is not a clear way to merge all these errors together to calculate the average error. Therefore, our concern hereafter is to focus only on short-time temporal errors (< 10 days) and provide a synthetic view of these errors. Indeed the Jason-2 cycle duration is about 10 days (like it was already the case for Jason-1 and Topex/Poseidon). The ocean is therefore globally covered within the 10 days period. Several diagnostics based on almost 10 days periods were already developed in the frame of the validation of the altimeter data (see also chapter 8.5.3.) and can be used for the estimation of the error budget. Furthermore, the ocean state varies only slightly within a 10 days period (except for high variability regions, such as the Gulf Stream). Notice also, that the spatial repartition of these errors has not been described. Only the global mean error have been calculated in order to simplify the approach.

8.5.3. Method to determine the error

Assessing the errors of the different altimeter parameters and geophysical corrections is not straight forward. Several methods can be used, in order to compute the errors. Furthermore errors are different in function of spatial and temporal scales. In the following, only global mean errors are considered. When not mentioned otherwise, errors within a 10-day period (which equals a Jason-2 cycle) are computed.

Using formation flight phase of Jason-2 with Jason-1
Concerning the altimeter parameters, the formation flight phase, when Jason-1 and Jason-2 overflew the same ground track with only 55 seconds delay, is very useful. During the first 20 cycles of Jason-2, direct differences of Jason-1 and Jason-2 (collocated) 1 Hz measurements can be computed. Due to the short time delay, the assumption that both satellites measure the same quantities can be made. These measurements contain errors compared to the unknown truth. Assuming that both missions contribute equally to the error, the standard deviation of the Jason-1/Jason-2 differences divided by square-root of 2, gives the error of the measured parameter. This error can potentially include the measurement noise (if it exists for the studied parameter), but also errors on time scales less than 10 days. Nevertheless, this is the minimum threshold of the error, since both missions might be impacted by the same errors, which can not be seen when just comparing Jason-2 and Jason-1. For instance, the similarity of altimeter and retracking method, as well as algorithms to retrieve the wet troposphere content derived from radiometers, the identical atmospherical and geophysical corrections (dry troposphere, ocean tides ...) prevent the estimation of the whole error budget.

Spectral analysis
The spectral analysis of a signal allows to identify the repartition of the energy of this signal in the frequency spectrum and contains information about the spatial (wavelength in km) scales implied. The method consists in averaging N Fast Fourrier Transform computed over samples of M along-track points. The length of the samples is 300 points or 15 s for 20 Hz data. The bandwidth analysed with this method concerns frequencies between the invers of the spectrogram window's size and Shannon frequency (inverse of two times the sampling period). These frequencies can also be converted into distances with the relation: $Distance = Ground\_Satellite\_Speed/Frequency$ with Ground_Satellite_Speed equal to 7 km/s.
For 20 Hz data, analysed frequencies are:

- between 0.1 and 15 s
- between 0.07 Hz (1/15 seconds) and 10 Hz (20 Hz/2)
- between 700 m and 105 km

The power spectrum of a real physical signal containing measurement noise can be regarded as decreasing spectrum added to a white noise spectrum which is an uniform plateau (energy equally distributed on all frequencies). The high frequency plateau can therefore be interpreted as the noise level of the data. The value of the plateau is

$$\alpha = 2 * \Delta t * \sigma^2 \quad (1)$$

where σ is the standard deviation of the white noise.

Analysing rms of 20Hz data (Range, SWH, Sigma0)
In the Jason-2 products, the rms of the 20 Hz altimeter parameters is available (for range, significant wave height, backscattering coefficient, ...). This rms of the elementary Ku-band parameters can be averaged over a certain period in function of significant wave height. Only valid data are used (using the method described in Ablain et al. (9 :RD 4)). The mean value of the rms of the 20 Hz altimeter parameters for significant wave height of 2 m (most of measurements have significant wave heights around 2 m), corresponds approximately to the 20 Hz measurement noise of the altimeter parameters. According to Zanife et al. (9 :RD 13), this value can be approximately related to the 1Hz using the decorrelation assumption of the high rate data over 1s. Assuming full decorrelation, the division by square root of 20 (20 elementary measurements) results in the 1 Hz data noise.
Therefore, this approach give the same kind of information (white noise of altimeter parameter) than the spectral analysis just previously described. It is easily applicable but only for the range, SWH and Sigma-0 parameters.

Comparison with other corrections
For some corrections, several versions exist (for example dry troposphere correction derived from different models). The mean and standard deviation of the correction differences gives an indication of the accuracy and the noise of the correction. Furthermore at crossover points, the impact of using either one or another correction in the Sea Surface Height computation can be analyzed. Therefore the explained variance of a correction is analyzed for the ascending / descending SSH differences at crossover points. These differences are computed for time differences less than 10 days between ascending and descending tracks. This allows us to minimize the contribution of the oceanic variability (mesoscale). Therefore the variance of the SSH differences at crossover points gives an information of the performance of the altimeter system. Computing the differences of these variances (one using one version of the correction, one using another version of the correction), allows to measure the ability of the correction to improve the computation of the SSH. Assuming the error is the same on both corrections, this difference of variance has to be divided by 2, as errors on ascending and descending tracks are additive. This type of analysis gives therefore access to errors concerning timescales less than 10 days (on average, the time differences at 10-day crossovers is 3.5 days for Jason missions). This means that analyzing 2 corrections where one has experienced improvements concerning long-term periods (e.g. annual signals, long-term trends, ...), this improvement will not be visible with this type of analysis.

Intercalibration with other altimeter missions
Another way to assess errors on parameters or corrections is to intercalibrate different altimeter missions. Especially correction (or parameter) differences at multi-mission crossover points with small temporal interval (1h or 3h) are useful. The drawback is that there are relatively few crossover points with such a small time interval. This gives access to errors concerning timescales of less than 1 or 3 hours.

Bibliography and theoretical considerations
Finally, several authors have already studied errors on several parameters and corrections. The studies, which are taken into account in this document are listed hereafter:

RD 1 Abdalla,S., P. Janssen, and J.-R. Bidlot. 2010. Jason-2 OGDR Wind and Wave Products: Monitoring, Validation and Assimilation. Marine Geodesy. Vol. 33 (S1):239-255.

RD 2 Abdalla,S., P. Janssen, and J.-R. Bidlot. 2011. Altimeter Near Real Time Wind and Wave Products: Random Error Estimation. Marine Geodesy. Vol. 34:393-406.

RD 3 Ablain, M., A. Cazenave, G. Valladeau, and S. Guinehut. 2009. A new assessment of the error budget of global mean sea level estimated by satellite altimetry over 1993-2008. Ocean Sci.. 5: 193-201.

RD 4 Ablain, M., S. Philipps, N. Picot, E. Bronner. 2010. Jason-2 Global Statistical Assessment and Cross-Calibration with Jason-1. Marine Geodesy. Vol. 33 (S1): 162-185.

RD 5 Cerri, L., J.P. Berthias, W.I. Bertiger, B.J. Haines, F.G. Lemoine, F. Mercier, J.C. Ries, P. Willis, N.P. Zelensky, and M. Ziebart. 2010. Precision Orbit Determination Standards for the Jason Series of Altimeter Missions. Marine Geodesy. Vol. 33 (S1):379-418.

RD 6 Chelton, D.B. 1994. The sea state bias in altimeter estimates of sea level from collinear analysis of TOPEX data. JGR vol. 99, C12, pp. 24995-25008.

RD 7 Chelton, D.B., J.C. Ries, B.J. Haines, L.-L. Fu, and P.S. Callahan. 2001. Satellite Altimetry. In Satellite Altimetry an Earth Sciences, eds. L.-L. Fu and A. Cazenave. San Diego, CA: Academic Press, pp. 1-132.

RD 8 Gaspar, G., F. Ogor, P.-Y. LeTraon, and O.-Z. Zanife. 1994. Estimating the sea state bias of the TOPEX and POSEIDON altimeters from crossover differences. JGR vol. 99, C12, pp. 24981-24994.

RD 9 Lambin, J. and C. Tourain. 2007. OSTM/ Jason-2 System Performances Budget. TP3-J0-NT-909-CNES.

RD 10 Lillibridge, J., R. Scharroo, G. Jacobs, L. Russell, and V. Tabor. 2011. Marine Geodesy. Vol. 34:191-213.

RD 11 Compte Rendu de la Réunion RESTO. 3rd January 2012.

RD 12 Salstein, D., R. Ponte, K. Cady-Pereira. 2008. Uncertainties in atmospheric surface pressure fields from global analyses. J. Geophys. Res., 113, D14107, doi:10.1029/2007JD009531.

RD 13 Zanife, O.Z., P. Vincent, L. Amarouche, J.P. Dumont, P. Thibaut, S. Labroue. 2003. Comparison of the Ku-Band Range Noise Level and the Relative Sea-State Bias of the Jason-1, TOPEX, and Poseidon-1 Radar Altimeters. Marine Geodesy. Vol. 26, 201-238.

RD 14 OSTM/Jason-2 Product Handbook. SALP-MU-M-OP-15815-CN. Issue 1 rev 4. August 3, 2009

Table 9: Reference documents

8.5.4. Description of the error budget

Description of the level-2 Product
All products for Jason-2 (ODGR, IGDR, and GDR) are generated using the MLE4 (maximum likelihood estimator) ground retracking algorithm. Therefore, the figures concerning the altimeter parameters derived from waveforms are identical whatever type (OGDR, IGDR, GDR) of product is used. In reality, this could slightly be different as time differences may occur between 1 Hz OGDR and IGDR data (see Lillibridge et al. 2011, 9 :RD 10). OGDR, IGDR, and GDR products differ mainly by the orbit, as well as some corrections coming from models (using either predicted or analyzed fields). For these corrections, the performance results are discussed separately for the three product types. The whole GDR data are homogeneous in version D. OGDR and IGDR data have been disseminated in product version D since August 2012.

Description of the parameters/corrections analysed
The analyzed parameter/corrections have either directly or indirectly an impact on the sea surface height. Hereafter we divide the parameters/corrections in 3 groups. The first group contains the parameters/ corrections for the raw sea-level height calculation. Raw sea surface height is here defined as: Orbit – range – corrections which have a direct impact on the path delay. The second group contains corrections which have not an impact on the path delay, but are used in the final sea surface height computation. Indeed it is necessary to apply them when looking on meso-scale features. The third group contains parameters which have not direct impact on the path delay, but are inputs for corrections used in the sea surface height computation. Detailed descriptions can be found in [9 :RD 7] or specifically for Jason-2 in the Jason-2 User Handbook (9 :RD 14). Hereafter a short description of the analyzed parameters and corrections:

- Parameters and corrections for raw sea surface height calculation:

- Altimeter range. This is the distance from the satellite to the surface of the Earth measured by the altimeter. It's derived from the waveforms. Only its white noise is easily accessible. This is analyzed in chapter 8.5.5..
- Altimeter Ionosphere correction. The ionosphere correction is necessary to correct for the path delay due to the free electrons of the Earth's Ionosphere. It is computed by using the dual-frequency measurements of the altimeter (Ku- and C-band). This correction is also dependant on the sea state bias. Errors of the dual-frequency ionosphere correction are analyzed in chapter 8.5.6..
- Sea state bias. This correction encloses corrections for the electromagnetic bias (troughs of waves tend to reflect altimeter pulses better than do crests, which overestimates the range), skewness bias and tracker bias. The sea state bias correction is highly dependant on significant wave height, but shows also a dependency on wind speed. The errors on the sea state bias correction are analyzed in chapter 8.5.7..
- Dry troposphere correction. This correction is necessary to account for path delay due to "dry" gases of the Earth's troposphere. This correction comes from models. Its errors are analyzed in chapter 8.5.8..

- Wet troposphere correction derived from radiometer. This correction is necessary to account for path delay due to water vapor in the Earth's troposphere. It is derived from radiometer measurements. Its errors are analyzed in chapter 8.5.9..
- Orbit. It corresponds to the distance of the satellite above the reference ellipsoid. Several techniques to determine the satellite ephemeris exist. The orbit solutions are different for the three products. The errors of the orbit determination are analyzed in chapter 8.5.10..

- Corrections for final sea-level height:
The following corrections are not actual corrections to the altimeter measurement itself, but they are necessary to apply, when computing meso-scale sea surface height (for example to analyze geostrophic currents). Tides are significant contributors to the observed sea surface height. In order to observe ocean circulation, tides have to be removed as otherwise they dominate the ocean signal. This is possible, as they are nowadays very good modeled.

- Geocentric Ocean tide. The geocentric ocean tide provided in the products is the sum of the ocean tide and the load tide. The ocean tide is related to the luni-solar forcing. The load tide is forced by the ocean tide.
- Pole tide. The pole tide is due to variations in the Earth's rotation and is unrelated to luni-solar forcing.
- Terrestrial tide. The solid earth tide is also related to luni-solar forcing of the earth. In the Jason-2 products the solid earth tide is computed as a purely radial elastic response of the solid Earth to the tidal potential.
- Dynamic Atmosphere Correction (DAC). The Dynamic Atmosphere Correction is the combination of the inverted barometer (hydrostatical response of the sea surface to the atmospheric pressure variation) and the barotropic/baroclinic response to atmospheric forcing (response of the sea surface due to high frequency wind and pressure).

- Altimeter parameters not directly involved in sea-level height calculation:

- Significant Wave Height (SWH). The significant wave height is derived from the waveforms measured by the altimeter. It is an input for the sea state bias correction computation. The errors of the significant wave height are analyzed in chapter 8.5.11..
- Altimeter Backscattering coefficient (Sigma-0). This coefficient is also retrieved from the altimeter waveforms. It corresponds to the power of the returned radar signal. It is important for the computation of the altimeter wind speed. Its errors are analyzed in chapter 8.5.12.
- Altimeter wind speed. The altimeter wind speed is derived from the backscattering coefficient, as well as (in a minor proportion) from significant wave height. The wind speed is an input for the sea state bias correction. Altimeter wind speed errors are analyzed in chapter 8.5.13..

Error bugdet
Table 70 shows the specifications and determined errors for each of the three Jason-2 products (O/I/GDR). The studied parameters/ corrections are divided into three groups (see chapter 8.5.4.). Furthermore, the specifications and errors of the raw and final sea surface height are shown.
The specifications of the error budget are taken from the Jason-2 handbook (9 :RD 14). These

specifications seem not always correct, especially when showing different figures (for example for altimeter derived ionosphere correction) between the three product types for altimeter parameters. As mentioned previously, these specifications should be the same for the altimeter parameters, as all three products (O/I/GDR) are generated using the same ground retracking algorithm. Furthermore some specification figures seem to concern errors and some only the noise part of the error.
Hereafter we choose to show in a first table (Table 70) the errors (noise estimation of the different corrections and parameters). Remind that errors described here do not take into account long-term errors impacting climate implications as long-term drift, periodic signals (annual, semi-annual or 60-day signals) and isolated jumps for instance. For most of the parameters presented in the table, the errors have been averaged spatially and temporally over a short period (10 days). In a second table (Table 71), the white noise (when useful) is shown.
Historically, these figures are specified for 1 Hz measurements with 2 m significant wave height. This is an average situation (the majority of data has wave height around 2 m). Nevertheless, in the following document, this is not always the case (depending on the method used for the error determination).
For some corrections, several error figures are given. This is the case when different methods were used to determine the errors. Furthermore most errors are given as a minimum threshold. Figures for each parameter/ correction are explained from chapter 8.5.5. onwards. For some corrections (the second group concerning corrections for final sea surface height), no figures are given. They did not appear in current altimeter error budgets. But we think, that they also can contain errors when computing sea surface height. The estimation of errors of these corrections will be addressed in the future.

Outlook
In this part, for the error budget estimation of Jason-2: GDR-D data have been used. Further work will include estimation of errors of corrections such as tides. Furthermore, noise estimation could be extended to sea state bias and altimeter wind speed.

	Error budget	Specifications			Error (<10 days)			GOAL
		OGDR	IGDR	GDR	OGDR	IGDR	GDR	
Parameters and corrections for raw sea surface height calculation	Altimeter range	>1.7 cm[a,b,c]			>1.6 - 1.7 cm			1.5 cm[a,b,c]
	Ionosphere	1 cm[d,c]	0.5 cm[d,c]		>1 cm[h] / >0.2 cm[i]			0.5 cm[d,c]
	Sea State Bias	3.5 cm	2 cm		>0.4 cm			1 cm
	Dry troposphere	1 cm	0.7 cm		0.4-0.7 cm	0.3-0.7 cm		0.7 cm
	Wet troposphere	1.2 cm			>0.2 cm			1 cm
	Rms Orbit (radial component)	10 cm[e]	2.5 cm	1.5 cm	>3.7 cm	>1.7 cm	>1.0 cm	1.5 cm
Corrections for final sea surface height	Ocean tide	?			?			?
	Polar tide	?			?			?
	Terrestrial tide	?			?			?
	DAC	?	?		?	?		?
Altimeter parameters	Significant wave height	10% or 50 cm[f]	10% or 50 cm[f]		13 cm			5% or 25 cm[f]
	Wind speed	1.6 m/s	1.5 m/s		1 m/s			1.5 m/s
	Sigma0 (absolute)	0.7 dB			0.11 dB			0.5 dB
Raw sea surface height		11 cm[A]	3.9 cm[A]	3.4 cm[A]	> 4.2 cm[A]/-	> 2.6 cm[A] - 2.8 cm[B]	>2.1 cm[A] - 2.4 cm[B]	2.5 cm[A]
Final sea surface height		?	?	?	< 5.0 cm[C]	< 4.1 cm[C]	< 4.0 cm[C]	

[a] Ku-band after ground retracking

[b] Averaged over 1 sec

[c] Assuming 320 MHz C-bandwidth

[d] Filtered over 100 km

[h] Non filtered value

[i] Filtered over 300 km

[e] Real time DORIS onboard ephemeris

[f] whichever is greater

[A] Computed with $\sqrt{\Sigma|\sigma|}$ Assuming that errors in the table are uncorrelated (which is not the case).

[B] from formation flight phase (Jason-2/Jason-1)

[C] from cross-over computations of Jason-2 data

Figure 70: *Jason-2 Error budget including white noise and correlated errors for timescales less than 10 days*

	White noise budget	Specifications			Error (<10 days)			GOAL
		OGDR	IGDR	GDR	OGDR	IGDR	GDR	
Parameters and corrections for raw sea surface height calculation	Altimeter range	1.7 cm[a,b,c]			1.6-1.7 cm			1.5 cm[a,b,c]
	Ionosphere	<1 cm[d,c]	<0.5 cm[d,c]		0.7 cm[h] / 0.1 cm[i]			<0.5 cm[d,c]
	Sea State Bias	<3.5 cm	<2 cm		?			<1 cm
Altimeter parameters	Significant wave height	<10% or 50 cm[f]	<10% or 50 cm[f]		11.2 cm			<5% or 25 cm[f]
	Wind speed	<1.6 m/s	<1.5 m/s		?			<1.5 m/s
	Sigma0 (absolute)	<0.7 dB			0.08 dB			<0.5 dB

[a] Ku-band after ground retracking
[b] Averaged over 1 sec
[c] Assuming 320 MHz C-bandwidth
[d] Filtered over 100 km
[h] Non filtered value
[i] Filtered over 300 km
[f] whichever is greater

Figure 71: *Jason-2 Error budget including only the white noise error*

8.5.5. Altimeter Range

Errors on the range measurements can depend on several sources: atmosphere state (rain, presence of water vapor ...), non-Gaussian distribution of the wave field, but also technical parameters such as altimeter calibration, platform mispointing, Doppler effect,... . The estimation of the altimeter range distance depends also on the retracking algorithm.

Error of altimeter range (timescale < 10 days)
The error of altimeter range (including the correlated error part) is difficult to estimate. Therefore only the white noise is estimated. The total error is therefore higher than just the noise figure.

White noise on altimeter range
In order to determine altimeter noise, two methods were used: the spectral analysis of the high-frequency content and the monitoring of rms of elementary Ku-band range measurements.
Figure 72 shows the power spectrum of the uncorrected SLA (orbit - range - MSS) of 20 Hz data. As the orbit and the mean sea surface (MSS) are low frequency quantities, the noise displayed on the spectrum, comes from the range. The plateau has a value of about 0.004 m^2. Using equation 1, the noise on 20 Hz data is 7.6 cm.

Assuming full decorrelation (dividing by $\sqrt{20}$), gives the 1 Hz noise: 1.7 cm.

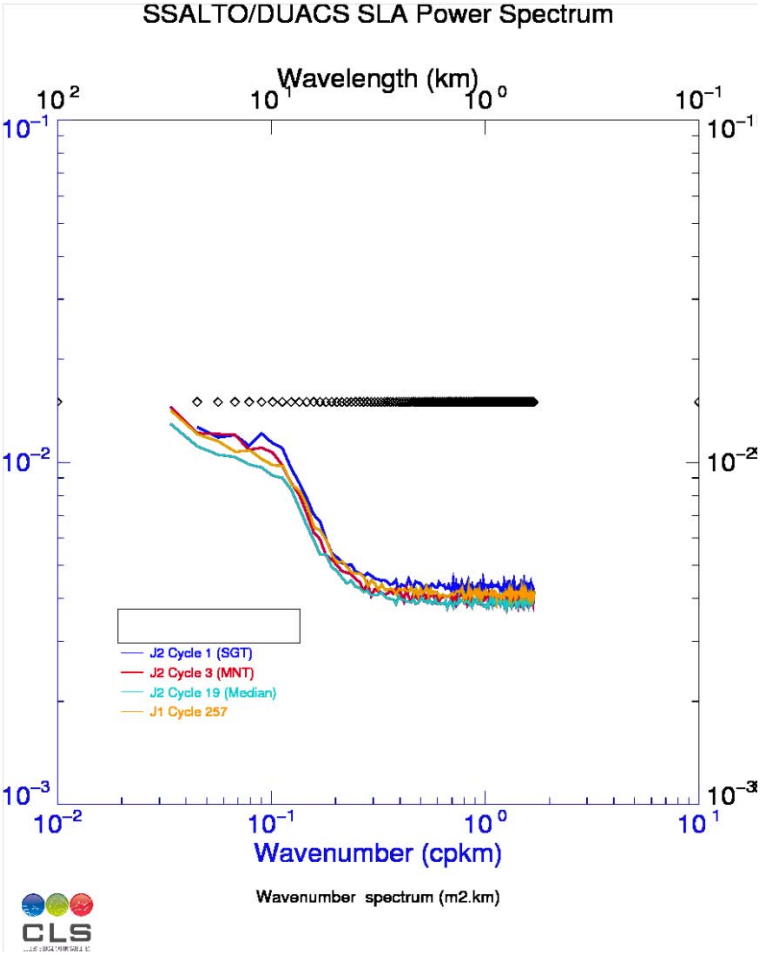

Figure 72: *Power spectrum of Jason-2 20 Hz SLA data*

Furthermore, the rms of the elementary Ku-band range (range_rms_ku) over 2011 was averaged in function of significant wave height (see Figure 73). Only valid data were used (using the method described in Ablain et al. (9 :RD 4).
For significant wave height of 2 m (most of measurements have significant wave heights around 2 m), the mean of range_rms_ku is 7.2 cm, which is the on the same order of magnitude as the value obtained by the power spectrum. Assuming full decorrelation, the division by sqrt20 (20 elementary measurements) results in 1.6 cm for the 1 Hz data. Note that using only 10 days of data gives the same results for significant wave heights around 2 m (noise of 1.6 cm for 1 Hz data).

The random noise of altimeter range is 1.6 cm to 1.7 cm for significant wave height of 2 m. The total error (due to correlations) for time scales less than 10 days is higher.

8.5.6. Ionosphere correction derived from altimeter

The ionosphere correction is dependent on the ranges (corrected for sea state bias) for Ku- and C-bands, as well as the frequencies used. As the OGDR, IGDR and GDR products use the same retracking algorithm, so computing the range the same way, there is no reason why requirements

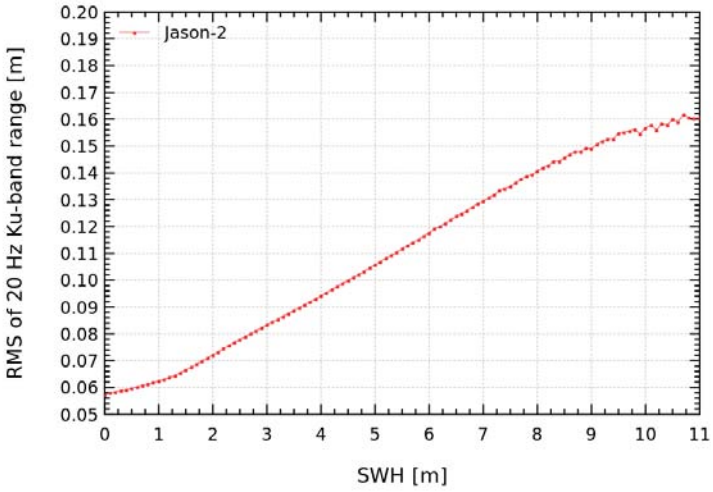

Figure 73: *Rms of elementaryKu-band range measurements in function of significant wave height for Jason-2 GDR over 2011.*

for ionosphere correction would be different for the 3 data types (as it is currently the case for the requirements in Table 70). Also we prefer to analyze errors for the un-filtered ionosphere correction (which is currently available in the O/I/GDR product) and also for a ionosphere correction filtered over 300 km.

Error of ionosphere correction (timescales less than 10 days)
One way to determine the error of the ionosphere correction is using the comparison between Jason-1 and Jason-2 during the formation flight phase (Jason-2 cycles 1 to 20), as described in (9 :RD 9). As during this phase, Jason-1 and Jason-2 were only 55 seconds apart on the same track, computing collinear measurement differences is possible. Figure 74 shows the cycle per cycle monitoring of the difference of dual-frequency ionosphere corrections (for un-filtered data and data filtered over 300 km). The standard deviation is 1.36 cm for un-filtered data and 0.35 cm for filtered data. Assuming that both altimeters contribute equally to the error, the error on the ionosphere correction on either Jason-1 or Jason-2 is 0.96 cm for non-filtered data and 0.25 cm for data filtered over 300 km.

White noise of ionosphere correction
The noise of the dual-frequency ionosphere correction can be computed theoretically by using the noise of the Ku- and C-band ranges. This is described in the Jason-2 System Performances Budget document (9 :RD 9). The Ku-band ionosphere correction formula is:

$$Iono\_corr\_Ku = \frac{1}{f_{Ku}^2}\left(\frac{f_{Ku}^2 * f_C^2}{f_{Ku}^2 - f_C^2}\right)(Range\_Ku - Range\_C) \quad (2)$$

$$\sigma_{Iono\_corr\_Ku} = \frac{1}{f_{Ku}^2}\left(\frac{f_{Ku}^2 * f_C^2}{f_{Ku}^2 - f_C^2}\right)\sqrt{\sigma_{Range\_Ku}^2 + \sigma_{Range\_C}^2} \quad (3)$$

For 2011, the rms of 20Hz range measurements (for significant wave heights of 2 m) is 7.2 cm for

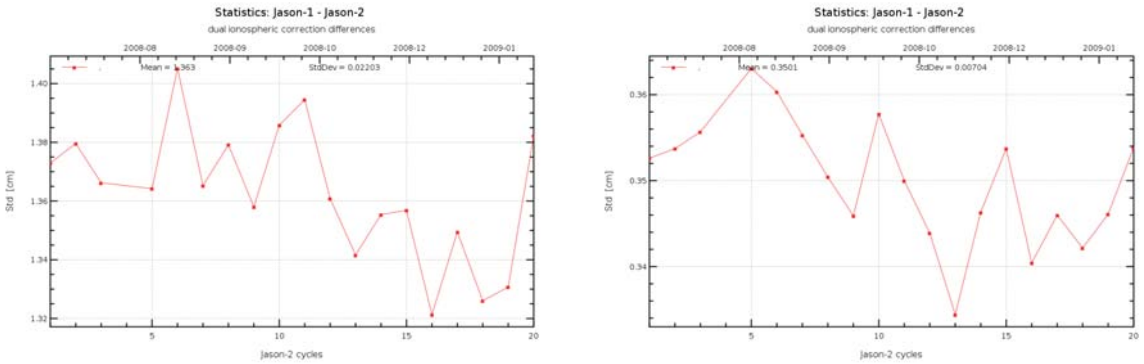

Figure 74: *Cycle per cycle monitoring (standard deviation) of the Jason-1 minus Jason2 dual-frequency ionospheric correction. Left: un-filtered correction, right: filtered correction (over 300 km)*

Ku-band (see 73) and 15.6 cm for C-band (not shown here). The computation gives therefore:

$$\sigma_{Iono\_corr\_Ku} = 0.179\sqrt{7.2^2 + 15.6^2} \cong 3.08cm \tag{4}$$

at 20 Hz.

$$\sigma_{Iono\_corr\_Ku} = 3.08/\sqrt{20} \cong 0.69cm \tag{5}$$

at 1 Hz.

When filtered at 300 km → 300 km / 7 km/s = 42.8 s: $\sigma_{(Ionocorrku)} = \frac{0.69}{\sqrt{42.8}} \cong 0.1cm$.
Nevertheless, as this value only takes into account range noise, it presents the minimum threshold of the error.

The error (including correlations for timescales less than 10 days) is at least 1 cm for un-filtered ionosphere correction and 0.2 cm for ionosphere correction filtered over 300 km. These figures are minimum values as the same errors might exist on both Jason-1 and Jason-2. The part of these errors due to random noise on the ionosphere correction (for data with significant wave height of 2 m) is 0.7 cm for un-filtered data and 0.1 cm for data filtered over 300 km.

8.5.7. Sea State Bias

The non-parametric sea state bias available on Jason-2 products is determined from a look-up table dependant on altimeter wind speed and significant wave height. Its quality is therefore directly dependant on the quality of this input values. The error of the resulting parameter therefore comes from the error made on the significant wave height and wind speed estimation, as well as the model estimation error. As the OGDR, IGDR and GDR products use the same retracking algorithm, so computing altimeter wind speed and significant wave height the same way, there is no reason why requirements for sea state bias would be different for the 3 data types. Historically, Chelton (9 :RD 6) considered 1% SWH for SSB uncertainty in his 1994 reference paper. It corresponds to a 2 cm SSB uncertainty level for 2m SWH. This high value is mainly due to the uncertainty of the constant offset term $\alpha 0$ in the regression used for the parameter based sea state bias models.

This error figure corresponds therefore rather to a bias. For non parametric models there is also an uncertainty on the determination of the constant (SSB for (SWH, Wind) = 0). Therefore non-parametric SSB solutions can have biases of several mm to several cm. Hereafter for the computation of the error figures (which are shown in Table 70) we do not take into account constant biases.

Error of sea state bias (timescales less than 10 days)

- SSB estimation error due to input error

Estimating the sea state bias correction error is relatively difficult. Since most SSB estimators are computed as a function of SWH and altimeter Wind Speed, the first approach is to use a Gaussian assumption, and a direct dependence between the errors on the input parameters. Taking a SWH value of 2m and a wind speed of 8m/s, the SSB model (table) gives a SSB value of -6.875074 cm for Jason-2 GDR-D. Taking into account the SWH and Wind speed errors (0.13 m and 1 m/s) , we select from the table the corresponding SSB values i.e. the SSB values indicated for a SWH varying from 1.87 to 2.13 m and a wind speed varying from 7.0 to 9.0m/s. Then we make the difference between each value and the consistent value (see Figure 75). This difference is the SSB error induced by the SWH error and the Wind speed error. The differences have a RMS value of about 0.34 cm for Jason-2 GDR-D. During the Jason-2 formation flight phase, sea state bias differences between Jason-1 and Jason-2 had a standard deviation of 7 mm (see 76), assuming that both missions contribute equally to the error, the error on Jason-2 sea state bias is 4.9 mm.

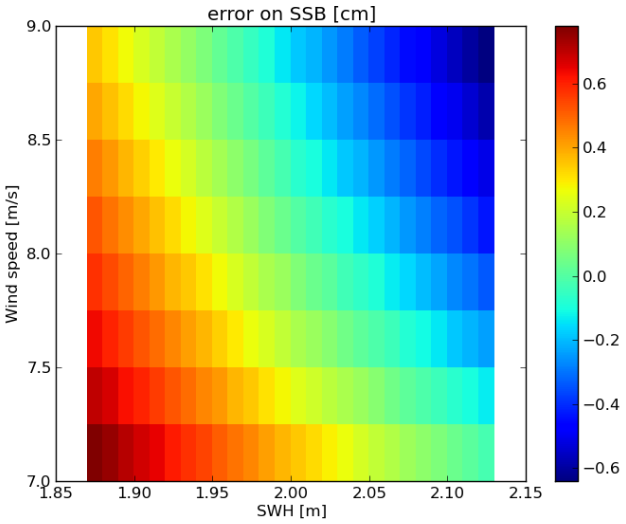

Figure 75: *Sensitivity of SSB to errors on SWH and wind speed (reference SWH=2m, wind speed=8m/s)*

- SSB estimation error due to different SSB models

When comparing over a 10-day period, two sea state bias models for Jason-2 (the non-parametric one used for GDR-D and a four-parameter model (Gaspar et al., (9 :RD 8)), the standard deviation of the difference (for valid measurements) is 7.3 mm. Assuming that both models contribute equally to the error, sea state bias error is 5.2 mm.

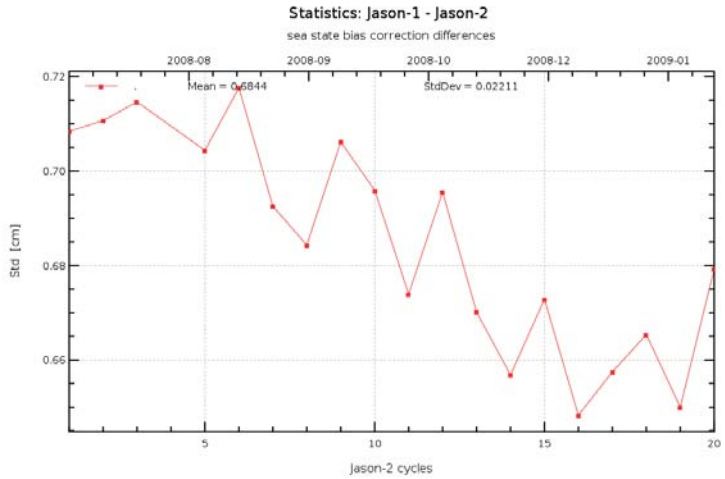

Figure 76: *Cycle per cycle monitoring standard deviation of the Jason-1 minus Jason2 non-parametric sea state bias correction.*

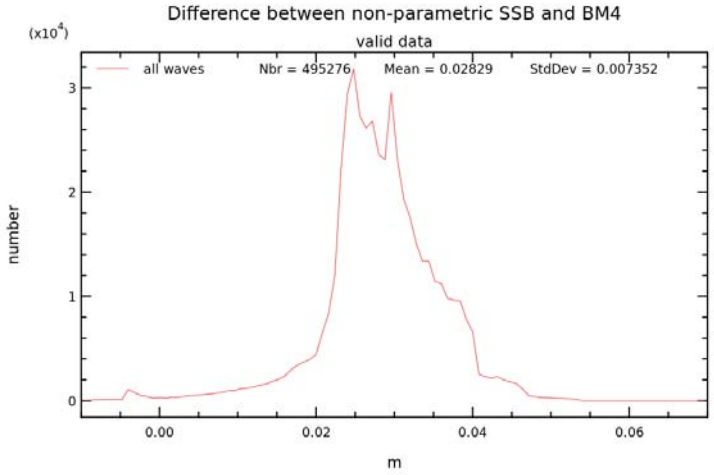

Figure 77: *Histogram of difference between non-parametric and BM4 sea state bias for Jason-2 cycle 193.*

The error of sea state bias (for timescales less than 10 days) is 0.5 cm.

8.5.8. Dry Troposphere Correction (from models)

Error of dry troposphere correction (for timescales less than 10 days)
The dry troposphere correction available in the products comes for IGDR and GDR products from restituated atmospheric pressure fields and model for S1 and S2 atmospheric tides (operational ECMWF model). For OGDR products the atmospheric pressure fields are predicted (operational ECMWF model). The dry troposphere correction value is proportional to the pressure value. To assess the error made on the dry troposphere correction (basically due to the error in the pressure field), a theoretical approach is possible. Salstein et al. (9 :RD 12) stated a rms error of 2-3 hPa

in the pressure fields, which translates to an error of approximately 0.7 cm in the dry troposphere correction. Another way to estimate the error is to asses the impact of using a dry troposphere correction from another model on altimetry data. Using either the dry troposphere correction (available in GDR-D) based on operational ECMWF model pressure fields or based on reanalyzed ERA-Interim pressure fields in sea surface height (SSH) computation, allows to assess its impact on crossover differences (maximal time interval of 10 days). Making the assumption that the ocean state does not vary within a 10 day interval, ascending/descending SSH differences should ideally have zero values. In reality this is not the case and is therefore an indication of the errors on the data. Computing the variance of crossover differences using successively both dry troposphere corrections, gives access to the difference of variance which is explained by the use of another type of the dry troposphere correction. Figure 78 shows the explained variance (converted to standard deviation) using other dry troposphere corrections (NCEP, ERA interim) compared to operational ECMWF model dry troposphere correction. Assuming that both models contribute equally to the error, the error of the dry troposphere correction is 0.2 to 0.3 cm.
In OGDR product, the dry troposphere correction is provided from the ECMWF forecast model run. The OGDR correction is therefore less precise than the GDR or IGDR one. Figure 79 shows a histogram of the difference of the forecast (OGDR) and analyzed (GRD-D) dry troposphere correction. Standard deviation is about 2 mm. When added to the error of the analyzed dry troposphere correction (sqrt(0.3^2+0.2^2), one yields approximately 4 mm. As the dry troposphere correction comes from a model, there is no white noise.

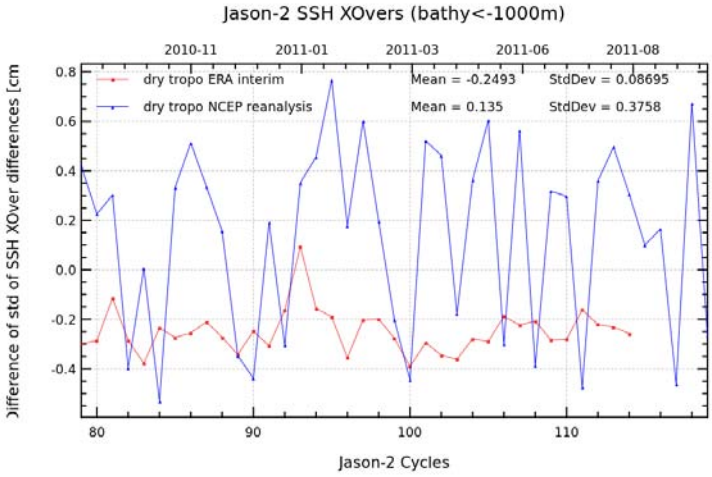

Figure 78: *Monitoring of difference of standard deviation of SSH differences at crossover points:* $\pm sqrt|Var_{(SSH\ using\ NCEP/ERA\ dry\ troposphere\ correction)} - Var_{(SSH\ using\ ECMWF\ dry\ troposphere\ correction)}|$. *The value is negative, when the variance difference was negative.*

The error of the dry troposphere correction (for timescales less than 10 days) is between 0.3 cm (comparison between models) and 0.7 cm (theoretical considerations) for IGDR and GDR products. For OGDR products the error ranges between 0.4 cm and 0.7 cm. There is no white noise for the dry troposphere correction.

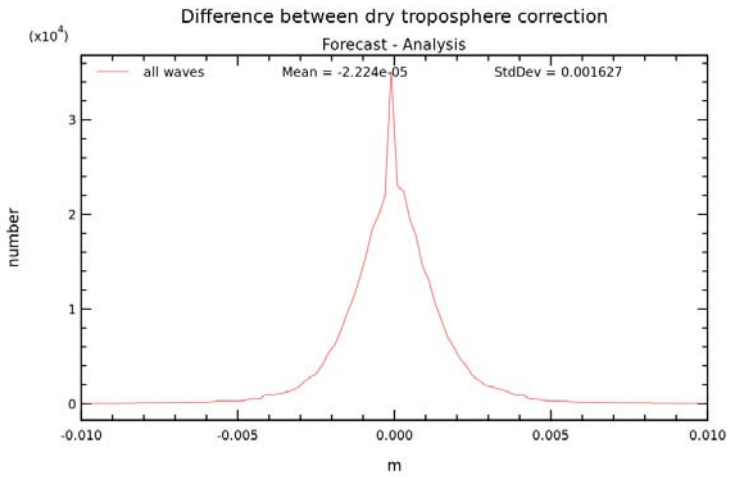

Figure 79: *Histogram of difference between dry troposphere correction from OGDR (forecast) and GDR (analysis), computed using data from cycle 193.*

8.5.9. Wet troposphere correction

Errors of the radiometer wet troposphere correction (for timescales < 10 days)
To determine the error on radiometer wet troposphere correction the comparison between Jason-1 and Jason-2 during the formation flight phase (Jason-2 cycles 1 to 20) is used. As during this phase, Jason-1 and Jason-2 were only 55 seconds apart on the same track, computing collinear measurement differences is possible. Figure 80 shows the cycle per cycle monitoring of the difference of the radiometer wet troposphere corrections. The standard deviation is 0.36 cm. Assuming that both altimeters contribute equally to the error, the error on wet troposphere correction on either Jason-1 or Jason-2 is 0.25 cm. Nevertheless this is a minimum value, as the same errors might exist on both radiometers. The radiometer wet troposphere correction has no white noise for 1 Hz measurements.

Jumps and drifts of the radiometer wet troposphere correction
The present document is focalized on errors for timescales less than 10 days. Nevertheless errors on longer timescales exist. The radiometer wet troposphere correction for example is impacted by drifts and jumps, especially for OGDR and IGDR products (the GDR product benefits from the ARCS processing which corrects most of these jumps and drifts). The jumps and drifts for IGDR data are easily recognizable on Figure 81, where radiometer and ECMWF model wet troposphere correction are compared.
The error of the radiometer wet troposphere correction (for timescales less than 10 days) is at least 0.2 cm (figure from formation flight phase of Jason-2 and Jason-1). There is no white noise for 1 Hz radiometer wet troposphere correction.

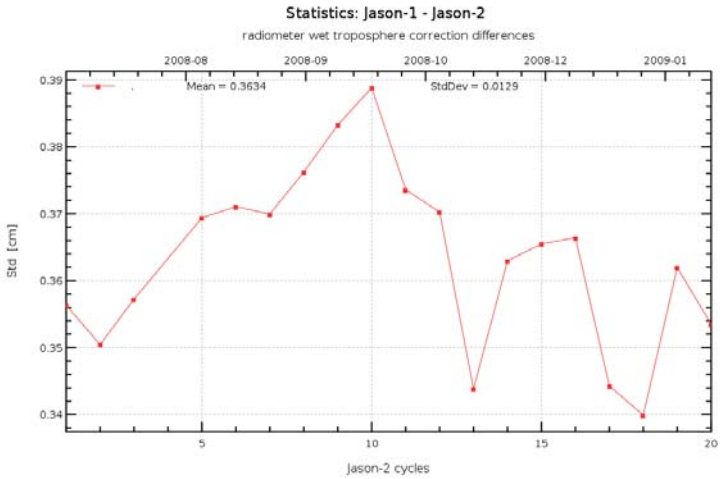

Figure 80: *Cycle per cycle monitoring (standard deviation) of the Jason-1 minus Jason2 radiometer wet tropospheric correction.*

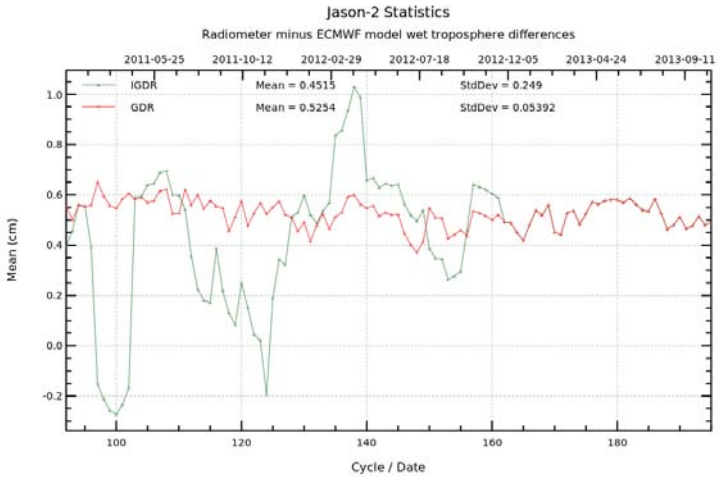

Figure 81: *Cycle per cycle monitoring (mean) of the radiometer minus ECMWF wet troposphere correction difference for Jason-2 GDR and IGDR.*

8.5.10. Orbit

The precise orbit ephemerides (POE) are computed using three orbit determination techniques: DORIS, GPS, and Laser. Cerri et al. (9 :RD 5) have estimated the radial error of the Jason GDR-C orbit standard (which is used for the Jason-2 GDR-T product). This error has a rms of 1.03 cm (see Figure 82 from Cerri et al).

The orbit determination noise from Figure 82 was estimated by Cerri at al. using several orbit solutions with similar models. Hereafter, two different orbit standards (GDR-C versus GDR-D) are compared for Jason-2 over 2011. They differ by the ITRF reference frame as well as by the gravity field used. Cycle per cycle standard deviation of this difference is shown in Figure 83. Its

Table 6
Radial error budget for Jason GDR orbit. When the errors in this table are assumed to be uncorrelated, the RSS value is 10.3 mm.

	Typical RMS	Systematic	Rationale
Orbit determination noise	<7 mm	1/rev with varying amplitude and phase, no significant geographical correlation	Inter-comparison of orbits using same or similar models or with low dependency from models
Static gravity field	<1 mm	static order-1 pattern	Comparison between EIGEN-GL04S and the following generation of mean field
Tide model	<2 mm	1–2 mm varying order-1 pattern	Comparison of FES2004 Vs GOT4.7 and of FES2004 Vs CSR3.0
Atmosphere/Ocean/ Hydrology	<6 mm	varying order-1 pattern	Comparison with orbits using the most complete TVG models
Solar radiation pressure	<3 mm	120-day variable pattern stronger at high and low latitudes, amplitude <3 mm	Comparison of orbits with UCL and GDR-C box models
Reference frame (long term)	2 mm	<1 mm/year drift along Z	Comparison of N/S centering of Jason-1 and Jason-2 ITRF2005 based orbits and analysis of drift of LAGEOS 1 and 2 geocenter series
Geocenter motion	2 mm	<5 mm annual variation along the N/S direction. Depends on the relative weight between SLR, DORIS and GPS tracking	Relative centering of orbits obtained by displacing the reference network of 5 mm along Z

Figure 82: *Radial error budget for Jason GDR orbit. Table 6 from Cerri et al. (9 :RD 5).*

mean value is 1.05 cm.

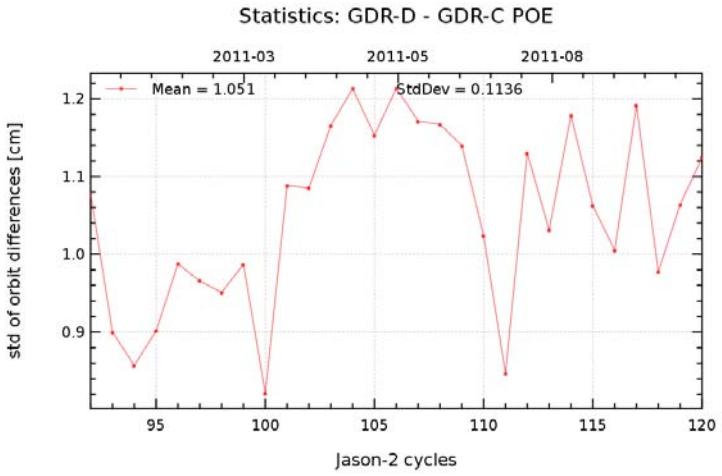

Figure 83: *Cycle per cycle monitoring of std of GDR-D - GDR-C POE standard for Jason-2 GDR over 2011.*

The medium orbit ephemerides (MOE) are computed using DORIS measurements (except for cycles 20 to 78, where also Laser data were used in MOE computation). The top left of Figure 84 shows the daily statistics of the differences between overlapping MOE arcs. This gives a hint of the stability of the MOE solution. It is about 1 cm. It varies in time and has generally higher values in summer. Lillibridge et al. (9 :RD 10) computed the differences between the different orbit types. Differences between MOE and POE are generally less than 2 cm. For a recent Jason-2 cycle, the standard deviation of this difference (POE - MOE) is approximately 1.1 cm (see bottom of Figure 84). Assuming that the errors between POE and MOE are uncorrelated, this gives an

error of 1.52 cm. The orbit of OGDR products is a DORIS/Diode navigator orbit. Right side of Figure 84 shows daily statistics of Navigator and MOE differences. Since a DIODE update on 18th of February 2010, the differences have decreased and its standard deviation is generally less than 4 cm. In the bottom part of Figure 84 the standard deviation of the POE minus Navigator orbit difference is 2.4 cm for a recent Jason-2 cycle. Assuming that the errors between POE and navigator orbit are uncorrelated, this gives an error of 2.62 cm. (see also, A. Couhert presentation at OSTST2013 : "Towards the 1mm/yr stability of the radial orbit error at regional scales").

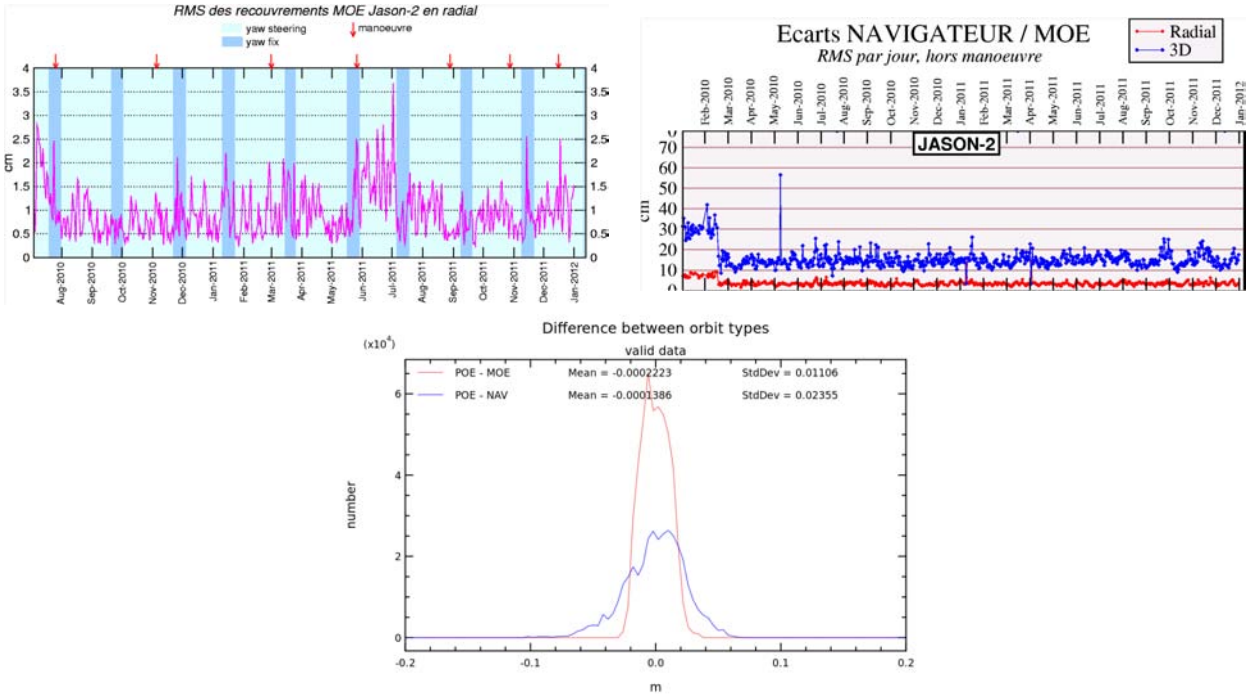

Figure 84: *Top left: Daily statistics of differences between overlapping arcs during MOE computation (from [10]). Top right: Daily statistics of differences between the Navigator and MOE (from [10]). Bottom: Histogram of difference between POE-D and MOE (red curve), as well as POE-D and Navigator (blue curve) for Jason-2 cycle 193.*

The errors of the different orbit types for timescales less than 10 days are approximately 1 cm for GDR, 1.5 cm for IGDR and 2.6 cm for OGDR.

8.5.11. Significant Wave Height

The figures of the specification of significant wave height are different for the three product type. As the retracking algorithm used for the Jason-2 product is the same no matter the product type, the specification and observed figures should be the same for the three product types.

Error of significant wave height (timescales less than 10 days)
During the formation flight phase, the standard deviation of the Jason-1 minus Jason-2 significant wave height difference was 17.2 cm (Figure 85). Assuming that both missions contribute equally to the error, the error on Jason-2 SWH is 12.2 cm. Abdalla et al. 2010 (9 :RD 1) compared

SWH from Jason-2 OGDR to wave buoys (mainly in the northern hemisphere). They found a mean difference of about 2 cm and a standard deviation of the difference of 39 cm. Using a triple collocation technique between Jason-2 OGDR SWH, wave buoys and model hindcasts, Abdalla et al. 2011 (9 :RD 2) estimate a error of 13 cm for Jason-2 SWH. As the retracking algorithm used for the Jason-2 OGDR is the same as the one used for the IGDR and GDR products, these figures should therefore also be valid for SWH of the IGDR and GDR products.

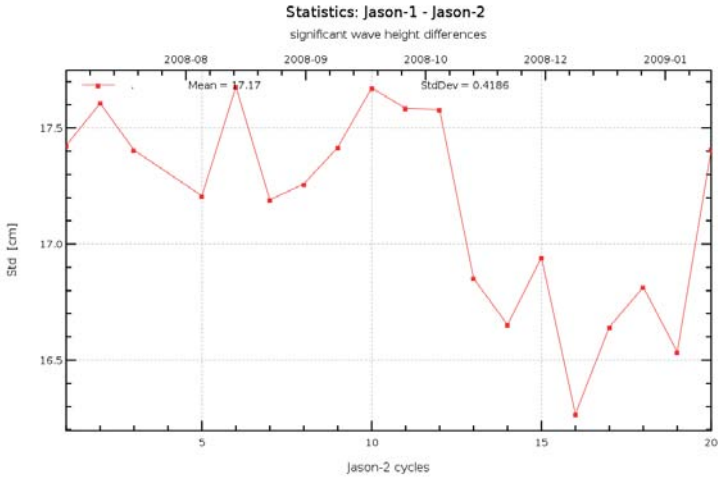

Figure 85: *Cycle per cycle monitoring of the standard deviation of the Jason-1 minus Jason-2 significant wave height.*

White noise of significant wave height

In order to assess the white noise of 1Hz significant wave height (SWH), the rms of the elementary Ku-band SWH (swh_rms_ku) over 2011 was averaged in function of significant wave height. Only valid data were used (using the method described in Ablain et al. (9 :RD 4). For significant wave height of 2 m, the mean of swh_rms_ku is 49.8 cm. Assuming full decorrelation, the division by square root of 20 (20 elementary measurements) results in 11.1 cm for the 1 Hz data.

Figure 73 shows the power spectrum of the significant wave height of 20 Hz data. The plateau has a value of about 0.175 m2. Using equation 1, the noise on 20 Hz data is 0.5 m. Assuming full decorrelation (dividing by sqrt20), gives the 1 Hz white noise: 11.2 cm.

The error of significant wave height (for timescales less than 10 days) is about 13 cm. The white noise is about 11.2 cm. These figures are valid for all three types of products (O/I/GDR).

8.5.12. Backscattering coefficient

Error of backscattering coefficient (timescales less than 10 days)

During the formation flight phase, the standard deviation of the Jason-1 minus Jason-2 backscattering coefficient difference was 0.157 dB (Figure 88). Assuming that both missions contribute equally to the error, the error on Jason-2 backscattering coefficient is 0.11 dB. Note, that the error of backscattering coefficient is probably higher for Jason-1 than Jason-2, as Jason-1 experienced

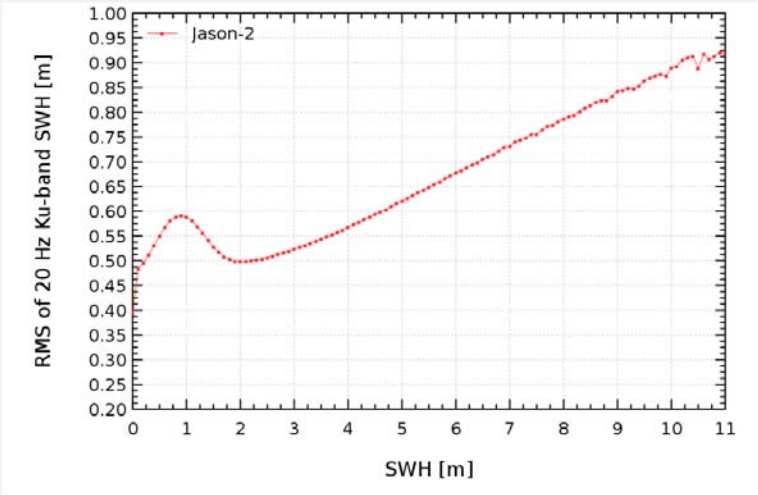

Figure 86: *Rms of elementary Ku-band SWH measurements in function of significant wave height for Jason-2 GDR over 2011.*

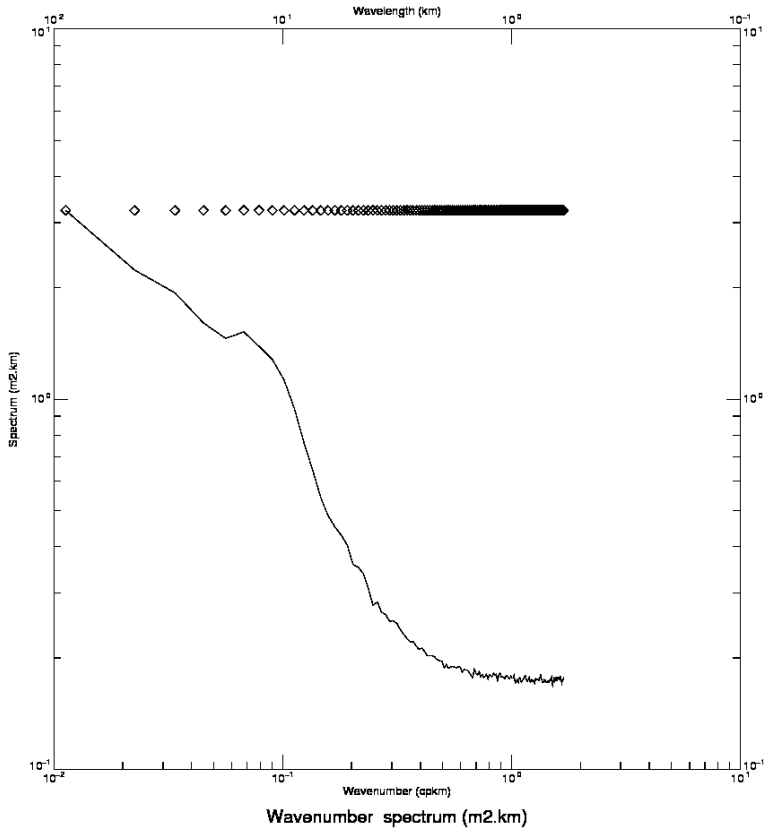

Figure 87: *Spectrum of 20 Hz significant wave height data.*

some increased mispointing periods (due to unavailability of star trackers). This also impacts the

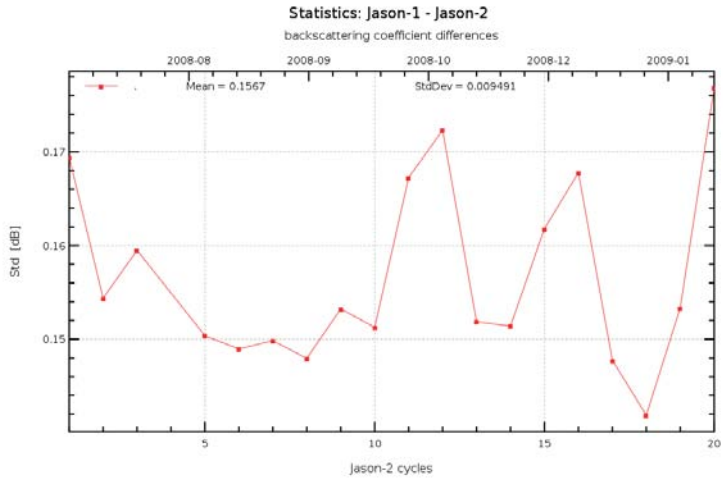

Figure 88: *Cycle per cycle monitoring of the standard deviation of the Jason-1 minus Jason-2 backscattering coefficient.*

backscattering coefficient.

White noise of backscattering coefficient

In order to assess the white noise of 1Hz backscattering coefficient (Sigma0), the rms of the elementary Ku-band sigma0 (sig0_rms_ku) over 2011 was averaged in function of significant wave height. Only valid data were used (using the method described in Ablain et al. (9 :RD 4). For significant wave height of 2 m, the mean of sig0_rms_ku is 0.374 dB. Assuming full decorrelation, the division by square root of 20, results in 0.08 dB for the 1 Hz data.

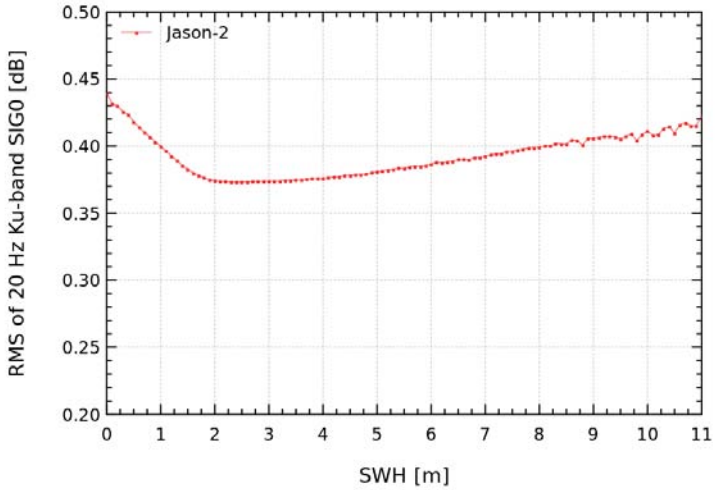

Figure 89: *Rms of elementary Ku-band Sigma0 measurements in function of significant wave height for Jason-2 GDR over 2011.*

Figure 90 shows the power spectrum of the backscattering coefficient of 20 Hz data. The plateau

has a value of about 0.08 dB2. Using equation 1, the noise on 20 Hz data is 0.34 dB. Assuming full decorrelation (dividing by $sqrt(20)$), gives the 1 Hz noise: 0.075 dB. The value is similar to the one determined with the previous method.

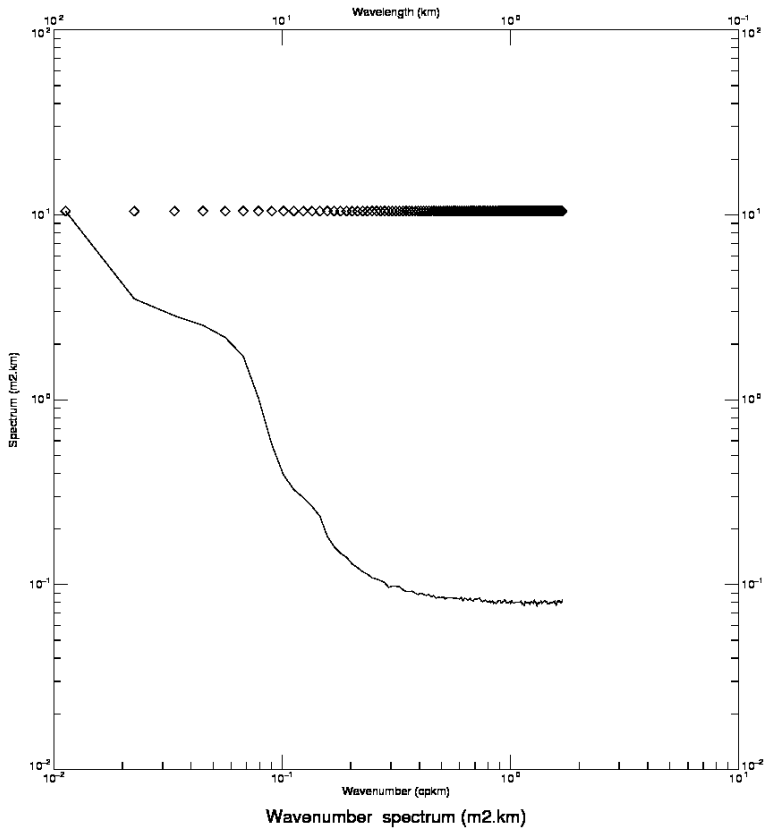

Figure 90: *Spectrum of 20 Hz backscattering coefficient.*

The error of the backscattering coefficient (for timescales less than 10 days) is 0.11 dB. The white noise of the backscattering coefficient has a value of 0.08 dB.

8.5.13. Altimeter wind speed

Error of the altimeter wind speed (for timescales less than 10 days)

During the formation flight phase, the standard deviation of the Jason-1 minus Jason-2 altimeter wind speed difference was 0.45 m/s (right part of Figure 91). Assuming that both missions contribute equally to the error, the error on Jason-2 altimeter wind speed is 0.32 m/s. This is a minimum value of the error.

Using a triple collocation technique between Jason-2 OGDR altimeter wind speed, buoys and model hindcasts, Abdalla et al. 2011 (9 :RD 2) estimate an error of 1 m/s for Jason-2 altimeter wind speed.

The error of the altimeter wind speed (for time scales less than 10 days) is about 1 m/s.

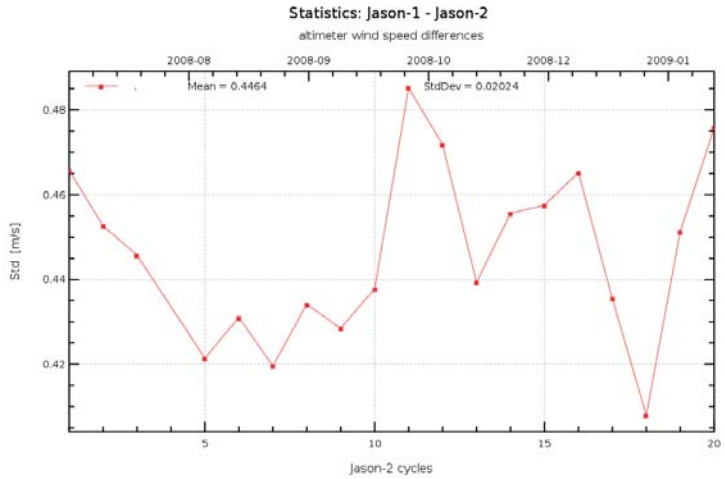

Figure 91: *Cycle per cycle monitoring (standard deviation) of the Jason-1 minus Jason-2 altimeter wind speed.*

8.5.14. Error on the raw Sea Surface Height (for timescales less than 10 days)

Generally, the raw SSH error specifications (Table 70) were computed by the square root of the sum of the squared individual errors ($sqrt(\Sigma_i.\sigma_i)$). This seems not very fortunate, as noises and correlated errors were mixed up. This can lead to an under-estimation of the error, as the white noise is only a part of the error. Furthermore, the values are not really uncorrelated (e.g. the ionosphere correction is computed using range and sea state bias). Concerning the observed/computed error budget, often only minimum thresholds of the error values are available. So this method leads to a minimum threshold of the error on raw sea surface height. Computing with this method the raw SSH error, yields: 4.2 cm for OGDR, 2.6 cm for IGDR and 2.1 cm for GDR (when using ionosphere correction filtered over 300 km). Hereafter we use the flight formation phase between Jason-2 and Jason-1. The sea level anomaly (SLA) contains the parameters and corrections presented in Table 70, as well as the mean sea surface. Note that the ionosphere correction used for the SLA computation was filtered over 300 km. The standard deviation of the Jason-1 minus Jason-2 sea level anomaly (SLA) difference was 3.9 cm for IGDR and 3.4 cm for GDR. Assuming that both missions contribute equally to the errors, the SLA error is 2.8 cm for IGDR and 2.4 cm for GDR. These figures are minimum values. Especially, as some corrections, like for example the ECMWF dry troposphere correction are identical for both missions. Nevertheless they are higher than the value computed with the previous method. This would confirm the hypothesis that some items which contribute to error on the SSH were not taken into account. For Ogdr the method to use the formation flight phase is not very relevant, as Jason-1 Osdr and Jason-2 Ogdr are not of the same level of quality (different tracking algorithm used and Jason-1 navigator orbit has much more error than Jason-2 navigator orbit).
The error of sea level anomaly (for timescales less than 10 days) is at least 4.2 cm for OGDR, 2.6 cm for IGDR and 2.1 cm for GDR when using the method which sums the individual errors. Using the flight formation phase, the errors rise to 2.8 cm for IGDR and 2.4 cm for GDR. These figures are also minimum values.

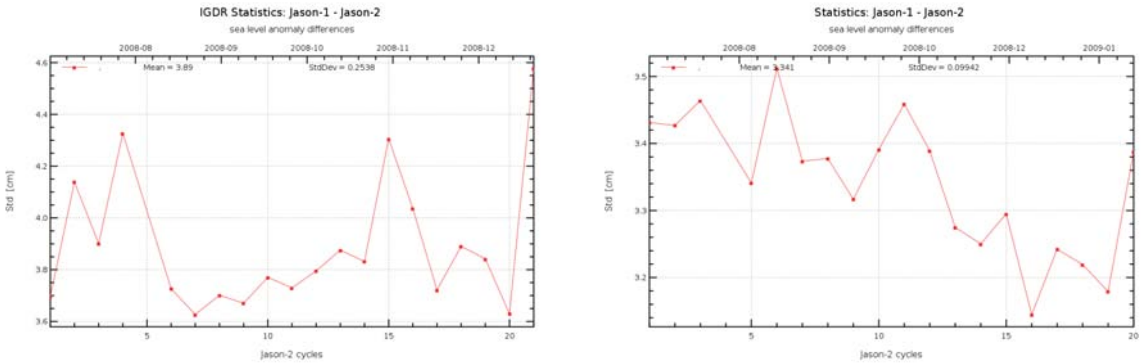

Figure 92: *Cycle per cycle monitoring (standard deviation) of the Jason-1 minus Jason-2 sea level anomaly.*

8.5.15. Error on the final Sea Surface Height (for timescales less than 10 days)

In the previous chapter, the error of the raw sea surface height was computed using the formation flight phase. This did only give access to the error of a part of the sea surface height computation, as many corrections (like tides) are the same for both satellites. In order to compute the error of the total sea surface height, mono-mission crossover points are used. Standard deviation of ascending/ descending sea surface height (which includes all corrections) yields 4.9 cm for GDR, 5.2 cm for IGDR and 6.5 cm for OGDR (Figure 93). Generally, range values at crossover points are interpolated per spline and allowing for a 3 cm noise, which reduces the standard deviation. Hereafter no noise was allowed during spline interpolation. As errors on sea surface height are on both tracks (ascending and descending), dividing the standard deviation by sqrt2 gives the errors of Jason-2 final sea surface height: 3.5 cm for GDR, 3.7 cm for IGDR and 4.6 cm for OGDR. These are maximum values.

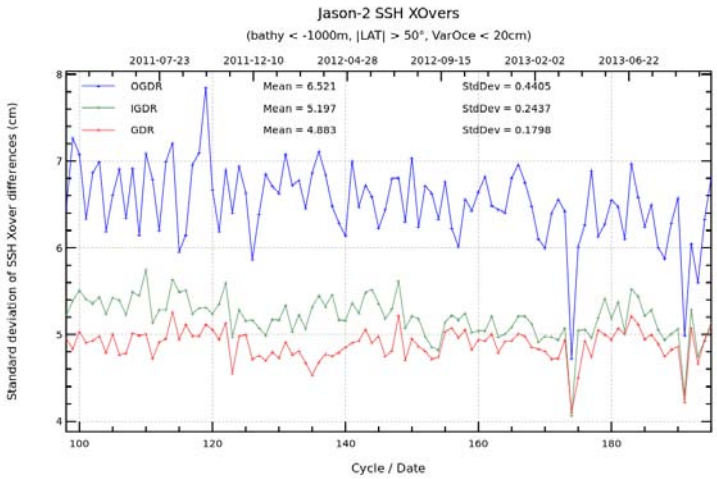

Figure 93: *Cycle per cycle monitoring standard deviation of ascending / descending sea surface height differences for Jason-2 OGDR, IGDR and GDR products.*

The errors of the final sea surface height are less than 4.6 cm for OGDR, 3.7 cm for IGDR and 3.5 cm for GDR.

9. Conclusion

Jason-2 is in orbit since 20th of June, 2008. During the flight formation phase, which lasted 20 cycles (till 2009-01-26), Jason-2 flew with Jason-1 (55s apart) over the same historical TOPEX/Poseidon ground track. This allowed extensive verification and validation of the data, as both satellites observed the same geophysical phenomena. OGDR and IGDR data quality was already approved during OSTST 2008 meeting in Nice. OGDR products were distributed to users since mid-December 2008 and IGDR since mid-January 2009. The GDR production started end of February 2009 and was released in version T to users since August 2009. More than 5 years of GDR data are now available. Note that during 2012, the whole mission was reprocessed in standard GDR-D. During 2013, Jason-2 entered Safe Hold Mode by three times (in February, March and September).

The flight formation phase has shown that Jason-2 data quality is excellent, at least of the same order as the Jason-1 one. The raw data coverage is similar to Jason-1's over ocean and improved in coastal areas. Thanks to the new altimeter tracking modes, the availability of land measurements is significantly improved. Over ocean, the valid data coverage is similar since the additional Jason-2 raw measurements are removed by the editing procedure. The additional measurements in coastal areas and over rivers and lakes benefit to projects such as PISTACH (see PISTACH handbook http://www.aviso.oceanobs.com/fileadmin/documents/data/tools/hdbk_Pistach.pdf).

The altimetric parameter analysis has shown a similar behavior compared to Jason-1. Some biases exist as between dual-frequency ionosphere correction, but they are stable. Though Jason-2 radiometer performances are improved especially near coasts, stability problems are observed in Jason-2 IGDR product (small jumps (versus JMR or ECMWF model) occurred in 34 GHz channel). During 2011, these stability problems became more frequent leading to jumps and drifts also in the 18.7 GHz channel. These stability problems are mostly corrected thanks to the ARCS system applied for GDR. For the GDR-D reprocessing, new calibration coefficients were used. According to the JPL, cycles 001 to 113 have climate data record quality calibrations, cycles 114 to 140 have intermediate quality calibrations and cycle 141 and onwards have operational (ARCS) quality calibrations. But even the new calibration coefficients are not able to correct rapid drifts which occur within a cycle (as happened around cycle 120).

The SSH performances analyzed at crossovers or along-track highlight similar performances between Jason-1 and Jason-2. The consistency between both SLA is remarkable with a small geographically correlated signal lower than 1 cm. This signal is removed using GSFC orbits proving the sensibility of the orbit calculation for the detection of geographically correlated biases. The fact that several production centers (CNES, JPL, GSFC) compute different kinds (tri-technic, GPS only, Doris+SRL) of Jason-2 precise orbit solutions, gives also a great opportunity to understand more about the impact of orbit on altimetry data and to explain some of the observed signals.

The flight formation phase between Jason-1 and Jason-2 allowed us to check accurately the Jason-2 mission. As during the Jason-1/TOPEX flight formation phase, we also learned a lot from Jason-1 measurement quality. To balance all these excellent results and especially the quasi-perfect SSH consistency between both missions, both systems can contain similar errors undetectable with the analyzes performed here. Comparisons with external and independent datasets (Tide gauges, Temperature/Salinity profiles, ...) are thus essential to detect potential errors.

The more of 5 years of Jason-2 data show excellent quality. Scientific studies and operational applications therefore benefit from the combination of Jason-2, Jason-1, and Envisat data. The 2012 reprocessing of the whole mission in GDR-D standard has improved the dataset in comparison to the GDR-T standard for meso-scales (improved coherence at crossover points), as well as on longer time scales (coherence between ascending and descending passes is improved).
The Jason-1 mission ended on 21st June 2013, so that cross calibration between Jason-1 and Jason-2 are no longer possible. The whole Jason-1 data will be reprocessed during 2014.
Finally, the launch of the AltiKa mission on 25th of February 2013 allows to complete the altimetry constellation from 2013 onwards, re-occupying the long-term ERS and Envisat ground track. Comparisons between AltiKa and Jason-2 data are available in [18].

The remaining open points which needs further investigation or surveillance are:

- the stability of the AMR
- the remaining signal of approximatly 120 days in the monitoring of the ascending/descending crossover differences.
- the exessive altimeter rain flag
- the sea state bias, which is quite different from the one of Jason-1 (nevertheless new sea state bias look-up tables (presented at OSTST 2012 by Tran et al.[[67]]) are available for Jason-1 and Jason-2)
- the radiometer processing is different between Jason-1 and Jason-2
- there remains a hemispherical bias linked to orbit solutions (see Special Investigations chapter in [17]).

10. Annex

10.1. Jason-1 and Jason-2 altimeter validation activities over ocean in the framework of the SALP project

Jason-1 and Jason-2 altimeter validation activities over ocean in the framework of the SALP project were presented at OSTST in October 2013 and the following poster is available at: http://www.aviso.oceanobs.com/fileadmin/documents/OSTST/2013/posters/Philipps_Poster_OSTST13_PerfoJ1J2.pdf

Jason-1 and Jason-2 altimeter validation activities over ocean in the framework of the SALP project

Sabine Philipps (CLS), Michaël Ablain (CLS), Hélène Roinard (CLS), J. Legeais (CLS), Nicolas Picot (CNES)
CLS, Space Oceanography Division, Toulouse, France, (mablain@cls.fr)
CNES, Centre National d'Etudes Spatiales, Toulouse, France

SALP Service Altimetrie & Localisation Precise

Overview

Global data quality assessment of Jason-1 and Jason-2 data are performed by CNES and CLS in the framework of the SALP project since the Jason-1 launch in 2002.
Our purpose is to underline the importance and the complexity of performance missions activities ("Cal/Val") through 3 relevant examples.

Cal/Val objectives are :
- -To check the data availability and validity
- -To analyze the physical content quality of product parameters
- -To estimate the system performances
- -To contribute to a better knowledge of the sea-level physical content
- -To check the system improvement
- -To provide information for users and production centre (My Ocean/DUCAS)

Example 1 : Mono-mission analyses

Check the internal consistency of an altimetric system by analysing the Sea Surface Height (SSH), its parameters and geophysical corrections

TIME

- 2005: detection of an hemispheric north/south bias on mono-mission crossover maps due to a time-tag bias of ~0.28 ms
- 2008: reprocessing of Jason-1 data in GDR-C version including a new parameter to correct empirically this time-tag bias, time-tag bias is also observable on Jason-2 data
- 2010: CNES experts find the explanation for the time-tag bias on Jason
- 2012: Reprocessing of Jason-2 data in GDR-D version: the datation in the GDR product is corrected for this time-tag bias

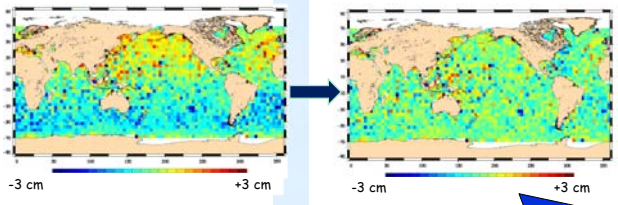

Example 2: Altimeter missions cross comparisons

Evaluate the coherence between two altimeter systems by comparing their SSH and estimate the potential improvement of the computation of a new altimeter standard in the SSH calculation.

TIME

- 2008: detection of an hemispheric north/south bias between JA1 and JA2 during flight formation phase for CNES POE_C - range - MSS. This bias was reduced using GSFC Doris/Laser orbit
- 2012: reprocessing of Jason-2 in GDR-D standard. Outside of formation flight phase geographically correlated bias observable on JA1-JA2 crossover points using : POE-D, GOT4V8, model WTC, SSB from products

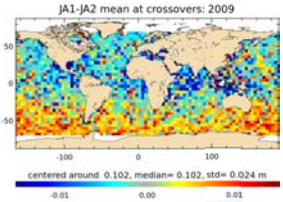

Hemispheric SSH bias: +/- 1 cm

- POE-D, GOT4V8, model WTC, **2012 SSB**: amplitude of geographically correlated bias is reduced (around Indonesia, around 50° S). Small North/South bias remains

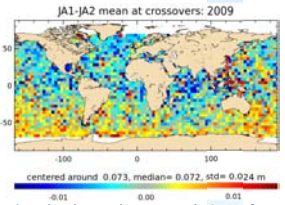

Hemispheric SSH bias: +/- 0.5 cm

- **Doris only orbit (without down-weighting of SAA stations for JA1)**, GOT4V8, model WTC, 2012 SSB

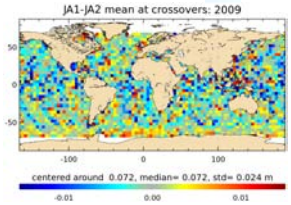

Hemispheric SSH bias: not detectable

Mono-mission analyses
Cross-comparisons
Cal/Val
In-Situ comparisons

Example 3 : In-Situ Comparisons

Compute the SSH differences between altimeter data and in-situ measurements (tide gauges, Argo T/S profiles,...) to detect potential drifts or jumps on the long-term time series

TIME

- 2005: Down-weighting of SAA stations for JA1 orbit solution improves performances at mesoscale, but creates a small North/South bias between JA1 and JA2 data. Compared to insitu data (T/S profile), which weighting solution is more coherent?
- 2013: Down-weighting of SAA stations for JA1 Doris only orbit shows North/South trend differences (between JA1 and T/S) of 0.6 mm/yr
- 2013: Without down-weighting of SAA stations for JA1 Doris only orbit the North/South trend differences (between JA1 and T/S) is reduced to 0.2 mm/yr

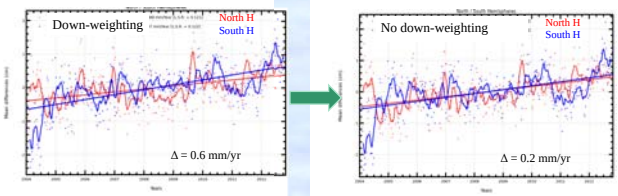

Conclusions

- Jason-1 and Jason-2 altimeter ocean validation activities performed by CNES and CLS have allowed us to strongly contribute to the improvement and the very good data quality
- The 3 examples presented here show that :
  - Altimeter Validation activities over ocean is not a "simple" data quality control but a very complex and exhaustive activity
  - The communication with experts is crucial to understand and correct the anomalies
- The key of success of these validation activities are :
  - Use other altimetry missions in operation
  - Use independent external data sources
  - Agility: iterate quickly : reactivity is essential in crises and commissioning
  - Skill diversity: integrating a wide panel of scientific & technical skills in the validation
  - Skills maintained on time : over all the altimetry period
- For future altimeter missions, 2 main recommendations should be applied for ocean validation activities:

Recommendation 1 "A strong effort is mandatory for the altimeter ocean validation activities"
- To provide for users and productions centers (My Ocean/DUACS, ECMWF) the best altimeter datasets possible for all the applications: oceanic variability, climate studies,...

- **Recommendation 2:** "An integrated team gathering validation & instrumental experts is necessary"
  - To have short feedback loops
  - To correct/validate the anomalies as soon as possible

These recommendations are emphasized with the upcoming launch of Sentinel-3A:
The SARM altimeter on board provides a new potential for high resolution topography but also many questions and challenges for Calibration / Validation activities.

Collecte Localisation Satellites
8-10 rue Hermes
31520 Ramonville Saint-Agne - France

OSTST
8-11 October 2013 | Boulder, US

11. References

References

[1] Ablain, M., A. Cazenave, G. Valladeau, and S. Guinehut. 2009 : A new assessment of the error budget of global mean sea level rate estimated by satellite altimetry over 1993-2008. *Ocean Sci*, **5, 193-201**. Available at http://www.ocean-sci.net/5/193/2009/os-5-193-2009.pdf

[2] Ablain, M., S. Philipps, M. Urvoy, N. Tran, and N. Picot (2012) Detection of Long-Term Instabilities on Altimeter Backscattering Coefficient Thanks to Wind Speed Data Comparisons from Altimeters and Models, *Marine Geodesy*, **35:S1, 258-275**. Available at http://www.tandfonline.com/doi/pdf/10.1080/01490419.2012.718675

[3] AVISO and PODAAC User Handbook. IGDR and GDR Jason-1 Products. Edition 4.1, October 2008. SMM-MU-M5-OP-13184-CN (AVISO), JPL D-21352 (PODAAC). Available at http://www.aviso.oceanobs.com/fileadmin/documents/data/tools/hdbk_j1_gdr.pdf.

[4] Beckley, B. D. , Zelensky, N. P. , Holmes, S. A. , Lemoine, F. G. , Ray, R. D. , Mitchum, G. T. , Desai, S. D. and Brown, S. T. (2010) Assessment of the Jason-2 Extension to the TOPEX/Poseidon, Jason-1 Sea-Surface Height Time Series for Global Mean Sea Level Monitoring, *Marine Geodesy*, **33:1, 447 - 471**. Available at http://pdfserve.informaworld.com/96442__925511460.pdf

[5] Bertiger, Willy , Desai, Shailen D. , Dorsey, Angie , Haines, Bruce J. , Harvey, Nate , Kuang, Da. , Sibthorpe, Ant and Weiss, Jan P. (2010) Sub-Centimeter Precision Orbit Determination with GPS for Ocean Altimetry. *Marine Geodesy*, **33:1, 363 - 378**. Available at http://pdfserve.informaworld.com/858128__925510150.pdf

[6] Bertiger, Willy , Desai, Shailen D. , Haines, Bruce J., R. DeCarvalho, and A. Dorsey (2010) Jason-2/OSTM Precision Orbit Determination with GPS *Oral presentation at OSTST meetting, Lisbon, Portugal*, Available at http://www.aviso.oceanobs.com/fileadmin/documents/OSTST/2010/oral/19_Tuesday/bertiger.pdf

[7] E. Bronner and G. Dibarboure, May 24th, 2012: Technical Note about the Jason-1 Geodetic Mission. *SALP-NT-MA-EA-16267-CNv1.0*. Available at: http://www.aviso.oceanobs.com/fileadmin/documents/data/duacs/Technical_Note_J1_Geodetic_Mission.pdf

[8] Philipps, S., M. Ablain, G. Valladeau, and J.-F. Legeais. Jason-2 validation and cross calibration activities (Annual report 2012). Reference: CLS.DOS/NT/12-223. Nomenclature: SALP-RP-MA-EA-22141-CLS. Available at http://www.aviso.oceanobs.com/fileadmin/documents/calval/validation_report/J2/annual_report_j2_2012.pdf.

[9] Philipps, S., M. Ablain, G. Valladeau, and J.-F. Legeais. Jason-2 validation and cross calibration activities (Annual report 2011). Reference: CLS.DOS/NT/12-005. Nomenclature: SALP-RP-MA-EA-22042-CLS. Available at http://www.aviso.oceanobs.com/fileadmin/documents/calval/validation_report/J2/annual_report_j2_2011.pdf.

[10] Ollivier A., M. Guibbaud. Envisat RA2/MWR ocean data validation and cross-calibration activities. Yearly report 2012. SALP-RP-MA-EA-22163-CLS, CLS.DOS/NT/12-292.

[11] Roinard, H., S. Philipps. Jason-2 reprocessing impact on ocean data (cycles 001 to 145). Comparison of Jason-2 Gdr-D with Gdr-T, as well as with Jason-1 Gdr-C and Envisat Gdr v2.1. SALP-RP-MA-EA-22140-CLS. CLS.DOS/NT/12.222.

[12] Roinard, H., S. Philipps. Jason-2 reprocessing impact on ocean data (cycles 001 to 020). Comparison of Jason-2 Gdr-D with Gdr-T, as well as with Jason-1 Gdr-C. SALP-RP-MA-EA-22118-CLS. CLS.DOS/NT/12.138. Available at ftp://avisoftp.cnes.fr/AVISO/pub/jason-2/documentation/gdr_d_calval_report/JA2_GDR_D_validation_report_cycles1to20_V1_1.pdf

[13] Valladeau, G.. Validation of altimetric data by comparison with tide gauge measurements for TOPEX/Poseidon, Jason-1, Jason-2 and Envisat. SALP-NT-MA-EA-22157-CLS, CLS.DOS/NT/12-259.

[14] Legeais J.-F. and S. Dupuy. 2012 annual report: Validation of altimeter data by comparison with in-situ T/S Argo profiles for T/P, Jason-1, Jason-2 and Envisat missions. CLS-DOS/NT/12-261. SALP-RP-MA-EA-22176-CLS.

[15] Valladeau G. and Prandi P., 2013:Validation of altimeter data by comparison with tide gauge measurements for TOPEX/Poseidon, Jason-1, Jason-2 and Envisat (Annual report 2013). [CLS.DOS/NT/13-262].

[16] Legeais J.F. and Ablain M., 2013: Validation of altimetric data by comparison with in-situ T/S Argo profiles (Annual Report 2013) [SALP-RP-MA-EA-22281-CLS, CLS.DOS/NT/13-256]

[17] H. Roinard, S. Philipps, M. Ablain, G. Valladeau, and J.-F. Legeais. Jason-1 validation and cross calibration activities (Annual report 2013). Reference: CLS.DOS/NT/13-226. Nomenclature: SALP-RP-MA-EA-22269-CLS. Available at http://www.aviso.oceanobs.com/fileadmin/documents/calval/validation_report/J1/annual_report_j1_2013.pdf.

[18] S. Philipps. Sara/AltiKa validation and cross calibration activities (Annual report 2013). Reference: CLS.DOS/NT/13-228. Nomenclature: SALP-RP-MA-EA-22271-CLS.

[19] A. Ollivier. M. Guibbaud. Envisat RA2/MWR ocean data validation and cross calibration activities (Yearly report 2013). Reference: CLS.DOS/NT/13-290. Nomenclature: SALP-RP-MA-EA-22293-CLS.

[20] Boening, C., J. K. Willis, F. W. Landerer, R. S. Nerem, and J. Fasullo (2012), The 2011 La Niña: So Strong, the Oceans Fell, *Geophys. Res. Lett.*, doi:10.1029/2012GL053055, in press.

[21] John T. Fasullo , C. Boening, F. W. Landerer, R. S. Nerem (2013), Australia's Unique Infuence on Global Sea Level in 2010-2011, doi:10.1002/grl.50834, in press.

[22] Boy, François and Jean-Damien Desjonqueres. 2010. Note technique datation de l'instant de reflexion des échos altimètres pour POSEIDON2 et POSEIDON3 *Reference: TP3-JPOS3-NT-1616-CNES*

[23] Brown G.S., "The average impulse response of a rough surface and its application", *IEEE Transactions on Antenna and Propagation*, Vol. AP 25, N1, pp. 67-74, Jan. 1977.

[24] Brown S., S. Desai, and W. Lu "Initial on-orbit performance assessment of the advanced microwave radiometer and performance of JMR GDR-C", *Oral presentation at OSTST meeting, Nice, France, 9-12 november 2008.* Available at http://www.aviso.oceanobs.com/fileadmin/documents/OSTST/2008/oral/brown_calval.pdf

[25] Brown, S., S. Desai, W. Lu, and A. Sibthorpe. 2009. Performance Assessment of the Advanced Microwave Radiometer after 1 Year in Orbit. *Oral presentation at OSTST meeting, Seattle, USA*. Available at: http://www.aviso.oceanobs.com/fileadmin/documents/OSTST/2009/oral/Brown.pdf

[26] S. Brown. 2010. A Novel Near-Land Radiometer Wet Path-Delay Retrieval Algorithm: Application to the Jason-2/OSTM Advanced Microwave radiometer. *IEEE TGRS vol. 48 n ° 4*. Available at ftp://podaac.jpl.nasa.gov/allData/ostm/preview/L2/AMR/docs/Brown_TGARS_2010.pdf

[27] Cerri, L. , Berthias, J. P. , Bertiger, W. I. , Haines, B. J. , Lemoine, F. G. , Mercier, F. , Ries, J. C. , Willis, P. , Zelensky, N. P. and Ziebart, M. (2010) Precision Orbit Determination Standards for the Jason Series of Altimeter Missions, *Marine Geodesy*, **33:1, 379 - 418**. Available at http://pdfserve.informaworld.com/816985__925509111.pdf

[28] Cerri, L., A. Couhert, S. Houry, F. Mercier. 2011. Improving the long-term stability of the GDR orbit solutions. *Oral presentation at OSTST meeting, San Diego, USA*. Available at http://www.aviso.oceanobs.com/fileadmin/documents/OSTST/2011/oral/02_Thursday/Splinter3POD/05_Cerri.pdf.

[29] Chambers, D., P., J. Ries, T. Urban, and S. Hayes. 2002. Results of global intercomparison between TOPEX and Jason measurements and models. *Paper presented at the Jason-1 and TOPEX/Poseidon Science Working Team Meeting, Biarritz (France), 10-12 June.*

[30] Collard, F. (2005). Algorithmes de vent et période moyenne des vagues JASON à base de réseaux de neurons. BO-021-CLS-0407-RF. Boost Technologies.

[31] Commien, L., S. Philipps, M. Ablain and N. Picot. 2009. SSALTO CALVAL Performance assessment Jason-1 GDR "C"/GDR "B". *Poster presented at OSTST meeting, Seattle, USA*. Available at: http://www.aviso.oceanobs.com/fileadmin/documents/OSTST/2009/poster/commien.pdf

[32] Couhert, A., L. Cerri, F. Mercier, S. Houry. 2010. Status of Jason-1 and Jason-2 GDR orbits. *Talk presented at OSTST meeting, Lisbon, Portugal*. Available at: http://www.aviso.oceanobs.com/fileadmin/documents/OSTST/2010/oral/couhert.pdf

[33] DeCarvalho, R., S. Brown, B. Haines and S. Desai. 2009. Global cross calibration and validation of the Jason-1 and Jason-2/OSTM data products. *Oral presentation at OSTST meeting, Seattle, USA*. Available at: http://www.aviso.oceanobs.com/fileadmin/documents/OSTST/2009/oral/deCarvalho.pdf

[34] Desjonqueres, J.-D., G. Carayon, J.-L. Courriere, and N. Steunou "POSEIDON-2 In-Flight results", *Oral presentation at OSTST meeting, Nice, France, 9-12 november 2008*. Available at http://www.aviso.oceanobs.com/fileadmin/documents/OSTST/2008/oral/desjonqueres.pdf

[35] Desjonquères, J. D. , Carayon, G. , Steunou, N. and Lambin, J. (2010) Poseidon-3 Radar Altimeter: New Modes and In-Flight Performances, *Marine Geodesy*, **33:1, 53 - 79**. Available at http://pdfserve.informaworld.com/542982__925503482.pdf

[36] Dettmering, Denise and Bosch, Wolfgang (2010) Global Calibration of Jason-2 by Multi-Mission Crossover Analysis, *Marine Geodesy*, **33:1, 150 - 161**. Available at http://pdfserve.informaworld.com/315039__925510361.pdf

[37] Dorandeu.,J., M. Ablain, Y. Faugère, F. Mertz, 2004 : Jason-1 global statistical evaluation and performance assessment. Calibration and cross-calibration results. *Marine Geodesy* **27: 345-372.**

[38] Faugère, Y. et al. 2009. The SLOOP project: preparing the next generation of altimetry products for open ocean. *Poster presented at OSTST meeting, Seattle, USA*. Available at: http://www.aviso.oceanobs.com/fileadmin/documents/OSTST/2009/poster/Faugere2.pdf

[39] Faugère, Y. et al. 2010. CROSS-CALIBRATION between ENVISAT and JASON-1/2. *Oral presentation at OSTST meeting, Lisbon, Portugal*. Available at: http://www.aviso.oceanobs.com/fileadmin/documents/OSTST/2010/oral/19_Tuesday/Tuesday_afternoon/faugere.pdf

[40] Jason-2 Version "T" Geophysical Data Records : Public Release, August 2009. Available at : http://www.aviso.oceanobs.com/fileadmin/documents/data/products/Jason-2_GDR_T_disclaimer.pdf

[41] Gourrion, J., Vandemark, D., Bailey, S., Chapron, B., Gommenginger, G.P., Challenor, P.G. and Srokosz, M.A., 2002: A two-parameter wind speed algorithm for Ku-band altimeters, *Journal of Atmospheric and Oceanic Technology*. **19(12) 2030-2048**.

[42] Dumont, J.-P., V. Rosmorduc, N. Picot, S. Desai, H. Bonekamp, J. Figa, J. Lillibridge, R. Sharroo, 2011: OSTM/Jason-2 Products Handbook. CNES: SALP-MU-M-OP-15815-CN. EUMETSAT: EUM/OPS-JAS/MAN/08/0041. JPL: OSTM-29-1237. NOAA/NESDIS: Polar Series/OSTM J400. Available at http://www.aviso.oceanobs.com/fileadmin/documents/data/tools/hdbk_j2.pdf

[43] Hernandez, F. and P. Schaeffer, 2000: Altimetric Mean Sea Surfaces and Gravity Anomaly maps inter-comparisons. AVI-NT-011-5242-CLS, 48 pp. CLS Ramonville St Agne.

[44] Huffman, G. and D.T.Bolvin, 2009: TRMM and Other Data Precipitation Data Set Documentation. Available at ftp://precip.gsfc.nasa.gov/pub/trmmdocs/3B42_3B43_doc.pdf

[45] Imel, D.A. 1994. Evaluation of the TOPEX/POSEIDON dual-frequency ionospheric correction. *J. Geophys. Res.*, **99, 24,895-24,906**.

[46] Lemoine, F., N.P. Zelensky, S. Melachroinos, D.S. Chinn, B.D. Beckley, D.D. Rowlands, and S.B. Luthcke. 2011. GSFC OSTM (Jason-2), Jason-1 & TOPEX POD Update. *Oral presentation at OSTST meeting, San Diego, USA*. Available at http://www.aviso.oceanobs.com/fileadmin/documents/OSTST/2011/oral/02_Thursday/SplinterPOD/03Lemoine_etal_SWT2011_v01.pdf.

[47] Le Traon, P.-Y., J. Stum, J. Dorandeu, P. Gaspar, and P. Vincent, 1994: Global statistical analysis of TOPEX and POSEIDON data. *J. Geophys. Res.*,**99, 24619-24631.**

[48] MSEs (CNES, NASA, NOAA, EUMETSAT). 2011. GDR Status. *Oral presentation (by N. Picot) at OSTST meeting, San Diego, USA*. Available at http://www.aviso.oceanobs.com/fileadmin/documents/OSTST/2011/oral/03_Friday/Plenary/GDRProducts/02PicotGDR_status_2011.pdf.

[49] Obligis, E., L. Eymard, M. Ablain, B. Picard, J.F. Legeais, Y. Faugere and N. Picot, 2010. The wet tropospheric correction for altimetry missions: A mean sea level issue. *Oral presentation at OSTST meeting, Lisbon, Portugal*. Available at http://www.aviso.oceanobs.com/fileadmin/documents/OSTST/2010/oral/19_Tuesday/OBLIGIS.pdf.

[50] Ollivier A., Faugere Y., Granier N., 2008: Envisat RA-2/MWR ocean data validation and cross-calibration activities. Yearly report. Technical Note CLS.DOS/NT/09.10, Contract N° SALP-RP-MA-EA-21633-CLS http://www.aviso.oceanobs.com/fileadmin/documents/calval/validation_report/EN/annual_report_en_2008.pdf

[51] Ollivier A., Faugere Y., P. Thibaut, G. Dibarboure, and J.-C. Poisson, 2008: Investigation on the high frequency content of Jason-1 and Jason-2. CLS.DOS/NT/09-027

[52] Ollivier A., M. Guibbaud, Faugere Y. Envisat RA2/MWR ocean data validation and cross-calibration activities. Yearly report 2011. SALP-RP-MA-EA-22062-CLS, CLS.DOS/NT/12-021.

[53] Otten M., C. Flohrer, T. Springer, and W. Enderle. 2011. Generating precise and homogeneous orbits for Jason-1 and Jason-2. *Oral presentation at OSTST meeting, San Diego, USA*. Available at http://www.aviso.oceanobs.com/fileadmin/documents/OSTST/2011/oral/03_Friday/Splinter6POD/01_Otten.pdf.

[54] Peltier, 2004, Global Glacial Isostasy And The Surface of The Ice-Age Earth: The ICE-5G (VM2) Model and GRACE. *Annual Review of Earth and Planetary Sciences*, May 2004, **Vol. 32, Pages 111-149**, doi: 10.1146/annurev.earth.32.082503.144359

[55] Philipps, S., M. Ablain, J. Dorandeu, P. Thibaut, N. Picot and J. Lambin. 2006. SSALTO CAL-VAL Performance assessment Jason-1 GDR 'B'/GDR 'A'. *Poster presented at OSTST meeting, Hobbart, Australia*. Available at: http://www.aviso.oceanobs.com/fileadmin/documents/OSTST/2006/ablain1.pdf

[56] Picot, N., P. Thibaut, N. Tran, S. Philipps, J.C. Poisson, T. Moreau, and E. Bronner. 2010. New Jason-2 GDR-C standards. *Oral presentation at OSTST meeting, Lisbon, Portugal*. Available at http://www.aviso.oceanobs.com/fileadmin/documents/OSTST/2010/oral/PThibaut_Jason2.pdf.

[57] Picot, N., P. Thibaut, N. Tran, S. Philipps, J.C. Poisson, E. Bronner, C. Garcia and many others. 2011. Jason-2 GDR-D standards. *Oral presentation at OSTST meeting, San Diego, USA*. Available at http://www.aviso.oceanobs.com/fileadmin/documents/OSTST/2011/oral/02_Thursday/Splinter5IP/05NPicot_et_al_OSTST_2011_J2-GDRD-Standards.pdf.

[58] Schaeffer, P., A. Ollivier, Y. Faugere, E. Bronner, and N. Picot. The new CNES CLS 2010 Mean Sea Surface. *Oral presentation at OSTST meeting, Lisbon, Portugal, 18-20 october 2010*. Available at http://www.aviso.oceanobs.com/fileadmin/documents/OSTST/2010/oral/19_Tuesday/Schaeffer.pdf.

[59] Schaeffer, P., Y. Faugere, J.-F. Legeais, A. Ollivier, T. Guinle, and N. Picot (2012). The CNES_CLS11 Global Mean Sea Surface Computed from 16 Years of Satellite Altimeter Data. *Marine Geodesy* **35: sup1, 3-19**. Available at http://www.tandfonline.com/doi/abs/10.1080/01490419.2012.718231

[60] Solar Radio Flux (10.7cm) (daily solar data). Available at http://www.swpc.noaa.gov/ftpmenu/indices/old_indices.html

[61] Thibaut, P. O.Z. Zanifé, J.P. Dumont, J. Dorandeu, N. Picot, and P. Vincent, 2002. Data editing: The MQE criterion. *Paper presented at the Jason-1 and TOPEX/Poseidon Science Working Team Meeting, New-Orleans (USA), 21-23 October*.

[62] Thibaut, P., J.-C. Poisson, A. Ollivier, S. Philipps, and M. Ablain: "Jason-2 waveforms, tracking and retracking analysis", *Oral presentation at OSTST meeting, Nice, France, 9-12 november 2008*. Available at http://www.aviso.oceanobs.com/fileadmin/documents/OSTST/2008/oral/thibaut.pdf

[63] Moreau, T., P. Thibaut, 2009. Etude dépointage Poseidon-3: optimisation de l'angle d'ouverture d'antenne. CLS-DOS-NT-09-028. 15 pp, CLS Ramonville St. Agne.

[64] P. Thibaut. Bilan des activités d'expertise altimétriques menées en 2009 : Lot 2D. SALP-RP-MA-EA-21808-CLS, CLS-DOS-NT-10-029.

[65] Tran, N. , Labroue, S. , Philipps, S. , Bronner, E. and Picot, N. (2010) Overview and Update of the Sea State Bias Corrections for the Jason-2, Jason-1 and TOPEX Missions, *Marine Geodesy*,**33:1, 348 - 362**. Avialable at http://pdfserve.informaworld.com/804727__925502357.pdf

[66] Tran, N., P. Thibaut, J.-C. Poisson, S. Philipps, E. Bronner, and N. Picot. Jason-1, Jason-2 and TOPEX Sea State Bias. Overview and Updates. *Oral presentation at OSTST meeting, Lisbon, Portugal, 18-20 october 2010*. Avialable at http://www.aviso.oceanobs.com/fileadmin/documents/OSTST/2010/oral/TRAN.pdf

[67] N. Tran, S. Philipps, J.-C. Poisson, S. Urien, E. Bronner, and N. Picot. Impact of GDR_D standards on SSB corrections. *Oral presentation at OSTST meeting, Venice, Italy, 27-28 September 2012*. Available at http://www.aviso.oceanobs.com/fileadmin/documents/OSTST/2012/oral/02_friday_28/01_instr_processing_I/01_IP1_Tran.pdf.

[68] World Meteorological Organization. 2010. El Nino/ La Nina Update (30 March 2010). Available at http://www.wmo.int/pages/prog/wcp/wcasp/documents/El_Nino_Mar10_Eng.pdf.

[69] World Meteorological Organization. 2011. El Nino/ La Nina Update (17 November 2011). Available at http://www.wmo.int/pages/prog/wcp/wcasp/documents/El_Nino_Nov11_Eng.pdf.

Jason-1, Jason-2 and Envisat. SALP-NT-MA-EA-22046-CLS, CLS.DOS/NT/12-016.

[70] Valladeau, G., S. Philipps. Jason-1 validation and cross calibration activities (Annual report 2009).SALP-RP-MA-EA-21795-CLS, CLS.DOS/NT/10-005.

[71] Valladeau, G., S. Philipps. Jason-1 validation and cross calibration activities (Annual report 2010).SALP-RP-MA-EA-21903-CLS, CLS.DOS/NT/10-332.

[72] Zlotnicky, V. 1994. Correlated environnemental corrections in TOPEX/POSEIDON, with a note on ionomospheric accuracy. *J. Geophys. Res.*, **99, 24,907-24,914**